Investigation of two diffusion problems using exact numerical methods:

I) Polymers in gels

II) Anomalous diffusion of particles in gels

by

Justin Boileau

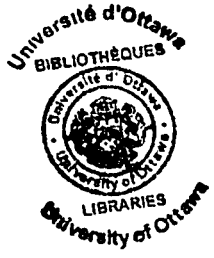

A thesis submitted to
The School of Graduate Studies and Research
In partial fulfillment of the requirements
For the degree of Master of Physics

University of Ottawa
Ottawa, Ontario
May 11, 2004

Summary

The concepts of diffusion and random walk have helped increase our understanding of the movement of molecules in biological, physical and chemical systems. The scope of applicability of the theory of diffusion is truly limitless. The theoretical study of diffusion was initially focussed on the movements of small particles in quenched media. Although narrow, this field has increased our knowledge concerning the diffusion of proteins along bio-membranes, the gel electrophoresis of particles for the purpose of separation, and the development of micro-fabricated devices used to separate molecules. In the first part of this thesis, we generalize an existing model used to find the exact diffusion coefficient of small particles among immobile obstacles. The model is expanded to include small oligomers and allows us to study the non-trivial effects of molecular architecture on the diffusion of molecules both in solution and in the presence of immobile obstacles.

The second part of this thesis deals with the short time anomalous diffusion of particles in disordered media. Historically, the steady state solution of molecular diffusion was studied and little to no effort was ever made towards an understanding of how molecules reach steady-state dynamics. An exact enumeration model is proposed to study the exact short-time dynamics of a particle in 3 dimensional space.

Sommaire

L'étude des processus de dérive et des marches aléatoires a amélioré notre compréhension de la dynamique moléculaire des systèmes biologiques, physiques et chimiques. Les champs d'applications de la théorie de diffusion sont très vastes. Initialement, cette théorie visait à expliquer le mouvement de petites particules évoluant dans des milieux denses. Aujourd'hui, elle nout permet de mieux comprendre plusieurs phénomène importants, comme par exemple la diffusion des protéines le long des membranes et l'électrophorèse des particules chargées. Elle facilite également le dévelopement d'équipement de séparation de molécules à échelle microscopique.

Dans la première partie de cette thèse, nous généralisons un modèle de diffusion qui nous permet de trouver des valeurs exactes pour la mobilité et le coefficient de diffusion de particules simples se déplaçant sur un réseau. Nous modifions le modèle existant qui ne permet que de calculer la mobilité et le coefficient de diffusion de petites molécules. Cette généralisation nous permet d'étudier certaines conséquences non triviales de l'architecture moléculaire sur la diffusion des molécles en solution et en présence d'obstacles.

Dans la deuxième partie de la thèse, nous présentons un nouveau modèle pour l'étude de la diffusion de particules pour de courts intervalles de temps. Traditionellement, l'étude de la diffusion visait le mouvement des particles en état stationnaire et très peu d'importance était accordée aux phénomènes transitoires. Nous proposons un modèle d'énumération exacte pour l'étude de la diffusion à temps court des particules en trois dimensions.

Statement of Originality

The work presented in this thesis is, to the best of my knowledge, new and original. It is my own work except for section 2.3 where I recapitulate an existing model published by the group of G.W. Slater over the last 8 years. All theoretical advances presented in this thesis derive from my own work with the helpful guidance of my supervisor. All analytical and numerical results shown herein have been realized through my own Maple IV and Fortran 77 codes.

Additionally, most results contained in chapters 2-6 have been published in the following article:

- J. Boileau and G.W. Slater, "An exactly solvable Ogston model of gel electrophoresis VI: Towards a theory for macromolecules", *Electrophoresis*, volume 22, pp. 673-683 (2001).

Furthermore, I had the opportunity to present my results at the following meetings:

- J. Boileau and G.W. Slater, "A lattice model of gel electrophoresis: A theory towards macromolecules", Poster presentation at the *Annual meeting of the Canadian Association of Physicists (CAP)*, June 2000, Toronto.
- J. Boileau and G.W. Slater, "A lattice model of gel electrophoresis", Oral presentation at the semi-annual graduate student seminars of the *Ottawa-Carleton Institute for Physics (OCIP),* May 2000, Ottawa.

Finally, I also had the opportunity to participate in a review article written jointly by the group of G. W. Slater:

- Gary W. Slater, Claude Desruisseaux, Sylvain J. Hubert, Jean-François Mercier, Josée Labrie, Justin Boileau, Frédéric Tessier, Marc P. Pépin, Theory of DNA electrophoresis: A look at some current challenges, *Electrophoresis*, volume 21, pp. 3873-3887 (2000).

Acknowledgements

I would first like to thank my supervisor Dr. Gary W. Slater. His constant devotion to the sciences, his continuous support and generous commitment of time have been key factors towards the completion of my Masters degree. You have greatly enriched my commitment to learning and been an inspiration that I can carry forward for the rest of my life.

I would also like to thank Jean-François Mercier whose previous work and helpful discussions has been a tremendous asset to the completion of this project. Thank you Jean-François.

To Frederic Tessier I also give my heartfelt thanks for his help in both theoretical and computational matters. Your experience and guidance have greatly enhanced the quality of this work.

To the Department of Physics, both the support and research staff for their kindness and devotion towards a productive research environment.

Lastly, but certainly not least, I would like to extend my gratitude to my wife, Crystal Boileau, who has supported and encouraged my throughout. Your persistence, support and faith in me have allowed me to bring this project to fruition. Thank you for believing in me, I could not have done it without you.

Table of Contents

List of Figures

List of Tables

PART I

Chapter 1

Introduction

The movement of particles and small molecules, including polymers, in viscous and porous media, has been a topic of considerable interest for many years. The study of diffusion has helped us to understand many phenomena in chemistry, biology and physics, ranging from the movement of molecules along cell membranes to protein folding. These models have also helped to understand the dynamics of molecules in the presence of a driving field, which has led to the development of sieving devices (e.g. capillary electrophoresis[1,2], ratchet-like devices[3] and even DNA prisms[4]) used to separate DNA molecules in support of the Human Genome Project. It is realistically a field of limitless application and deserves all the attention that can be spared to it.

To study these problems, models have been developed such as the Lattice Monte Carlo (LMC) and the Ogston-Morris-Rodbard-Chrambach (OMRC) models[5-7]. The OMRC model is a mean field theory designed to study the movement of charged particles in a liquid in the presence of an electric field, often referred to as electrophoresis. The LMC model exploits the Brownian or random motion of particles along the framework of a lattice to study static and dynamic properties of molecules. This thesis is divided in two mutually exclusive parts. The first section deals with a model developed by Slater et al.[8-13] designed to find numerically exact diffusion coefficients of particles both in a good solvent and within a lattice of steric obstacles. In my work, the model was improved to

include small polymers in those same conditions. Our study of this new model deals with the free diffusion of oligomers, reptation problems, and finally entropic trapping devices. The second part develops a numerical model which studies the short-time anomalous diffusion of particles in various media. The short time dynamics of particles is a sub-field of statistical physics that has not received much attention and deserves to be studied more extensively in order to understand how a molecule reaches a state of steady movement in its environment.

1.1 Introduction to Polymer physics

Polymers are fascinating molecules that are applied and fabricated for virtually all our day-to-day activities. The diversity with which polymers are used these days is truly staggering. This section will give the reader enough background information on polymer physics to allow navigation through this thesis without a great deal of previous expertise in the field. We will begin by defining polymers and briefly describe their relevant static and dynamic properties.

What is a polymer? From the most general point of view, any plastics or rubbers are considered polymers. Your glasses are likely made of polymers. The "ink" on this page is a polymer. From a scientific point of view the actual definition of a polymer may well depend on whom you ask. A mathematician will tell you that it is a molecule whose form is depicted as a random walk. A chemist will say that a polymer is a series of identical molecules that are covalently bonded to form long chains. A physicist may compare polymers with a fluid containing fewer degrees of freedom. While these descriptions are essentially valid, they each provide only a portion of the answer to our question. By taking each perspective into consideration, we achieve a better understanding of what a polymer is.

So what makes the study of polymers so attractive? Firstly, polymers can both be fabricated or found in nature. DNA molecules, for example, are considered polymers. Secondly, dilute solutions of polymers can be seen as liquids whose molecules are not strongly correlated to their neighbours. This makes their study far easier than a normal fluid. For example, since polymers are strongly bonded in long chains, the shape of individual monomers becomes unimportant on long time scales. In simple fluids,

geometrical effect associated with the shape of the molecules strongly affects the behaviour. With polymers, the knowledge of just a few properties such as stiffness and size allow us to accurately discern many thermodynamic properties. This inherent simplicity is exploited to develop applications for use in industry. Let's discuss some of the properties polymers possess that we can study.

The number of monomers (M) forming a polymer molecule ranges from just a few monomers (we then talk about oligomers) to over one million monomers. Typically, the topology of a polymer is linear but the definition has lately been loosened to include ring and branched polymers to name but a few. The monomers need not be identical molecular subunits. A DNA molecule is considered a polymer with 4 different types of monomer units that coalesce into a very specific structure (double helix). Polymers whose monomers are identical are termed homopolymers while a polymer that has at least 2 different monomers is called a heteropolymer.

The shape of a polymer molecule is the first step in understanding its behaviour. The typical conformation of a linear polymer is much like a random walk, each monomer positioned randomly in sequence. Several models were developed to study the shape and size of linear polymers such as the freely jointed chain[14]. These models mirror the concept that a polymer is shaped using random walk statistics but fail to account for the physical dimensions of the individual monomers. This is known as the excluded volume effect. Simply put, a monomer cannot occupy the same physical space as another monomer. Taking the excluded volume into account will cause the molecule or conformation to be larger than predicted by random walk models. This is called the 'swelling' of the polymer chain.

There are two popular properties by which the spatial size of a polymer is characterized. The first is the mean end-to-end distance $\langle h^2 \rangle$, where $\vec{h}$ is simply the (vector) distance between the first and last monomer and the brackets depict an ensemble average. Another method is the molecule's mean radius of gyration $\langle R_g^2 \rangle$, which is an average of every monomers' square distance from the polymers' centre of mass (CM), mathematically defined by[14]:

$$\left\langle R_g{}^2 \right\rangle = \frac{1}{M}\sum_{i=1}^{M}\left\langle \left(\vec{R}_i - \vec{R}_{CM}\right)^2 \right\rangle \tag{1.1}$$

where $\vec{R}_i$ and $\vec{R}_{CM}$ are the position of the i-th monomer and the position of the polymer's centre of mass, respectively. The values of $\left\langle R_g{}^2 \right\rangle$ and $\left\langle h^2 \right\rangle$ will be a function of the number and size of monomers and the stiffness imposed by the chemical bonds between them.

Another aspect that we will study in this paper is the diffusion of polymers. To understand how a polymer diffuses it would be useful to describe the displacement of a single particle. The diffusion equation in one-dimension provides an excellent starting point:

$$\frac{\partial}{\partial t}P(x,t) = D_o \frac{\partial^2}{\partial x^2}P(x,t) \tag{1.2}$$

where P(x,t) denotes the probability of a particle being at position x at time t and D_o is the diffusion constant. Solving this linear differential equation we obtain the first two moments of the distribution function P(x,t)[15]:

$$\begin{aligned} \langle x \rangle &= 0 \\ \langle x^2 \rangle &= 2D_o t \end{aligned} \tag{1.3}$$

where $\langle x^2 \rangle$ is termed the mean square displacement. In $d \geq 1$ dimensions, the solution is easily extrapolated to:

$$\langle r^2(t) \rangle = 2dD_o t \tag{1.4}$$

Eq (1.4) can be reordered to provide an expression for the diffusion constant:

$$D_o = \frac{\langle r^2(t) \rangle}{2dt} \tag{1.5}$$

This last expression defines the diffusion constant whether we are describing the motion of a single particle or the centre of mass (CM) motion of a larger molecule (including polymers). However, because one often observes transient effect for short times, it is common to replace this relationship by:

$$D_o = \frac{1}{2d}\lim_{t\to\infty}\frac{\langle r^2(t) \rangle}{t} \tag{1.5'}$$

It is logical that the mean square displacement of a polymer molecule will be quite different than that of a single particle. While eq (1.5) provides a universal definition of the diffusion constant, the value of $\langle r^2(t) \rangle$ will be a function of the molecule being studied. The Rouse model[14] was developed to describe the dynamics of a polymer molecule in solution. It is a bead-spring model that replaces solvent interactions with a friction force, ξ and simulates the movement of the monomers using a stochastic force f_{sto}. The model considers neither hydrodynamic interactions nor the excluded volume effect. The resulting equation of motion is called the Langevin equation and it can be solved using simple mathematics. The Rouse model predicts that the mean square displacement $\langle r^2(t) \rangle$ of the molecule's CM is:

$$\langle r^2(t) \rangle = 2d \frac{k_B T}{M\zeta} t \tag{1.6}$$

where k_B is Boltzmann's constant, T is the temperature, ξ is the friction coefficient of one monomer and M is the number of monomers. Substituting with eq (1.5) we have for the free solution diffusion constant:

$$D_o = \frac{k_B T}{M\zeta} \tag{1.7}$$

or,

$$D_o \propto M^{-1} \tag{1.8}$$

This model does not correspond well to experimental results since hydrodynamic interactions are not taken into consideration. Nevertheless, the Rouse model is still very important and has served as the basis of numerous theoretical investigations of polymer dynamics in solutions[14]. Since our model also disregards hydrodynamic interactions, we will be using the Rouse predictions to test our model's validity. It is also important to note that the Rouse model was intended for very long chains where the end effects imposed by the first and last monomers can be neglected.

Of course, polymer dynamics may deviate from Rouse predictions depending on the environment. For example, in a polymer melt, linear polymers will typically diffuse along their backbone. Because of the high density of polymers, transverse diffusion is inhibited. This type of movement is dubbed reptation and the restriction imposed on the

polymers' degree of freedom will of course decrease the diffusion coefficient of the polymer. The diffusion coefficient of a polymer chain undergoing reptation[14] scales to the order of: $D \sim 1/M^2$. Another example of an environment affecting diffusion is a polymer chain inside a gel. Polymers and particles alike may then exhibit anomalous diffusion due to the disordered nature of the gel-like structure. In other words, molecular displacement may scale as: $\langle r^2 \rangle \propto t^{\beta}$, where $\beta<1$, which does not correspond to normal diffusion. It is often believed that the "anomalous" diffusion of particles in gels is due to the fractal nature of the gel although there are no firm indications that the gels are indeed fractal[16]. A safer statement would be that the anomalous diffusion of molecules is linked with the level of disorder in the gel. The disorder will cause the chain to be trapped in certain areas and flow freely where there is more available free volume. These are but 2 common examples of situations where the diffusion of molecules may not correspond to Rouse dynamics. Since molecules invariably diffuse in non-homogeneous solutions, these special cases are truly relevant.

It is quite astounding that with these simple concepts of polymers such as shape and movement, described using only basic mathematics and physics, we can predict the behaviour of polymers in very complex systems. These basic building blocks will allow a better comprehension throughout this work. The next 2 sections describe the computational work that was historically accomplished to determine the behaviour of polymers in quenched disordered systems.

1.2 Molecular Dynamics Simulations

Before getting too far ahead of ourselves, let's examine how the study of the movement of particles began. By following through some historical notions we can gain a better appreciation of how our work becomes a stepping stone towards the modelling of more realistic systems. Brownian motion is the apparent random movement of particles associated with the bombardment of a molecule with neighbouring particles. Early in the 20th century, Einstein formalised the concept by using statistical arguments and introducing the random walk problem. The diffusion of particles has since been modeled and observed as random walks. With the advent of computers, algorithms were developed to study molecules by simulating their collective random motion. Thus the

study of Molecular Dynamics began. Although useful in theory, Molecular Dynamics simulations require a large commitment of time and processing power. The proper simulation of molecules requires several interactions to be considered simultaneously and it can become very time consuming for a molecule to cover enough of phase space to properly discern thermodynamic properties. It may thus become important to simplify the models in a manner which do not compromise the physical behaviour of the system. Randomly moving molecules along a lattice is a popular alternative to Molecular Dynamics simulation. The Lattice Monte Carlo (LMC) algorithm is such an example. This model simulates the movement of particles by making random jumps along the framework of a lattice. The fact that the molecule is constrained in its movement by a lattice allows the molecule to easily cover its phase space without undermining physical properties. In other words, we generally retain the proper dynamics and thermodynamic properties while greatly reducing the number of molecular degrees of freedom. The only problem with LMC methods is that the fluid, which would be treated explicitly in Molecular Dynamics simulations, is now replaced by stochastic rules. Consequently, the precision becomes dependent upon the duration of the simulation, and collective fluid effects (e.g. hydrodynamics) do not exist. Moreover, we rarely achieve a precision of greater than 0.1%, which somewhat limits its scope of applicability.

Analytical models have also been developed as alternatives to allow researchers to quickly and efficiently predict the approximate behaviour of molecules in given systems. For a long time, the OMRC model (see Section 1.4) was considered one of the leading methods for predicting the mobility of small molecules during gel electrophoresis.

1.3. Electrophoresis

Electrophoresis is the study of the movement of charged particles immersed in a liquid and subjected to an electric field. Much of the human genome project relied on electrophoresis for the separation of DNA fragments[2]. Many sub-fields have been developed for the electrophoretic separation of molecules. One such field is gel electrophoresis. Molecules are immersed in a gel to counter electro-osmotic flow and convection in the fluid. This causes the motion of the molecules to rely solely on the electric force and their natural diffusion. The gel is usually a solution of cross-linked

polymers, like agarose, and molecular species are separated according to their size since larger molecules collide more frequently with the gel and take longer to elute. Another subfield is capillary gel electrophoresis[2] where molecules are injected in a gel-filled capillary and then separated. This offers a cheaper and faster alternative for the separation of molecular (or ionic) species. Although this thesis investigates the electrophoretic mobility of analytes, our analysis will be limited to very weak applied fields. In this limit, the mobility is directly proportional to the diffusion coefficient; therefore, our results are equally valid for the study of standard (zero-field) diffusion problems.

1.4 The Ogston or OMRC Model

The OMRC model, commonly referred to as the Ogston model, was first developed to explain the sieving effect of the gel on the electrophoretic mobility of small analytes[5,6,17,18]. The model was used to predict the electrophoretic mobility of charged particles in inhomogeneous media such as agarose gels. These cross-linked gels offer a sieving effect because larger molecules tend to collide more frequently with the gel fibres thus impeding their motion. The typical quantity sought in electrophoresis experiments is the mobility μ, defined as the drift velocity acquired by a particle divided by the magnitude of the applied external field. This model links the electrophoretic mobility of a solute with the volume available to it:

$$\mu^*(C) = \frac{\mu(C)}{\mu_0} = F(C) \tag{1.9}$$

where C is the concentration, $\mu^*(C)$ is the scaled mobility, $\mu(C)$ is the mobility, μ_o is the mobility of the particle in the absence of a gel (C=0), and F(C) is the fraction of the total gel volume available to the particle. The fraction $\mu(C)/\mu_o$ is called the scaled mobility (μ^*) which is a useful quantity to isolate the effect of obstacles for a given system.

The Ogston model became so widely accepted that much effort was devoted to finding the fractional available volume F(C). Ogston showed that F(C) for a spherical particle in an array of randomly oriented fibres is given by an exponential function whose only parameters are the size of the solute and gel fibres respectively. Indeed, the model (apparently) correlated rather well to experiments using small molecules in randomly

arranged gels of low concentrations (far from the percolation limit). The simplicity of the model was so attractive that molecular architecture even disappeared from the models. It wasn't until recently[10,11,19,20] that the Ogston model was challenged for its apparent lacunae. The OMRC model [5-7,13,17,18,21], shown to be equivalent to a mean field theory, fails to consider the finer details of molecular interactions and trajectories. Unfortunately, this model was never successfully verified using experimental measurements due to the difficulty in measuring the scaled mobility $\mu^*(C)$ and the available volume F(C) independently.

The first part of this thesis (chapters 1 through 6) will put the OMRC model to a continued test (since it was initially tested using rigid isotropic analytes). Of particular importance is the fact that the OMRC model is still used quite extensively to analyze the mobility of short polymers. This may appear a little counter-intuitive because the OMRC model was designed for spherical and rigid molecules whereas a polymer is defined by a linear sequence of like molecules that are covalently bonded. The reason for the apparent validity of the OMRC model as applied to linear polymer molecules is because the shape of a polymer appears to follow a random walk and the final average shape of the polymer is more or less spherical in situations where gel concentrations are very low. Therefore, for the purpose of the OMRC model, the polymer is often modelled as a spherical molecule whose size is given by its radius of gyration, R_g, which is essentially a reasonably valid mean field statement.

The fact remains that the Ogston model is still a mean field approximation that disregards molecular details and the measure of disorder in a gel when predicting the electrophoretic mobility of the molecule. We shall later demonstrate how both of these factors can play a crucial role in the diffusion of molecules.

1.5 Presentation of the Thesis

As mentioned before, this thesis is divided in two separate parts. The first part studies the electrophoretic mobility of small oligomers in a vanishing electric field and is subdivided as follows: Chapter 2 introduces the original model and reveals how we improved the model to include molecular degrees of freedom. Chapter 3 presents and discusses our results for the mobility of linear polymers in 1 dimension (1D). Chapter 4

extends our analysis to the study of polymers in 2D without the presence of obstacles. Chapter 5 discusses the mobility of analytes in the presence of obstacles and finally, Chapter 6 contains a discussion of the results obtained thus far. In chapter 7 we introduce the second part of the thesis. We present a model for the study of the short time anomalous biased diffusion of a single particle. We use an enumerative method to analyse the progression of the diffusion constant towards the steady state regime. We start by introducing theoretical concepts followed by a short introduction to the model. We then utilize simple systems to validate the model before progressing to more complex systems whose diffusive behaviour has been difficult to ascertain.

Chapter 2

Numerically Exact Diffusion Coefficients and Electrophoretic Mobilities

2.1. Introduction

Over the last few years, a new mathematical model was put forward to compute the exact diffusion coefficients of rigid isotropic particles in various media[8-13]. This model neglected hydrodynamic interactions and intra-molecular degrees of freedom but was nevertheless an invaluable tool for the study of diffusion in porous media and provided insight into the future possibilities of this field. Although it was extremely useful for the study of point particles, it was unable to deal with certain important problems. Amongst these are the diffusion and electrophoresis of rod-like molecules (viruses, short dsDNA fragments, etc.), the dynamics of molecules of identical weight but with differing architecture, the migration of soft globules or vesicles and the effects of conformational entropy during electrophoresis. In this thesis we present a generalized version of the model which includes intra-molecular degrees of freedom. This will give us the opportunity to increase the scope of our study and gain a better understanding of the basic principles governing the dynamics of polymers.

The purpose of this chapter is to present the model that will be used to study the properties of small molecules. Since we are presenting an improvement to an existing model developed by the group of Gary W. Slater, it will be necessary to first present the original model. In section 2.2 we will discuss in general terms the diffusion constant and the mobility of a particle in the presence of a weak electric field. We will also describe how these concepts are applied when using a lattice model. In section 2.3 we will discuss

the lattice description that will be used to describe the molecules. The original model will be presented in section 2.4. This will establish a theoretical foothold that will be necessary to understand the generalization of the model. Sections 2.5 and 2.6 present the improved model. We will discuss the necessary changes to the original model necessary to accomplish the generalization. This new model will allow us to include, for the first time, intra-molecular degrees of freedom in the electrophoretic study of molecules and will permit us to study many more problems that were not within its original scope.

2.2. Free Diffusion and Drift on a Lattice

We first examine the movement of a particle in a free solution (no obstacles). The free solution electrophoretic mobility μ_o of an analyte is defined by the ratio of its electrophoretic velocity v to the electric field E[15]:

$$\mu_o = \frac{v}{E} \tag{2.1}$$

Typically, the mobility is defined by μ=v/F. Since we are dealing with the steady state motion of the particle, the acceleration becomes zero and the mobility is defined by its terminal averaged velocity, hence μ= v/E.[15] In the absence of a driving force, the spatial fluctuations of a particle of size R result from its thermal motion and the friction coefficient f(R) resulting from the fluid's viscosity. We then have a general expression for the free solution diffusion constant D_o:[22]

$$D_o = \frac{k_B T}{f(R)} \tag{2.2}$$

The mean drift velocity in the presence of a driving force is given by the ratio of the applied external force F_{ext} to the friction coefficient f(R):[22]

$$v = \frac{F_{ext}}{f(R)} \tag{2.3}$$

In the special case where the external force is an electric field we have:

$$v = \frac{QE}{f(R)} \tag{2.4}$$

where Q is the charge of the particle. Combining eqs (2.1), (2.2) and (2.4) we have:

$$D_o = \frac{k_B T}{Q} \mu_o \tag{2.5}$$

otherwise known as the Nerst-Einstein relation. The latter links the mobility μ_o with the diffusion constant D_o. This relation is generally valid only for low field intensities.

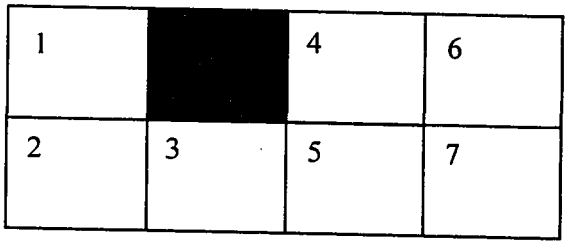

Figure 2.1: Conceptual drawing of the lattice model. The obstacle on the lattice is depicted by the black square. The physical dimensions the individual lattice sites is a x a. The available lattice sites are numbered 1 to 7. We use periodic boundary conditions along both Cartesian axes.

The lattice model used to describe the motion of a single particle is depicted in Figure 2.1. The particle can be located on any of the 7 numbered lattice sites and its size coincides with the dimensions of the lattice sites (a x a). The Brownian time step associated with each move is given by:

$$\tau_B = \frac{a^2}{2D_o} \tag{2.6}$$

where D_o is the diffusion constant in free solution given by eq 2.2.

To define the probabilities associated with the discretized movement of particles we will be using an approach developed by Slater and Rousseau[23]. This approach, which is reminiscent of the Glauber[24] approach, is summarized as follows:

Given a system of one charged particle in one dimension, the probability of jumping in the ± x-direction in the presence of an electric field is given by:

$$p_{\pm x} = \frac{e^{\pm\varepsilon}}{e^{+\varepsilon} + e^{-\varepsilon}} \cong \frac{1}{2}\left(1 \pm \varepsilon + O\left(\varepsilon^3\right)\right) \tag{2.7}$$

where ε is the scaled dimensionless value of the electric field given by:

$$\varepsilon = \frac{QEa}{k_B T} \tag{2.8}$$

where Q is the charge of the particle. This probability function allows us to increase the probability of movement in the +x direction and decrease it proportionally in the –x-direction such that the normalization condition: ($p_{+x}+p_{-x}=1$) is still satisfied. The time

step associated with these jumps is thus also changed by the presence of an external electric field:[25]

$$\tau = \frac{\tanh(\varepsilon)}{\varepsilon}\tau_B \tag{2.9}$$

or, we can use a dimensionless value of time, defined by:

$$\tau^* = \frac{\tau}{\tau_B} = \frac{\tanh(\varepsilon)}{\varepsilon} \tag{2.10}$$

For $\varepsilon << 1$ we can expand eq (2.10):

$$\tau^* \approx 1 - \frac{\varepsilon^2}{3} + O(\varepsilon^4) \tag{2.11}$$

This expansion is of particular importance since it will allow us to simplify the problem. Note that while the time step, τ^*, is a function of the applied electric field, eq (2.11) reveals that the time step is not perturbed to the first order of ε. This means that the jumps will be evenly distributed in time regardless of the direction of movement as long as the second order term of the scaled electric field remains negligeable. We can also make use of a dimensionless expression for the velocity:

$$\upsilon = \frac{v\tau_B}{a} \tag{2.12}$$

Using eq (2.10) we can derive a dimensionless expression for the velocity of our particle in terms of probabilities:

$$\upsilon = \frac{p_{+x} - p_{-x}}{\tau} \times \frac{\tau_B}{a} = \frac{e^{+\varepsilon} - e^{-\varepsilon}}{\tau\left(e^{+\varepsilon} + e^{-\varepsilon}\right)} \times \frac{\tau_B}{a} = \frac{\tanh(\varepsilon)}{\tanh(\varepsilon)/\varepsilon} = \varepsilon \tag{2.13}$$

Combining (2.13) and eq (2.8) we have a dimensionless expression for zero-field mobility of a molecule:

$$\mu_o = \lim_{\varepsilon \to 0} \frac{\upsilon}{\varepsilon} = 1. \tag{2.14}$$

Using eq (1.9) and the Nerst-Einstein relation (eq 2.5) we can relate the scaled values of the mobility and the diffusion constant of our particle:

$$\mu^* = \frac{\mu}{\mu_o} = \frac{D}{D_o} = D^* \tag{2.15}$$

Note again that this is generally valid only in the $\varepsilon \to 0$ limit. Defining these scaled quantities is a useful tool by which we can isolate the effect of obstacles on the mobility

and diffusion constants. It can also then be claimed that this model is appropriate for the study of the zero field diffusion of particles in gels.

Finally, extending our analysis to 2 dimensions and in the limit of small ε we have:

$$p_{\pm x} = \frac{1}{d}\frac{1}{1+e^{\mp 2\varepsilon}} \approx \frac{1 \pm \varepsilon}{4} + O(\varepsilon^3) \qquad p_{\pm y} = \frac{1}{2d} = \frac{1}{4} \tag{2.16}$$

where d=2 is the dimensionality.

By now, it has become quite clear that we plan on conducting a dimensionless analysis of results. This approach allows us to apply our results to a plethora of polymer systems without having to consider the finer details of a specific polymer system such as stiffness and individual monomer composition. Consequently, a dimensionless analysis is more conducive to our goals. Unfortunately, it is also useful to give experimentalists an idea of how our results can be applied in practice. We will now offer an approximate analysis of how our results would compare to experimental results by relating the length and time scales associated with our lattice system.

By linking the contour length $L_c = (M-1)b_o$ of a polymer chain (where M is the number of monomers and b_o~2.89 from the BFM) with the persistence length $L_p = h^2/2L_c$ (where h^2=(M-1)b^2) we have: l_p~5 lattice spacings would be a reasonable value. Given that the persistence length of a double stranded DNA is 53nm with each base pair measuring bp~0.38 nm, we have 1 lattice site=30bp~10nm. From here we can compute the relaxation time through the molecules' radius of gyration and diffusion constant through the relations[14]:

$$D = k_B T / 6\pi\eta R_g$$
$$D = R_g^2 / 4\tau \tag{2.17}$$

Isolating for τ we have: $\tau = 6\pi\eta R_g^3 / 4k_B$ ~10μsec (using typical values of the solution viscosity and radius of gyration). Linking the relaxation time with the number of Monte Carlo Steps (MCS)[29] we can compute the time step for each MCS. We then arrive at an approximate solution of τ~1/4 μsec.

2.3. Lattice Model of Gel Electrophoresis

This section describes the original lattice model of Slater and co-workers. For a more complete overview of the model along with detailed examples refer to [8-13,21]. Now that we have defined the probabilities associated with the movement of a particle and the appropriate dimensionless quantities, we can proceed to explain the details of the lattice model. Referring once again to Figure 2.1 we see a lattice in two-dimensions containing S=7 available sites which are numbered for clarity. In this lattice model, we will be using periodic boundary conditions (PBC). Referring to the lattice system in Figure 2.1, a particle moving from site number 7 in the +x direction would reappear at site 2. Likewise, a particle at site 3 moving in the ±y direction would remain at site 3 due to the obstacle depicted by the blackened square. Using PBC, we can simulate an infinite volume in which the particle can evolve.

As mentioned, any such lattice will have S available sites in which the particle can be legally placed (ie: a site which does not have an obstacle). To find the mobility of the particle in our lattice system we will rewrite eq (2.14) and (2.15) to correspond more appropriately to our lattice system:

$$D^* = \mu^* = \lim_{\varepsilon \to 0} \frac{\langle v|n\rangle}{\mu_o \varepsilon} \tag{2.18}$$

where $|n\rangle$ is the vector whose elements n_i correspond to the probability of the particle being located at site i=1..S in the steady-state. $\langle v|$ is the vector whose elements v_i correspond with the particle's velocity while located at site i=1..S in the steady-state. Note that we use Dirac notation in this work: bras and kets represent Row and Column vectors ($|n\rangle$ and $\langle n|$), while uppercase and lower case letters depict matrices and scalars respectively. The rationale behind eq (2.18) is that the presence of an external field will create anisotropy in the system causing the probability of occupation of the particle to be a function of its position (i) within the lattice. Equation 2.18 is simply the weighted average over all sites.

Using eq (2.16) for the probabilities we can write linear equations of motion corresponding to the probability of a particle being located on a lattice cell. Generally, we have for $n_{\{x,y\}}(t+1)$:

$$n_{\{x,y\}}(t+1) = p_{\rightarrow} n_{\{x-1,y\}}(t) + p_{\leftarrow} n_{\{x+1,y\}}(t) + p_{\uparrow} n_{\{x,y-1\}}(t) + p_{\downarrow} n_{\{x,y+1\}}(t) \tag{2.19}$$

As an example, for the lattice shown in Figure 2.1 we have for $n_1(t+1)$:

$$n_1(t+1) = p_{\rightarrow} n_1(t) + p_{\uparrow} n_2(t) + p_{\rightarrow} n_6(t) \tag{2.20}$$

A similar equation can be written for the six other sites. We can rewrite the system of equations to include all 7 equations as:

$$T|n(t)\rangle = |n(t+1)\rangle \tag{2.21}$$

where T is an SxS transition matrix whose elements denote the transition probabilities from one system state to the next and $|n(t)\rangle = \{n_1(t), n_2(t), ..., n_7(t)\}$ is the probability vector. Given that we are dealing with the steady state solution of the mobility we have:

$$|n(t)\rangle = |n(t+1)\rangle \tag{2.22}$$

meaning that we can re-write eq (2.20) as:

$$T|n(t)\rangle = |n(t)\rangle \tag{2.23}$$

and, by factoring we obtain,

$$(T - I)|n\rangle = |0\rangle \tag{2.24}$$

where I is the Identity matrix and $|0\rangle$ is the null vector.

Before we can solve the system of equations shown in Eq (2.24) we must acknowledge that eq (2.24) has only (S-1) independent equations. We must then impose a normalization condition. Replacing the last row (by convention) of the matrix T with

$$\sum_i n_i = 1 \tag{2.25}$$

accounts for the fact that the sum of all probabilities is always 1. Equation (2.24) then becomes:

$$A|n\rangle = |b\rangle \tag{2.26}$$

where $|b\rangle$ = {0, ... , 1} and A is the matrix modified by including a normalization condition to the transition matrix T.

Recall that to find the mobility of the particle we had to link the particle's velocity with the local probability (eq. 2.16). The velocity of the particle is defined quite simply. We have for the components v_i of $\langle v|$:

$$\upsilon_i = p_{\rightarrow} L_{\rightarrow} - p_{\leftarrow} L_{\leftarrow} \tag{2.27}$$

where the probabilities $p_{\{\rightarrow,\leftarrow\}}$ are defined by eq (2.16) and $L_{\{\rightarrow,\leftarrow\}} = 0$ if the jump is illegal and $L_{\{\rightarrow,\leftarrow\}}=1$ is the jump is accepted.

Using eq (2.25) to find probability vector $|n\rangle$ and eq (2.27) to define the velocity vector $\langle\upsilon|$ we have all that we need to find the particle's mean mobility. The only remaining issue is that the probability and mobility equations are a function of the, as yet undefined, parameter ε. To circumvent having to define a specific numerical value to the scaled electric field, ε, we use a useful algebraic simplification. Writing each mathematical object A, $|n\rangle$ and $|v\rangle$ as the sum of field-independent and (first order) field-dependent terms we have:

$$A = A_I + \varepsilon A_\varepsilon \tag{2.28}$$

$$|n\rangle = |n_I\rangle + \varepsilon |n_\varepsilon\rangle \tag{2.29}$$

$$|\upsilon\rangle = |\upsilon_I\rangle + \varepsilon |\upsilon_\varepsilon\rangle \tag{2.30}$$

Replacing eq (2.28) and (2.29) into eq (2.26) we have:

$$A_I|n_I\rangle + \varepsilon\left(A_I|n_\varepsilon\rangle + A_\varepsilon|n_I\rangle\right) + \varepsilon^2 A_\varepsilon|n_\varepsilon\rangle = |b_I\rangle \tag{2.31}$$

To first order in ε we are reduced to 2 equations:

$$A_I|n_I\rangle = |b_I\rangle \tag{2.32}$$

$$A_I|n_\varepsilon\rangle = -A_\varepsilon|n_I\rangle \tag{2.33}$$

The first of the two equations shown above corresponds to the trivial case without the presence of applied electric field and leads to the homogeneous solution $n_i = 1/S$. Equation (2.33) deals with the non-trivial effect of fixed obstacles being introduced into the system in the presence of a driving force. The presence of obstacles removes the translation symmetry of the system effectively skewing the probabilities. Since A_I, A_ε, and n_I are all quantities that can be readily found without calculation we only need to solve for the vector $|n_\varepsilon\rangle$. With this in mind we will go over an identical simplification done in terms of the particle's velocity.

Clearly, the velocity of the particle must be a function of the particle's local probability of presence. Using eq (2.30) we have:

$$\begin{aligned} \upsilon = \langle \upsilon | n \rangle &= \left(\langle \upsilon_l | + \varepsilon \langle \upsilon_\varepsilon | \right) \cdot \left(| n_l \rangle + \varepsilon | n_\varepsilon \rangle \right) \\ &= \langle \upsilon_l | n_l \rangle + \varepsilon \left(\langle \upsilon_l | n_\varepsilon \rangle + \langle \upsilon_\varepsilon | n_l \rangle \right) + O(\varepsilon^2) \end{aligned} \tag{2.34}$$

The first term on the right hand side (RHS) of eq (2.34) is zero since it corresponds to the velocity in the absence of an applied electric field. Ignoring the term in ε^2 we are left with the term in ε^1. Finally, using eq (2.18) for the mobility and eq (2.15) the scaled mobility we have:

$$\mu^* = \frac{\left(\langle \upsilon_l | n_\varepsilon \rangle + \langle \upsilon_\varepsilon | n_l \rangle \right)}{\mu_o} = D^* \tag{2.35}$$

We see that the value of the low-field scaled mobility is no longer a function of the scaled electric field! Therefore, using this simplification, we do not have to declare any value of the scaled electric field to the first order. This simplification can only be used in the presence of a small electric field where second order terms can be neglected. A stronger field would force us to consider these second order terms and oblige us to reconsider using a uniform time step. References [8-13] provide a detailed derivation of these simplifications and provide useful examples.

So far in this chapter, we have introduced a model that can allow us to compute the electrophoretic mobility and the diffusion coefficient of a particle in a vanishing electric field. We have seen that, using a simple probabilistic approach, we can reduce this seemingly complex problem to solving a system of equations where each unknown corresponds to the probability of occupation of a lattice site. We also applied an algebraic simplification that relieved us of the responsibility of having to declare an arbitrary value of the applied electric field. In the following section I describe the rules governing the behaviour of polymeric molecules on a lattice. In other words, I will present that lattice description of my generalized model.

2.4 The Bond Fluctuation Model for Polymers

In section 2.3 we described the original model as it pertains to a particle evolving on the framework of a lattice. Our goal in this thesis is to generalize the model to include small flexible polymers and molecules. The first step towards this end is to provide a lattice description of the molecules studied. Several models for the simulation of polymers already exist. We require a model that properly simulates both the static and

dynamic properties of polymers. Additionally, we want a lattice description that allows for the simulation of both two and three-dimensional polymers. Finally, it is important that the model be able to study molecules that are not strictly linear. One of the goals of this project is to study ring and star polymers as well as linear polymers. It would be fruitless to compare results if we were obligated to use a different lattice description with different types of molecules. Despite our previous statement that any bond description could be used with this model our needs have greatly limited the number of descriptors which were deemed adequate for the purpose of this study.

The Bond Fluctuation Model (BFM)[26] was chosen to describe macromolecular dynamics in this thesis. This model was selected because it represents a self-avoiding walk and the simulation algorithm is ergodic in two and three dimensions. The model exhibits proper Rouse dynamics and the radius of gyration scales according to the Flory exponent in LMC simulations thus exhibiting proper static properties. Moreover, the variable bond length increases the 'realism' of the macromolecule being studied. Although initially devised with linear polymers in mind the BFM can be used to study other types of molecules such as ring and branched polymers. For completeness, the model will be briefly described. Refer to [26] for a more detailed description and analysis of this lattice model.

The BFM can be used in both 2 and 3 dimensional studies. The precept of the model is that the bond length between 2 connected monomers is variable. In 2 dimensions, a maximum bond length of less than $l=16^{1/2}$ was chosen between 2 connected monomers. This restriction was necessary to avoid bond cutting. Furthermore, the minimum distance between any two monomers is $l=2$. This fulfills our excluded volume requirement since this restriction ensures that 2 monomers do not occupy sites adjacent to one another. Figure 2.2 shows four two-dimensional systems based on the BFM. This model's high coordination number in two dimensions ($Z=36$, meaning that a second monomer can find itself bound to the first in 36 different positions) can be seen as a disadvantage because it will greatly limit the size of molecule that we will be able to study. Nevertheless, we chose this algorithm because of the realism it conveyed with regards to polymer dynamics and static polymer descriptions.

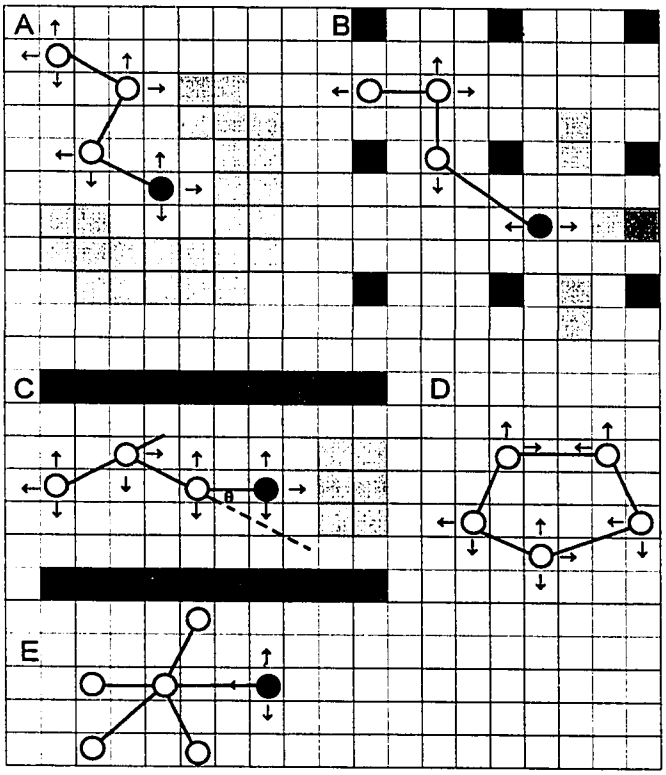

Figure 2.2: Four different two-dimensional systems based on the bond fluctuation model. Circles represent the monomers. Arrows show the possible moves of single monomer jumps, the blackened squares represent obstacles, and the shaded area in Figures 1A, 1B and 1C show the allowable positions of the next monomer in the chain following the monomer depicted by a filled circle. A) A free linear chain with M=4 monomers; B) The same chain in a lattice of periodic obstacles representing the densest gel. Obstacle plaquettes are placed periodically with lattice parameters Lx=Ly=4. We see that the obstacles follow the same excluded volume rules as depicted by the bond fluctuation model; C) A semi-rigid linear chain with M=4 monomers in a narrow tube. The angle θ between two consecutive bonds are restricted to $|\theta| \leq \pi/4$. D) A linked or circular chain is shown with M=5 monomers. E) A star polymer with all monomers linked to the centre and all branches have only 1 monomer.

The following section will introduce the generalized model.

2.5. The Generalized Model

As mentioned, the model discussed in section 2.3 can allow us to compute the exact diffusion coefficient of a particle evolving in an obstacle-laden environment. It has been demonstrated that using this model offers many advantages over the more traditional lattice Monte Carlo algorithms. In this section we will go over the fundamental changes that were necessary to allow for the study of small flexible molecules. Once we have developed the generalized model we will be able to study their static and dynamic properties. Our first challenge to generalize this model is to consider the conformational phase space of the molecule when enumerating the possible states of the system. Using the assumption that the molecular conformations and the position of the molecule are independent quantities will greatly simplify this task. In fact, given that the system is ergodic, there is no reason to believe that our assumption is false. The model introduced in section 2.3 enumerated the system states based on position alone. This

model will need to include the molecular conformation as well as the position when determining the states our molecule can have. Molecular states can then be viewed as possessing two "properties": The first is position and the second is conformation. The total number of states, S′, will then be a function of both of these properties and is given by:

$$S' = \sum_{k=1}^{S} F_k \tag{2.36A}$$

where S is the number of available sites and F_k is the total number of conformations allowable on site k. The quantity F_k is a function of the position of the molecule since interactions with obstacles will limit the allowable number of conformations. Section 2.6 discusses the exact procedure used to enumerate the possible states of the system. They would be named (k,C_i), where k is the position of monomer 1 and C_i is the conformation of the molecule. We then clearly have:

$$F_k = \sum L \tag{2.36B}$$

where the summation is over the total number of conformations and L=1 if the conformation C_i is legal for position k and zero otherwise.

When we presented the original model we discussed how the probabilities associated with a change of state is based on the Glauber approach. Specifically, eq (2.16) deals with the probabilities of transition when only 1 particle is used. Clearly, eq (2.16) is no longer applicable when we have more than one monomer to consider. To account for the added monomers we must redefine the way the transition is made. Since we define all monomers as being equally likely to make a move we define our probabilities to account for the fact that our molecule consists of M monomers:

$$P_{\leftarrow,\rightarrow} = \frac{1}{M} \cdot \frac{1 \pm \varepsilon}{2d} \tag{2.37}$$

$$P_{\uparrow,\downarrow} = \frac{1}{M} \cdot \frac{1}{2d} \tag{2.38}$$

The final step used to generalize the model is defining the velocity of the molecule. The original model used the simple relation shown in eq (2.27) to find particle velocities. Our first thoughts towards finding the molecular velocity were to use eq (2.27) and apply it to each particle in the molecule. Taking the subsequent average is an effective way to

ensure the proper velocity is found. Another method to find the molecular velocity was found which minimizes the computing time. We reasoned that taking a reference monomer would yield the same result since the reference monomer is restricted to following the centre of mass (CM) of the molecule. Our reasoning turned out to be correct (results not shown) and we will be choosing the first monomer of any molecule by convention when determining both the position and the mean velocity of the molecule.

2.6. Enumerating the Phase Space

Having discussed how the probabilities and the velocity equations were modified in the generalized model, we need only discuss how the enumeration of states is accomplished. We also discussed how the system states are defined using 2 properties: the position of the first monomer and the molecule's conformation. This system state is annotated: (k,C_i), where $k=(x,y)$ is the position of the molecule on the lattice and C_i represents the molecule's conformation.

Obviously, the two properties of the molecule must be considered simultaneously since the original model's focus was the determination of probabilities of transition from one state to the next. To find the probabilities of transition we need to enumerate all the possible states (k,C_i) of the system. We considered two strategies for finding these system states.

The first strategy used was to place the first monomer of the molecule in each available position, i, and then find all legal conformations keeping the reference particle in the same position. For example, consider a dimer in a lattice containing 2 available positions. The reference particle (#1 for example) is kept fixed on the lattice site while the second particle is moved around the first to find all conformations which would not violate monomer-monomer and monomer-obstacle interactions. Once this is done we move the reference particle in the second available site and repeat the procedure. In principle, once we have accomplished the procedure for all available positions, the system states have all been found and we can start building our transition matrix by linking one state to the next by using Monte Carlo moves. Once the transition matrix is built, the process of finding the electrophoretic mobility is done in the same manner as described in section 2.3.

Using this first strategy has certain disadvantages. The first is that building the transition matrix is a two-step process. The first step is the state finding process and the second is finding all transitions to build the transition matrix A. It would be more efficient if both these steps could be accomplished at the same time since this would greatly reduce the computing time of our simulations. The second disadvantage involves the manner in which system states are found. Since our conformation search is done independently of the determination of transitions, certain legal system states are not linked to any other legal conformation. In other words, all transitions made from this state lead to some form of violation making it an illegal system state. Consequently, all transitions are made unto itself. Physically speaking, the state would never be achieved by the system. This would violate the ergodicity of the lattice system studied. We only encountered such situations where the obstacle concentration is high and the number of monomers was greater than 3. Moreover, the existence of such a state will cause a singularity when solving the system of equations and must therefore be removed. Therefore, a second strategy for finding all system states and for building the transition matrix was needed.

The second strategy was specifically designed to ensure that all system states can be linked to a single initial state. We start with an established legal state defined by C(1,1) and start making Monte Carlo moves. We make the moves systematically to ensure each monomer is moved in each of the 2d Cartesian coordinates. Each time a legal move is made we note the system state and then update the transition matrix. Once we have made all possible moves from the first legal state we move to the second state and so forth. Gradually, the number of found states will grow. We will know that we have found all the legal conformations when there are no longer any conformations to investigate in our list which was methodically built from the first legal state. Using this strategy offers us the advantage of finding all legal states and building the transition matrix in one step.

The only difficulty with using the second strategy is that we have to manipulate the movement of our reference particle to ensure that it stays within the bounds of our lattice. Figure 2.3 shows how we accomplish this. The lattice shown in Figure 2.3 is two-dimensional which periodic obstacles. The greyed out area is the base lattice used and the remainder of the lattice is our depiction of periodic boundary conditions. The particle

pictured within this lattice is a trimer (depicted by circles). The reference monomer #1 is shown in grey. If a move of the reference monomer is made that will place it outside of the reference lattice we must move it to the other side of the lattice (shown in Figure 2.3B). Failing to ensure the reference monomer stays within the lattice will lead to an infinite number of states since the molecule is free to explore an infinite volume. However, it is permitted to have any other particle exit the reference lattice. Figure 2.3C shows what happens when we make a move that is not legal. In this case, the move shown in Figure 2.3B places the second particle to a position adjacent to an obstacle. Such a move is rejected on the basis of monomer-obstacle excluded volume interactions and the resulting transition is made to the original state. Mathematically speaking, the diagonal elements of our transition matrix would be updated as a transition made unto itself.

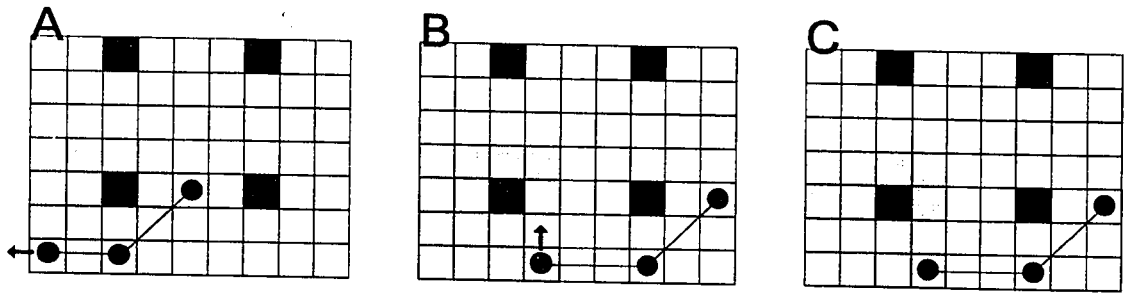

Figure 2.3: A trimer is shown in a lattice of periodic obstacles. The reference lattice is shown in grey. Obstacles are shown as black squares and the monomers are circles. The reference monomer is depicted by the grey circle. In Figure A we see the reference molecule being moved to a position outside the reference lattice. The resulting system state is shown in Figure B. We clearly see that the reference monomer has been moved to the other side of the reference lattice. From Figure B we move the reference monomer to a position that is adjacent to an obstacle. Since this is a transition to a state that violates monomer-obstacle excluded volume interactions, the resulting transition is then made back to the original system state, shown in Figure C.

The next chapter is devoted to the study of linear chains in 1 dimension. Chapter 4 is dedicated to the study of free polymeric molecules in 2 dimensions. Chapter 5 is the study of those same molecules in lattices where obstacles are present. Finally, we will be discussing the global results of this model in chapter 6 before undertaking another topic in chapter 7.

Chapter 3

Polymers in one dimension

A useful introduction to the diffusion of polymers is the problem of a polymer chain in one dimension. The purpose of the study of one-dimensional chains is to test the feasibility of this venue with the added benefit that the polymer chain can be viewed as a reptation problem (a polymer chain in a narrow tube). Since the constraints imposed in one dimension are not very realistic we did not expect true reptation behaviour but rather view this as a first step towards achieving better results. Moreover, a one-dimensional treatment of this problem serves us well in describing the model more thoroughly.

In this first example we start with a trimer (3 connected monomers) whose 4 available conformations are shown in Figure 3.1. Equation (2.16) provides the values of $P_{\leftarrow}$ and $P_{\rightarrow}$ respectively and n_i is the probability of the trimer being in conformation i in the steady state regime. The rules set forth in this problem for polymers are consistent with the Bond Fluctuation Model discussed in section 2.4. The minimum distance between monomers is 2 and the maximum distance is 3. In other words, we are forbidding the monomers from touching (excluded volume) and preventing them from getting too far thus maintaining the idea behind allowing variable bond lengths in the interest of realism and consistency. The transition matrix must now be compiled. For example, the transition equation corresponding to the first trimer conformation (Fig 3.1A) is given by:

$$n_A(t+1)=(2P_{\rightarrow} + 2P_{\leftarrow})n_A(t)+P_{\leftarrow}n_B(t)+P_{\rightarrow}n_C(t) + 0*n_D(t) \qquad (3.1)$$

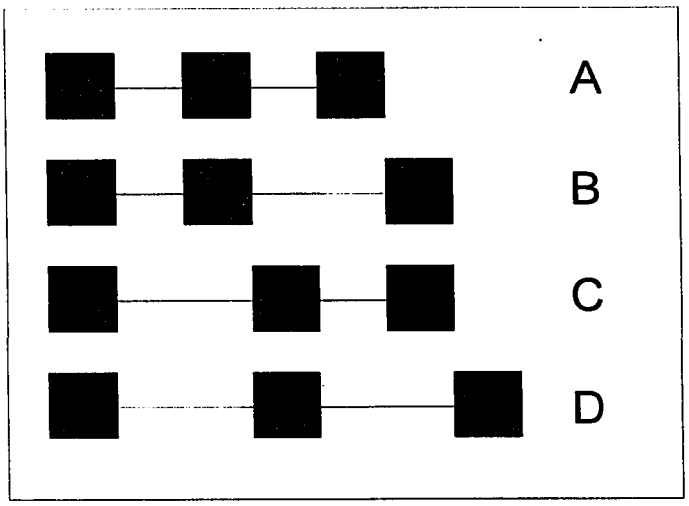

Figure 3.1: The different conformations of our one-dimensional trimer are shown. The bond lengths are restricted to sizes two and three. The conformational phase space has only 4 components.

We see from Figure 3.1 that, using a polymer containing 3 monomers, we have 6 possible moves in 1D (2 per monomer). We also see from the first term on the RHS of equation (3.1) that 4 moves from conformation A lead to an illegal polymer conformation. This is clearly seen in Figure 3.1A where the end monomers cannot move towards the centre monomer and the centre monomer cannot move at all since excluded volume interactions prevent such jumps. Note also that there is no direct path between conformations 1 and 4 because 2 moves are required to make that particular transition. Strictly speaking, this example does not include any obstacles. Our lattice description is then used for the purpose of finding molecular conformations only. As such, the system states are solely defined by the molecules' conformations. What we define as 'monomers' in Figure 3.1A are actually a coarse grain description of a polymer. We will be going over more precise physical parameters later. For the time being, it is sufficient to describe each lattice block as a predetermined number of monomers that will depend on the Kuhn length of the polymer. The Kuhn length is a measure of the polymers' stiffness.[14] That being said, we have a total of four conformations (ie: system states) and the complete 4x4 transition matrix is given by:

$$T = \begin{bmatrix} 4 & 1-\varepsilon & 1-\varepsilon & 0 \\ 1+\varepsilon & 3+\varepsilon & 1-\varepsilon & 1+\varepsilon \\ 1-\varepsilon & 1+\varepsilon & 3-\varepsilon & 1-\varepsilon \\ 0 & 1-\varepsilon & 1+\varepsilon & 4 \end{bmatrix} \tag{3.2}$$

To first order in ε, the normalized steady state solution to Eq (2.16) is then:

$$|n\rangle = |n_1\rangle + \varepsilon|n_\varepsilon\rangle = \begin{bmatrix} 1/4 \\ 1/4 \\ 1/4 \\ 1/4 \end{bmatrix} + \frac{\varepsilon}{8}\begin{bmatrix} 0 \\ 1 \\ -1 \\ 0 \end{bmatrix} \tag{3.3}$$

Separating the zero field and first order field dependent correction terms provides us with useful insight: in the absence of an electric field the system states are ergodic (equal probability). Our solution clearly indicates that the application of a small driving force effectively skews the probabilities making certain system states more probable than others. For example, state B is more likely than state C as shown by the second and third row of eq (3.3), respectively. Taking the first monomer as a reference for the velocity vector and using eq (2.27) we have:

$$\langle \upsilon| = \frac{1}{6}(-1,-1,1,1) + \frac{\varepsilon}{6}(1,1,1,1) \tag{3.4}$$

The electrophoretic mobility of a one-dimensional trimer is thus given by:

$$\mu = M \times \frac{\langle \upsilon|n\rangle}{\varepsilon} = M \times \frac{1}{8} = \frac{3}{8} \tag{3.5}$$

where the factor M (=3) comes from the fact that one Monte Carlo step (the unit of time here) actually consists of each monomer attempting a move or state transition (on average). We have solved this problem for larger oligomers in one-dimension and have deduced the general (exact) solution:

$$\mu(M) = \frac{1}{4} \times \left(1 + \frac{1}{M-1}\right), \quad M \geq 2 \tag{3.6}$$

We then see that large oligomers (ie: M→∞) are free draining, meaning that their mobility is size independent (μ→ ¼ as M→∞). The $1/(M-1)$ correction term is a finite-size factor due to the ends of the molecule. As mentioned, the Nerst-Einstein relation allows us to relate the zero field mobility to the diffusion coefficient[8-9]:

$$D = \frac{\mu}{M} \tag{3.7}$$

Using eq (3.7) we see that for large M, the diffusion coefficient is reduced to the well-known D~1/M Rouse scaling law for a free-draining polymer[14]. This gives us an indication of the validity of our method.

The concept of jump acceptance is a useful tool for making a distinction between model effects and the actual mobility or diffusion. The mobility of our 1D chain can be seen as the product of 2 terms:

$$\mu(M) = R(M) \times \mu_R(M) \tag{3.8}$$

where $\mu_R(M)$ is the intrinsic mobility. Equivalently, for the diffusion coefficient we would have:

$$D(M) = R(M) \times D_R(M) \tag{3.9}$$

where R(M) is the fraction of the possible jumps that were accepted and $\mu_R(M)$ (or $D_R(M)$) is the portion of the net mobility (diffusion) that is due to jump acceptance. Most finite-size and model-dependent effects are included in the R(M) factor while the fundamental aspects of chain dynamics are mostly restricted to the $\mu_R(M)$ (or D_R) factor. It can easily be shown that for our 1D chain we have,

$$R(M) = \frac{M+2}{4M}. \tag{3.10}$$

Consequently, the intrinsic mobility is given by:

$$\mu_R(M) = \frac{M^2}{(M-1)(M+2)}. \tag{3.11}$$

Figure 3.2 shows a plot of Eqs (3.6), (3.10) and (3.11). We see that as M goes from 2 to infinity the jump acceptance factor goes down from ½ to ¼ and the intrinsic mobility varies from 1 falls to a minimum at around $\mu_R(M) \sim 0.89$ (for M=4) and then slowly reverts to $\mu_R(M)=1$ for very large M. These results indicate that the mobility of a 1D analyte is highly correlated to the jump acceptance factor and, at the large M limit, it is constant (typical of a free-draining chain). The concept of jump acceptance will be revisited when discussing the same problem in 2 dimensions.

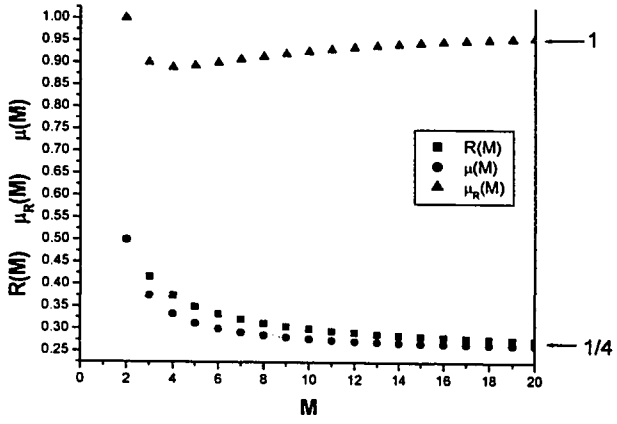

Figure 3.2: Plots of the mobility, μ(M), the jump acceptance factor R(M) and the intrinsic mobility $\mu_R(M)$ for a 1D linear chain.

Another aspect of the 1D chain that can be investigated in the mean end-to-end distance $\langle h \rangle$, given by:

$$\langle h \rangle = \sum_{i=1}^{S} (x_M - x_1) \cdot n_i \tag{3.12}$$

where x_i denotes the i-th monomer position and S is the total number of states. Interestingly, in the example shown above, the mean end-to-end distance calculation yields the same result as if all conformations were equally likely (which would be the case in the absence of an applied electric field). This means that, on average, the electric field has no effect of the chain's shape. This lends credence to our result that, for large M, the linear chain in 1D is free draining since no chain deformation is observed.

$$\begin{aligned} &\text{Without field}: \langle h \rangle = 4\left(\frac{1}{4}\right) + 5\left(\frac{1}{4}\right) + 5\left(\frac{1}{4}\right) + 6\left(\frac{1}{4}\right) = 5 \\ &\text{With field}: \langle \mathrm{h} \rangle = 4\left(\frac{1}{4}\right) + 5\left(\frac{1}{4} + \frac{\varepsilon}{8}\right) + 5\left(\frac{1}{4} - \frac{\varepsilon}{8}\right) + 6\left(\frac{1}{4}\right) = 5 \end{aligned} \tag{3.13}$$

As we can see from eq. (3.13), the 2 middle conformations cancel each other out in terms of their probabilities (probabilities were taken from eq. 3.3).

Unfortunately, not much more can be gleaned from the study of a 1D chain. Nevertheless, it provided us with a useful example to show how the model is put into practice. Additionally, we learned how the modelling of a one-dimensional linear chain followed dynamical behaviour consistent with the Rouse model. Only by studying higher dimensionalities will we be able to gather more useful and interesting results. In chapter

4 we will extend our analysis to the study of various molecules in two-dimensions in the absence of obstacles.

Chapter 4

Free Macromolecules in two dimensions

4.1 Introduction

This chapter takes our model to its intended area of study: The 2 dimensional analysis of small oligomers. Using the BFM (Bond Fluctuation Model) already discussed we will show how our model represents an attractive alternative to the study of macromolecules and produces exact results more rapidly than Lattice Monte Carlo (LMC) simulations have ever achieved. We will study various types of molecules, ranging from flexible oligomers and rod-like molecules to ring and star polymers. The study of 2 dimensional polymer systems are an important problem in physics. It allows us to study physical systems such as the diffusion of small DNA fragments confined to interfaces[49] and the lateral diffusion of proteins and lipids along cell membrane[50]. Moreover, 2D lattice systems exhibit stronger excluded volume and crowding effects[51] which are important considerations in many biological systems. Chapter 4 is further subdivided into 4 sections: Section 4.2 offers an example of our model in two-dimensions and provides useful computational details of our calculations. Section 4.3 discusses the theories on polymer physics that we will be using to analyze our results. Section 4.4 presents our results for the mobility and diffusion of macromolecules in solution (without obstacles).

4.2. A Flexible Polymer in a Lattice of Dense Periodic Obstacles.

An example is now shown to illustrate the challenges associated with the generalization of the model as well as certain computational difficulties that needed to be overcome. In our example, we use a flexible polymer chain (M=5 monomers) in a lattice of dense periodic obstacles. Figure 4.1A shows the lattice used as well as our polymer. We have already discussed the generalization of our model as it deals with the consideration of the molecular conformation as well as the molecule's position within the lattice. We also described how the enumeration of states will take place in parallel to building the transition matrix T. Figure 4.1B shows another sample model that will be studied later in an attempt to exploit molecular entropy to sieve analytes using capillary electrophoresis (CE) and microfluidic devices. There are, however, computational obstacles that will need to be overcome before we can solve such systems. In this example, we will discuss the challenges inherent in the study of molecules when the number of system states makes it impractical, or even impossible, to solve the system of equations in a traditional manner.

A

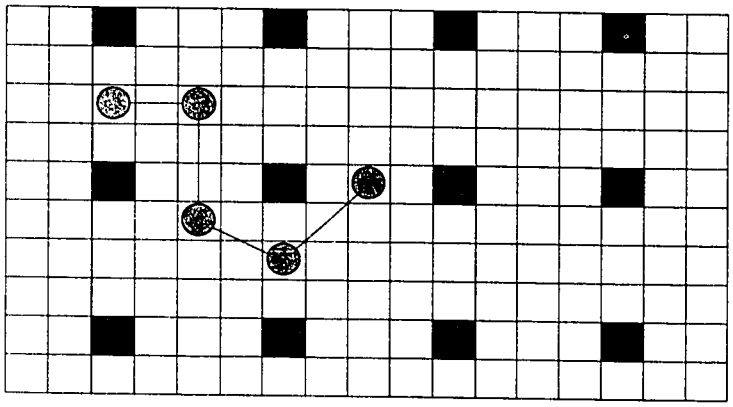

Figure 4.1A: a flexible polymer is shown in a lattice of periodic obstacles. The circles represent monomers and the obstacles are shown as squares (this is a convention used throughout the thesis). Of note is the fact that monomers and obstacles follow the same excluded volume rules, ie: they are not permitted to be adjacent.

B

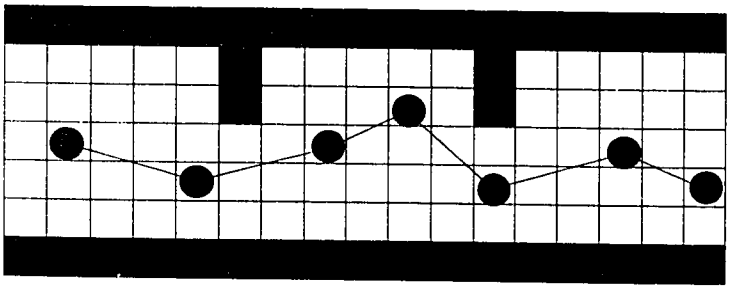

Figure 4.1B: a flexible polymer in a tube. This is a system that will be studied in section 5.3. The idea is to create entropic traps within a tube. The walls of the tube as well as the periodic dividing barriers follow the same excluded volume rules as obstacles.

Once we have built the transition matrix through the exhaustive process of finding all legal system states and linking them through transitions, we must solve the relevant equations. Since the BFM has a high coordination number (Z=36), the number of states of a system can easily exceed the computational limits when larger molecules are studied. In our example (Fig. 4.1A) we have 78 920 possible states in the system, meaning that we would effectively have to solve for a matrix that has over 10^{11} elements. To help deal with this issue we exploit the fact that our transition matrix is very sparse, meaning that few elements are non-zero. To see this, we note that each element of the transition matrix describes a probability of transition between states. Since every row of our transition matrix T corresponds to a separate system state, the elements within that row list all transitions that would lead to the system state corresponding to that row. The upper limit of the number of transitions is given by 2dM, where d is the dimensionality and M is the number of monomers. In our example (M=5, d=2), the upper limit is 20. Realistically, most conformations lead to less than ½ of this upper limit since many moves are rejected and lead to the original state. Hence, even though 2dM moves were made for each system state, each move that was deemed illegal will only succeed in updating the diagonal element of the transition matrix. Hence, for rejected moves, new elements of the transition matrix beyond the diagonal are not created. Consequently, in this particular example, each row of our transition matrix has a maximum of 20 non-zero elements, effectively reducing our system to about 10^6 non-zero elements. Unfortunately, the number of elements is still too high for us to solve using conventional methods. To solve for this system, we use the conjugate gradient method[27], which allows us to solve the system storing only the non-zero elements of our transition matrix by using an iterative method. The conjugate gradient method was chosen because of its rapidity. Other sparse techniques exist, however.

In short, using the described method for state enumeration and using the conjugate gradient method to solve our system of equations, we found an exact mobility of μ= 0.0014886 and a mean square end-to-end distance of $\langle h^2 \rangle$=54.537. This was found using a low-end Pentium computer with 32MB of RAM in about 90 minutes. In section 4.3 we will be discussing certain theoretical predictions that will be used to assist us in

the analysis of our results. This will serve as a validation of our model to confirm that it can be used as an adequate predictor of the static and dynamic properties of macromolecules.

4.3. Theory

The goal in this section is to briefly go over some theoretical and computational results we will be using throughout as a basis for comparison to determine the validity of our method. The first point of verification is the mobility of the analyte. This will be done by comparing published Lattice Monte Carlo results using the BFM. Another quantity that can be used to verify the validity of the model is the mean end-to-end distance, $\langle h^2 \rangle$ defined by:

$$\langle h^2 \rangle = \frac{1}{S} \sum_{i}^{S} \left(\vec{R}_M - \vec{R}_1 \right)^2 \tag{4.1}$$

where $\vec{R}_M$ and $\vec{R}_1$ are the position vectors of the last and first momoners, respectively, and the summation is over all (S) states of the system being examined. In addition to comparing these actual results, we will also be verifying the scaling properties which provide us with a means to track the average size of a molecule as the degree of polymerization increases. The scaling values are very well established for large linear polymers. We want to ensure that, in the large M limit, we have [14]

$$\langle h^2 \rangle \propto (M-1)^{2\upsilon} \tag{4.2}$$

where (M-1) depicts the number of bonds in a linear chain and υ is the Flory exponent ($\upsilon = 3/4$ is 2D). Also, for the diffusion constant, the scaling equation is given by:

$$D \propto M^{-\alpha} \tag{4.3}$$

where $\alpha=1$ is the Rouse prediction in all dimensions. Given these well-accepted parameters we can determine whether this model behaves properly both in the static and dynamic regimes. Of course, since our model is limited to the study of small oligomers, we will have to extrapolate results to the large M limit in order to test these scaling parameters.

4.4. Free Macromolecules: Results

In this section we will be investigating the properties of small macromolecules in solution. This means that the solution is homogeneous and there is nothing to obstruct the migration of our molecules. This is a good place to start since we can easily compare our results with the static and dynamic scaling properties described in section 4.3. We will be using four different types of molecules for our investigation. The first is a linear flexible polymer: particles are linked linearly like a polymer chain as allowed by the BFM. The second type of molecule is what we call a stiff chain. Similar to the linear chain, we then impose an additional constraint on the angle, θ, between successive bonds ($-\pi/4 < \theta < \pi/4$); Figure 2.2C illustrates the angular restrictions. Of note is that we did not consider bending energies between the bonds of the monomers when imposing the angular restriction. In the absence of an external force, no polymer conformation is energetically more favourable then the next. These stiff chains make for good models of rod-like molecules and stiff DNA fragments. The third molecule is the ring chain. These are linear chains whose first and last bonds are linked together in the same manner as the other bonds, forming a molecule with a circular geometry. The ring chains can be a good model for soft round objects (such as vesicles) or circular DNA molecules. Figure 2.2D shows an example of a ring chain. The last molecule studied is the star chain. All particles in the star chain have a bond to the central monomer. Typically, a star chain will have more than one monomer per branch but because of the rather extensive demands on memory imposed by the model we will be limited to the study of small star chains. Figure 2.2E shows a star chain.

4.4.1 Flexible linear chains

The study of flexible linear chains has a limitless scope of application. Results for these chains are shown in Table 4.1. We also tested our numerical algorithm using Monte Carlo (MC) simulations (based on the BFM) [26]. For example, these MC simulations gave D=0.0269(9) and $\langle h^2 \rangle$=53.81(6) for a flexible polymer with 5 monomers (M=5). This is in excellent agreement with the data of Table 4.1. Of note is the fact that our Monte Carlo result required substantially more CPU time than our model due to the stochastic nature of MC simulations. Also shown in Table 4.1 is the number of

conformations a linear polymer chain can yield. For M=5 we have 781,380 conformations using the BFM.

Table 4.1: Results for a flexible chain in solution (no obstacles)

LEGEND: M=# of monomers, D=Diffusion Coefficient, $\langle h^2 \rangle$ =end-to-end distance, R(M)=jump acceptance factor, α(M)=scaling exponent for D, α_R(M)= scaling exponent for $D \times R(M)$, υ(M)= scaling exponent for $\langle h^2 \rangle$

M	D	Number of conformations	$\langle h^2 \rangle$	R(M)	Diffusion exponents		$\langle h^2 \rangle$ Exponent
					α(M+½)	α_R(M+½)	υ(M+½)
2	0.090277	36	8.555	0.772	1.4496	0.92943	1.06943
3	0.050155	1076	20.36	0.6252	1.3125	**1.06839**	0.97464
4	0.034382	29 436	35.68	0.5828	1.2384	**1.04667**	0.91718
5	0.026081	781 380	53.72	0.5584	α(∞)=0.97± 0.01	α_R(∞)=0.97065	ν(∞)=0.73 ±0.01

To study the scaling laws (4.2) and (4.3) for these molecules, we define two "local" effective exponents:.

$$\alpha\left(M+\frac{1}{2}\right)=\frac{\log[D(M)/D(M+1)]}{\log[M/(M+1)]} \tag{4.4}$$

and,

$$\upsilon\left(M+\frac{1}{2}\right)=\frac{\log\left[\langle h^2(M+1)\rangle/\langle h^2(M)\rangle\right]}{2\log[M/(M+1)]} \tag{4.5}$$

We use eqs (4.4) and (4.5) to verify the convergence of these scaling parameters to the large M limit (since eqs (4.2) and (4.3) are only valid in the limit of very large M). Figures 4.2A and 4.2B show the results of our extrapolation analysis for α(M) and υ(M). Our extrapolated results for M→ ∞ are also shown in Table 4.1 (last line). In Figure 4.2 we simply used linear fits: we also attempted second order polynomial fits (results not shown) but the linear fits provided a closer approximation of the expected large M scaling exponents. Note that it is not our intent to determine the manner in which these molecules reach the proper Rouse and size scaling parameters since, for small molecules, it is expected that there will exist some strong finite-size and lattice effects. A better venue to determine how these scaling parameters are reached would be to study a wide range of molecular sizes, a study that is not presently feasible using this model due to computational constraints. Another important consideration is that these extrapolated values are found using only a few data points. Nevertheless the goal was to foster more

confidence into the validity of the model. A goal well achieved by viewing the extrapolated results of Table 4.1 where we have $\alpha \rightarrow 0.97$ and $\nu \rightarrow 0.73$ as $M \rightarrow \infty$, which are both close to the accepted theoretical results $\alpha \rightarrow 1$ and $\upsilon \rightarrow 3/4$ for the scaling of polymers in solution described in section 4.3.[14]

We already mentioned how the jump acceptance factor R(M) (eq 3.8) can be used to filter out the lattice and model dependent effects when discussing our results for a one-dimensional polymer. We can define an intrinsic diffusion coefficient $D_R(M)$:

$$D_R(M) = \frac{D}{R(M)} \tag{4.6}$$

combined with eq (4.3) we have,

$$D_R(M) \propto \frac{1}{M^{\alpha_R}} \tag{4.7}$$

where α_R is the scaling parameter of the intrinsic diffusion coefficient. In principle, we should have $\alpha_R = \alpha$. The finite-size scaling parameter $\alpha_R(M)$ of the intrinsic diffusion coefficient is also found using eq (4.4). Table 4.1 provides the values of the finite-size scaling parameter $\alpha_R(M)$. From Table 4.1, we see that the convergence of $\alpha_R(M)$ to 1 is just as apparent as the convergence of $\alpha(M)$. In fact, the convergence is also somewhat faster. The extrapolation, in this case, is done using only the last 2 points.

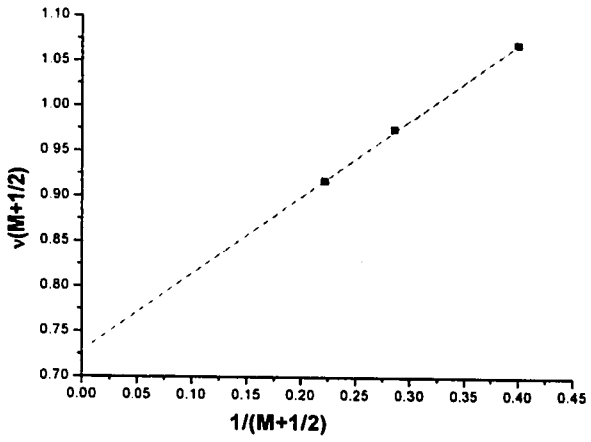

Figure 4.2A: the scaling exponent of the end-to-end distance, $\nu(M+½)$ vs. $1/(M+½)$. The line represents a linear fit of the data. The extrapolated value of the Flory exponent is: $\upsilon(\infty)=0.73(1)$

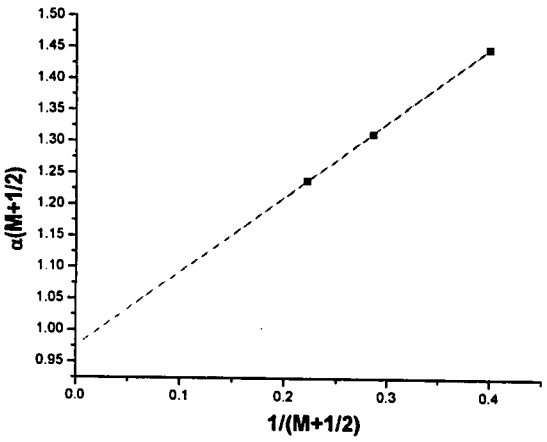

Figure 4.2B: the scaling exponent of the diffusion coefficient, $\alpha(M+½)$ vs. $1/(M+½)$. The solid line represents a linear fit of the data. Extrapolated value is $\alpha(\infty)=0.97(1)$

4.4.2 Stiff Chains

These chains are characterized by the restriction that the angle θ between 2 consecutive bonds is limited to $-\pi/4<\theta<\pi/4$. Figure 2.2C illustrates the angular constraints between bonds. This restriction allows us to study semi-flexible polymers with a varying Kuhn segment, or even rod-like molecules. Although we chose an angle of $\pi/4$ it is worthwhile to note that several other angles could have been used with this model. Furthermore, the limited degree of freedom imposed by the angular restrictions will effectively reduce the number of conformations a molecule can possess and allow us to study longer chains. Results are shown in Table 4.2. We see that the scaling of the diffusion constant and end-to-end distance still approach acceptable theoretical limits ($\alpha\rightarrow 1$, $\upsilon\rightarrow ¾$). Once again, we used linear extrapolations but discounted the results for the dimer (M=2) since no angular restriction can be imposed between only 2 monomers. We see that the chain stiffness has no effect on either chain dynamics or its static properties in the large M limit. This was expected since it can be seen as a consequence of the central-limit theorem.

We also studied the factor R(M) and note that convergence of $\alpha_R(M)\rightarrow 1$ is not as good. We also see that the angular restriction imposed on the polymer has lowered the asymptotic value of $R(M\rightarrow\infty) \approx 1/3$ here. This is expected since the additional restriction will lead to more moves being rejected.

To be thorough, we describe how polymer states can defined to account for the energy of bending in the polymer. We can use different energy landscapes to modify the

probabilities of polymer conformation to account for its stiffness (or persistence length).. This would accentuate the excluded volume effect and make certain conformations more probable than others. Note that this would not affect the ergodicity of the system since each conformation (or system state) would still have a non-zero probability of existence. Although this would, in principle, pose no problems with the current model, a method would need to be devised to ensure that the solution is still normalized to 1 (ie: the sum of all state probabilities must be unity). Otherwise, the system of equations could not be solved.

Table 4.2: Results for a stiff linear polymer in solution

LEGEND: M=# of monomers, D=Diffusion Coefficient, $\langle h^2 \rangle$=end-to-end distance, R(M)=jump acceptance factor, α(M)=scaling exponent for D, α_R(M)= scaling exponent for $D \times R(M)$, υ(M)= scaling exponent for $\langle h^2 \rangle$

M	D	Number of conformations	$\langle h^2 \rangle$	R(M)	Diffusion exponents		$\langle h^2 \rangle$ Exponent
					α(M+½)	α_R(M+½)	ν(M+ ½)
2	0.090277	36	8.555	0.772	1.8903	1.0338	1.5964
3	0.041948	380	31.221	0.5455	1.7165	**1.26531**	1.3025
4	0.025601	4020	66.055	0.4791	1.5776	**1.20628**	1.1713
5	0.018004	42 524	111.41	0.4410	1.4789	**1.15349**	1.0916
6	0.013749	449 836	165.88	0.4156	α(∞)=1.06 ±0.02	α_R(∞)=0.94 ±0.03	ν(∞)=0.72 ±0.01

4.4.3 Ring Chains

The results for ring chains are shown in Table 4.3. Ring chains, or circular polymers, are polymers where the first monomer is attached to the last. We see from Table 4.3 that the values of all scaling exponents (υ(M), α(M) and $\alpha_R(M)$) are sporadic and non-monotonous and the errors associated with their extrapolation to the large M limit are very large. Consequently, the manner in which we achieve convergence is suspect at best and doesn't lead to any firm conclusions Since the ring chains have no ends we relied on the mean radius of gyration, which scales the same as the $\langle h^2 \rangle$, to study the convergence of the scaling parameter ν. We then have:

$$R_g^{\,2} \propto M^{2\upsilon} \tag{4.7}$$

and,

$$\upsilon\left(M+1/2\right)=\frac{\log\left[R_g^{\,2}(M+1)/R_g^{\,2}(M)\right]}{2\log\left[(M+1)/M\right]} \tag{4.8}$$

Once again, the bond between first and last monomer reduces the freedom of the chain and allows us to study larger chains (up to M=6). A better test, perhaps, is to study the ratio of the asymptotic result [28] that $R_{g;circ}/R_{g;lin} \approx 0.73$. Our data agree with this prediction in limit of large molecular sizes. Results are shown in Table 4.4. Finally, we note that the factor R(M) for linear and circular chains lead to the same asymptotic value for large M (R(M)→0.45) . This was expected since end effects become less relevant (for linear chains) as the molecular size increases.

Table 4.3: Results for a circular or ring polymer in solution

LEGEND: M=# of monomers, D=Diffusion Coefficient, $\langle R_g^{\,2}\rangle$=mean radius of gyration squared, R(M)=jump acceptance factor, α(M)=scaling exponent for D, α_R(M)= scaling exponent for $D\times R(M)$, υ(M)= scaling exponent for $\langle R_g^{\,2}\rangle$

M	Diffusion Coefficient	Number of conformations	$\langle R_g^{\,2}\rangle$	R(M)	Diffusion exponents		$\langle R_g^{\,2}\rangle$ Exponent
					α(M)	α_R (M)	ν(M)
3	0.038990	192	2.6528	0.5104	1.1254	0.5607	0.74354
4	0.028207	2 300	4.0691	0.4635	1.2745	0.8928	0.65464
5	0.021225	33 580	5.4498	0.4509	1.0282	0.8401	0.69144
6	0.017597	571 548	7.0126	0.4509	α(∞)=1.0± 0.6	α_R(∞)=1.44 ±0.42	ν(∞)=0.56± 0.12

Table 4.4: Radii of gyration of free linear and circular chains with M=3 – 5.

M	R_g (Linear)	R_g (Circular)	$R_{g;circ}/R_{g;lin}$
3	2.0439	1.6287	0.7969
4	2.5566	2.0172	0.7890
5	3.0322	2.3345	0.7700
M→∞			0.74(2)

4.4.4. Star chains

The last molecule studied here is the star macromolecule. Figure 2.2E shows the macromolecule in question. In practice, a star would have a greater molecular weight along its arms but due to computational constraints we are limited to arms with a singular monomer. Results for the diffusion coefficient are shown in Table 4.5 and Figures 4.3 and 4.4. Interestingly, we see an initial increase in the number of conformations as we increase M until M=8. Greater molecular weights (M>8) show a substantial decrease in the number of conformations. In fact, we could not study M>10 without violating the rules of the BFM. Consequently, we expect to encounter very important lattice effects when studying star chains. In Figure 4.3, we plot the diffusion constant D versus the molecular weight M. We see a drastic decrease in the diffusion coefficient as we increase molecular size. It is quite clear from Figure 4.3 that the star macromolecule is not exhibiting Rouse behaviour. Figure 4.4 illustrates this by plotting the finite-size scaling parameter $\alpha(M)$ against molecular size M. Unlike the linear and circular chains, the scaling parameter $\alpha(M)$ diverges from expected results as we increase the molecular size.

These anomalous results are due to lattice effects. Despite the fact that the BFM provides realistic dynamic results for linear and circular chains, certain molecules are inadequately simulated. Moreover, a decrease in entropy (# of conformations) as we increase molecular size is an appropriate warning that results may not correspond properly to theoretical predictions. These effects are even more pronounced since we are dealing with molecules in 2 dimensions. We expect to see less serious deviations from expected results in 3 dimensions.

Despite the fact that our model did not succeed in the simulation of star chains, these small molecules can become useful in the simulation of soft vesicles where the radius of gyration can be compressed or extended through entropic effects. We would be simulating molecules that are circular (or spherical in 3D) in shape.

Table 4.5: Results for a star polymer in solution

LEGEND: M=# of monomers, D=Diffusion Coefficient, R(M)=jump acceptance factor
$\langle R_g^2 \rangle$=radius of gyration, α(M)= scaling exponent for D, α_R(M)= scaling exponent for $D \times R(M)$

M	D	Number of conformations	R(M)	$\langle R_g^2 \rangle$	α(M+½)	α_R(M+½)
4	0.03151	12 984	0.5764	8.6876	1.87739	1.07947
5	0.02073	81 388	0.5173	8.7688	2.3343	1.45962
6	0.013541	284 520	0.4680	8.8624	3.13179	1.98192
7	0.008356	555 132	0.4145	8.9700	4.63359	3.00643
8	0.004501	573 860	0.3549	9.0917	7.82887	5.36190
9	0.001790	278 152	0.2888	9.2253	18.52107	14.0865
10	0.0002543	48 096	0.2156	9.3663		

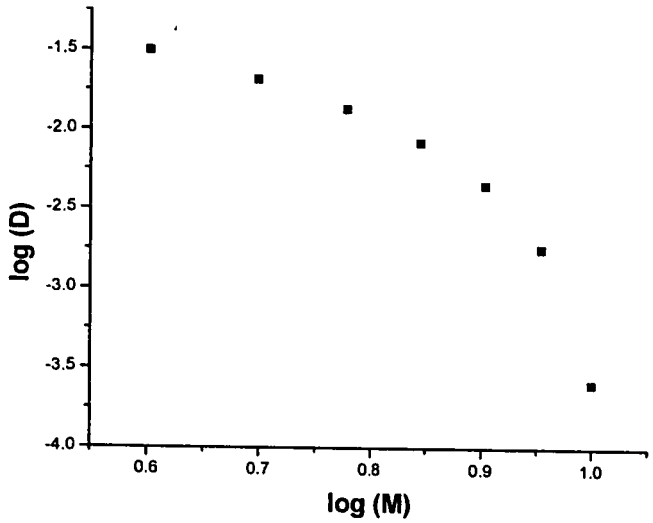

Figure 4.3: log-log plot of the diffusion coefficient D vs. molecular weight M of the star polymer in solution

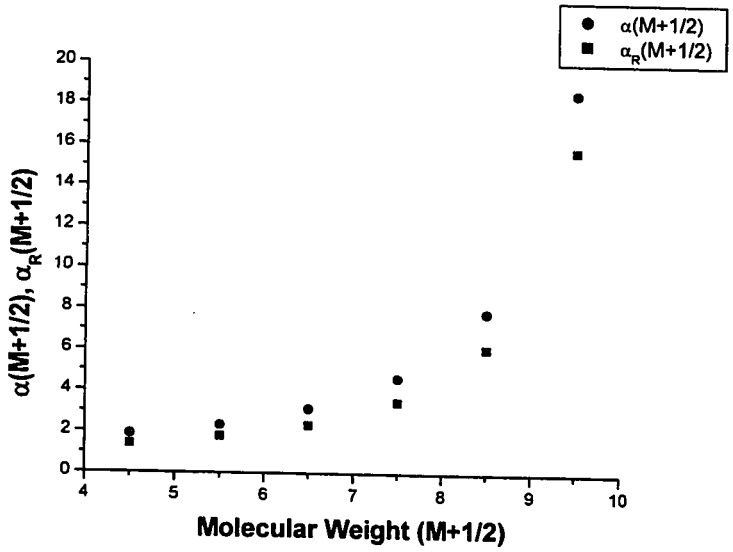

Figure 4.4: finite-size scaling parameter $\alpha(M+1/2)$, $\alpha_R(M+1/2)$ vs. molecular weight (M+1/2) for a star polymer in solution.

4.5 Conclusion

This concludes our analysis of free macromolecules in solution. The purpose of section 4.4 was to verify that the static and dynamic properties of molecules correspond to theoretical predictions and accepted published results in an attempt to validate our model. We have shown that most molecules obey the Rouse limit extrapolated to large molecular weights. Furthermore, the conformational sizes (h and R_g) scale according for the Flory prediction in the asymptotic limit. In addition to proper scaling properties, we have also shown that our results are consistent with LMC simulations using the BFM.

We were also able to exploit the jump acceptance factor R(M). Using R(M) to filter lattice-dependent effects we were able to achieve faster convergence to the expected scaling laws of flexible and semi-rigid polymers. In star macromolecules, the jump acceptance factor allowed us to see the extent of the lattice effects on our simulations and provided us with an indication that results may be suspect. The overall results presented in this chapter are sufficient to convince us of the model's validity and we can follow on to more important investigations: the mobility of macromolecules in a non-homogeneous solution.

Chapter 5

Molecules with the presence of obstacles: Results

Now that we have verified that the model provides accurate results for macromolecules in homogeneous solutions, we can focus our efforts on the study of these same molecules in inhomogeneous environments. With the presence of obstacles we must take into account the actual position of the monomers (e.g., using monomer #1 as the reference monomer) when enumerating states and building our transition matrix. A system state will then be defined by its molecular conformation as well as the position of the first monomer within the lattice. In section 4.2 we dealt with a flexible linear polymer in a periodic lattice of obstacles and have shown how the static and dynamic properties agree with LMC simulations, thus demonstrating the validity of our model. In this chapter we will deal with a variety of toy systems, discovering a plethora of interesting types of polymer dynamics ranging from reptation to entropic trapping. In our analysis, we will be using ideas from the original Ogston model as well as from the theory of polymer physics to examine our results.

This chapter is subdivided into four sections. In section 5.1 we will present some additional theory that will be used to analyze our results. In Section 5.2, we study various small oligomers in a lattice of periodic obstacles. Section 5.3 deals with anisotropic periodic gels where the periodicity is different in each cartesian direction. In Section 5.4 we study linear polymers in various tube-like systems (or channels).

5.1. Theory

For our analysis, we will be using the scaled mobility μ^*, defined by the ratio of the molecules' mobility in the gel with the mobility in a homogeneous solution. We then have:

$$\mu^*(C,M) = \frac{\mu(C,M)}{\mu(C=0,M)} \tag{5.1}$$

where M is the molecular size (number of monomers) and C is the gel concentration. Recall the premise behind the Ogston model that the scaled mobility was solely a function of the volume available to the molecule, F(C). Ogston revealed that the available volume for a spherical analyte of size R in a lattice of long and thin fibres is given by[17]:

$$\frac{\mu(C)}{\mu_o} \sim f(C) = \exp\left[-\pi\kappa l\left(R+R_f\right)^2\right] \tag{5.2}$$

where κ is the fibre concentration (in fibers per unit volume), l is the average fibre length and R_f is the average fibre radius of the gel. Consequently, semi-log graphs depicting eq. (5.2), called Ferguson plots, were widely studied to determine the dependence of the scaled mobility of analytes on the mass concentration ($C=\kappa l$) during gel electrophoresis. Moreover, the slope of the Ferguson plot, $(R+R_f)^2$, is called the retardation factor, K, and can be plotted against the radius of gyration to ascertain the effective fibre radius, R_f. Despite the popularity of the Ferguson plot, it was determined by Slater and Guo[10] that polynomial fits were better suited to fit the dependence of the scaled mobility on the concentration. Accordingly, we will also be fitting our data using the polynomial form:

$$\mu^*(C,M) = 1 - \sum_i a_i(M)C^i \tag{5.3}$$

where we will stop the sum at i=2 and use only low concentration data. In fact, using these scaled values, we have $\mu^*=D^*$ so the data can be seen as either the zero-field scaled mobility or the scaled diffusion constant. We will use the first coefficient, a_1, of the polynomial fit to estimate the retardation factor. We then have[7]:

$$K = a_1 = \left(-\frac{\partial\mu^*}{\partial C}\right)_{C\to 0} = \left(-\frac{\partial \ln(\mu^*)}{\partial C}\right)_{C\to 0} \tag{5.4}$$

where the last equality stands for small concentrations since $\mu^*(0)=1$ (see eq (2.14)). Therefore, the first coefficient a_1 of our polynomial fit also provides the Ferguson retardation factor K.

5.2. Periodic Gels

The simplest system that can be conceived is that of periodically placed obstacles. We note that obstacles will be following the same excluded volume restriction applied with the BFM, meaning that they are not allowed to be adjacent to one another. Therefore, each obstacle effectively blocks 9 sites, and the (v/v) concentration must be defined as $C=9/(L_xL_y)$, where L_x and L_y depict the periodicity of the obstacles in the x and y directions respectively. Figure 5.1 shows our results for isotropic periodic lattices ($L_x=L_y$). The actual coefficients of our polynomial fit are depicted in Table 5.1. At first view of Figure 5.1, we see that larger molecular sizes have lower mobility for all gel concentrations C. This appears to be a universal phenomenon, regardless of the type of molecule used and was an expected result. We also note inflection points when larger concentrations are used. In fact, the M=2 dimer shows evidence of several changes in curvature.

M	Polymer type	a_1	a_2
2	F	-2.50±0.02	3.3±0.2
3	F	-3.29±0.04	5.27±0.36
4	F	-3.87±0.02	5.31±0.12
3	C	-2.99±0.01	5.60±0.16
4	C	-3.97±0.03	7.99±0.41
5	C	-4.2±0.4	4.1±2.2
3	S	-3.78±0.02	6.69±0.28
4	S	-5.01±0.05	9.85±0.37
5	S	-6.09±0.11	13.4±0.6

Table 5.1: Coefficients of the polynomial expansion of the scaled mobility, $\mu^*(C)$, for various molecules in a lattice of periodic obstacles.
Legend: **M**=molecular mass,
$\mathbf{a_1}$,$\mathbf{a_2}$=coefficients in the polynomial expansion
F= flexible linear polymer
S= stiff linear polymer
C= circular polymer

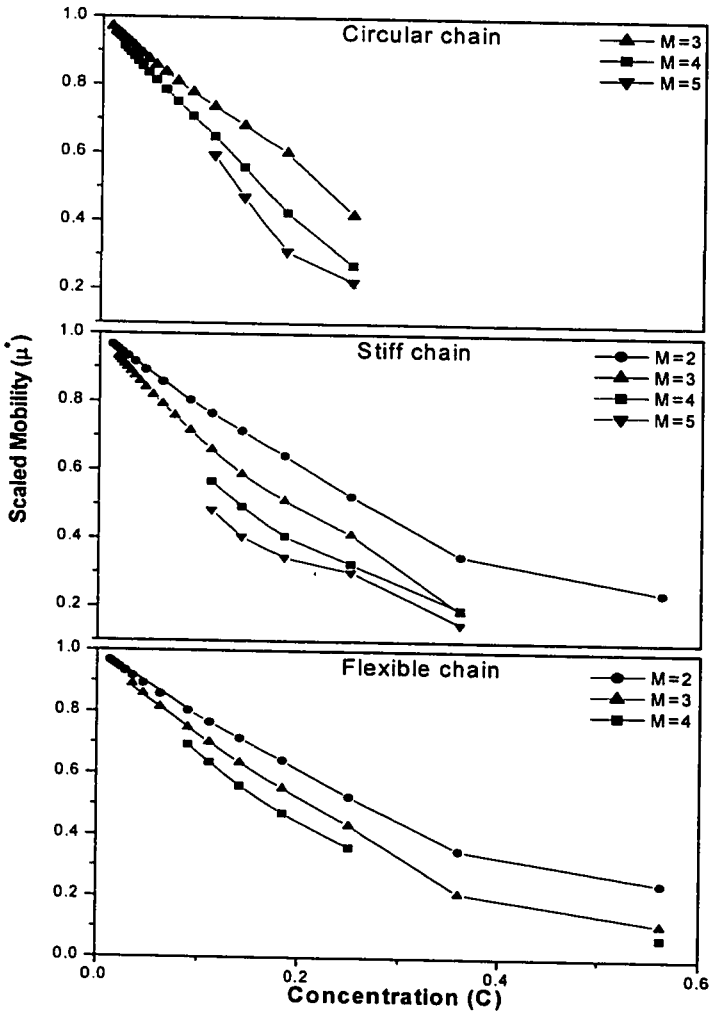

Figure 5.1: Mobility data for the periodic gel system shown in Fig 2.2. The data points are joined for clarity. We see that for the smaller chains (up to M=3), we were able to find the exact diffusion coefficient leading to the 0 concentration limit.

We also plotted the square root of the retardation factor, $K^{1/2}$, versus the radius of gyration R_g in Figure 5.2. This is a standard data analysis method suggested by the Ogston model[6,7,10-12]. The extrapolated values indicated in Figure 5.2 provide an effective obstacle radius for our periodic system. We expect an obstacle radius r=1 and for our circular chain, we achieve a similar result ($r \approx 0.9$). However, for linear chains (flexible and stiff) we have an average value $r \approx 2.8$, which is much larger than anticipated. This could mean that obstacles have a much larger effect on linear chains since they actually reduce their mobility (translation and rotation) and their entropy even when the molecule and the obstacles are far apart. This is an important finding since we must now consider

the analyte along with the gel used in order to determine the effective obstacle radius. In other words, certain molecules can approach the obstacles more closely than others before being dynamically affected. We can understand how this new phenomenon can occur by considering the average radius of gyration of the molecule. The linear chain, being less constrained than the circular chain, will see a larger variance in its size and it may feel the effects of obstacles from further away. These subtle effects would have been lost in the noise of other stochastically driven algorithms and offer us an opportunity to better understand polymer dynamics.

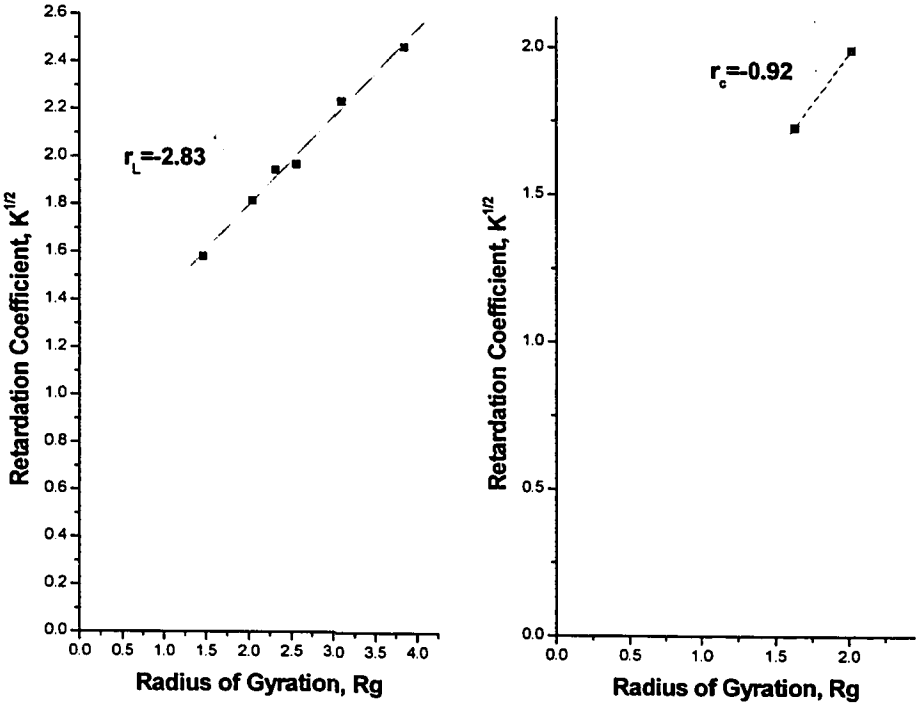

Figure 5.2: Square root of the retardation factor, $K^{1/2}$, vs the Radius of Gyration of the analytes is shown for the circular molecule and the linear chains (flexible and stiff). The line joining the 2 points for the circular chain is depicted by the equation: $K^{1/2}=(R_g+0.92)$ x0.678, thus giving an effective fibre radius of $r_c=0.92$. The fit for the flexible/stiff linear molecules is given by: $K^{1/2}=(R_g+2.83)$ x0.37 and the related fibre radius is thus: $r_L=2.83$, as shown.

Another common analysis tool used in the Ogston model is the Ferguson plot ($\ln(\mu^*)$ vs. C). Ferguson plots were a useful tool used to confirm the validity of the Ogston

model since the available volume can often be expressed in terms of exponentials (see Eq. 5.2). It also provided clues to the fibre radius and the retardation factor. However, several authors[8-13,21] have reported that these Ferguson plots are generally not linear and the available volume to the molecule was not always an accurate predictor of the scaled mobility. Figure 5.3A shows the Ferguson plot of 2 circular chains (M=3 and M=4) while Figure 5.3B shows the same plot for flexible linear chains (M=2,3 and 4). We see that for low concentrations (C<0.2) the data seem to agree with a linear fit. This apparent linearity is due to the fact that the polynomial coefficients a_1, a_2 have opposite signs (shown in Table 5.1). The resulting semi-log graph would then appear somewhat linear. It was shown previously[8-13,21] that these same coefficients have the same sign when a point-like analyte (M=1) is placed in a 'random' gel (obstacles placed randomly on a lattice). We would then see a more pronounced curvature in random gels. These facts reveal that Ferguson plots can lead to erroneous conclusions in the presence of non-negligible error bars. Furthermore, the curvature of the Ferguson plot can provide clues to the disorder of the system being studied[52].

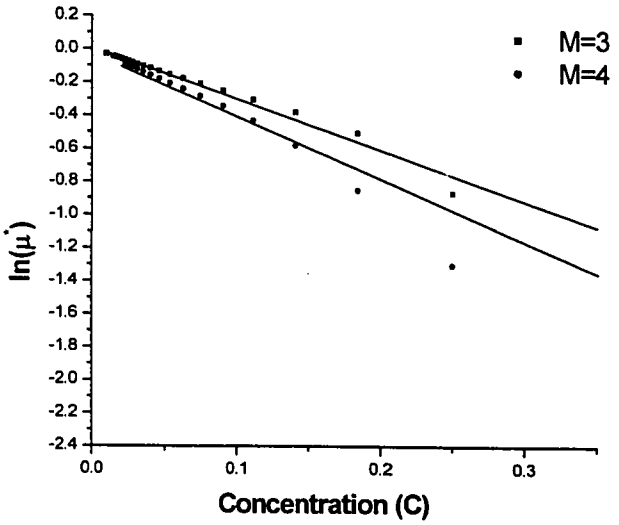

Figure 5.3A: Ferguson plot ($\ln(\dot{\mu})$ vs Concentration) for circular molecules (M=3 and M=4) in a periodic gel. The lines represent linear fits to the data using concentrations C<0.1.

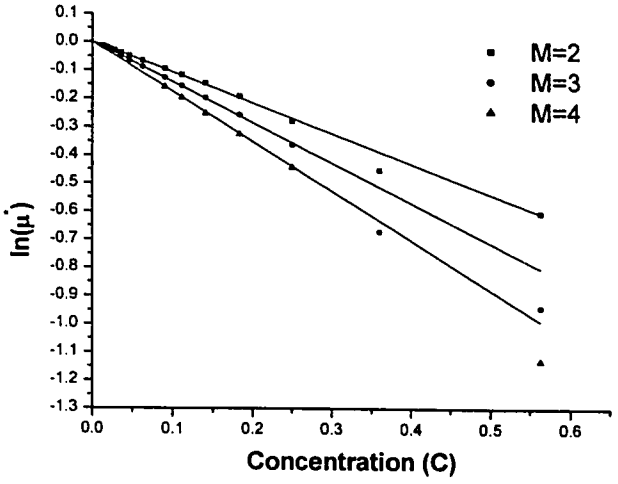

Figure 5.3B: Ferguson plot ($\ln(\dot{\mu})$ vs Concentration) for flexible linear chains (M=2,3 and 4) in a periodic gel. The lines represent linear fits to the data using concentrations C<0.1.

The linear fit from Figure 5.3B was obtained using concentrations less than C=0.1. The Ogston model only applied to gels of low concentration. We can see in Figures 5.3 how the linear fit fails to account for higher concentration results.

What happens when high concentrations are used? We found in earlier sections that our model provides good results for the scaling of the diffusion constant, D, and the end-to-end distance, $\langle h^2 \rangle$ for polymers in solution. When the concentration of our periodic

gel becomes very high, linear polymers manoeuvre through the lattice by a process known as reptation[14]. Figure 4.1A shows the densest lattice system that can be studied. We used this gel to see if our model properly simulates reptation dynamics in terms of the expected scaling parameters. Our results for flexible linear chains in a dense lattice of obstacles are shown in Table 5.2 and Figure 5.4ABC. In terms of scaling parameters, 2D reptation dynamics[38] should yield:

$$D \sim \frac{1}{M^{3/2}} \tag{5.5}$$

and,

$$\left\langle R_g^{\,2} \right\rangle \sim M^{2\upsilon} = M^{3/2} \tag{5.6}$$

Table 5.2: Results for a flexible linear polymer in a dense lattice of periodic obstacles

LEGEND: M=# of monomers, D=Diffusion Coefficient, $\left\langle R_g^{\,2} \right\rangle$=mean square radius of gyration, α(M+½) =scaling exponent for D, ν(M+½)= scaling exponent for $\left\langle R_g^{\,2} \right\rangle$					
M	Diffusion Coefficient	Number of conformations	$\left\langle R_g^{\,2} \right\rangle$	Diffusion exponents	$\left\langle R_g^{\,2} \right\rangle$ Exponent
				α(M+½)	ν(M+½)
2	0.022418	88	2.0455	4.73134	1.2045
3	0.005748	904	4.0905	3.65236	1.02451
4	0.002544	8584	6.4617	2.93955	0.95572
5	0.001489	78 920	9.1558	2.53722	0.90772
6	0.001007	719 288	12.113		
∞				α(∞)=0.71(8)	ν(∞)=0.80(6)

In Figure 5.4AB we show two representations to find the asymptotic scaling exponent of the diffusion constant. In Figure 5.4A we see a simple log-log plot of the scaled diffusion constant D^* vs. the molecular mass M. Using the largest 3 values of M, the scaling parameter depicted by the slope of Figure 5.4A reveals: α=2.29(8) which is higher than expected (see eq 5.5). However, the curvature indicates that larger molecular sizes would yield a lower, and hence more appropriate, value of the scaling parameter. A better approach may be our traditional one where we take consecutive local slope values shown

in eqs (4.4) and (4.5). Figure 5.4B shows these results. We see the linear extrapolation of our large M scaling parameter still does not yield what we would have expected for reptation dynamics. This lack of correspondence to the theoretical predictions established in eq. 5.5 and eq. 5.6 is not very surprising since reptation dynamics was only intended for very large chains. Furthermore, the use of small chains to simulate reptation dynamics will incur finite-size effects, which are of the order of $1/\sqrt{M}$ [14]. Consequently, reptation cannot be observed using values M=2,3 and the larger molecules studied in this lattice would necessarily yield skewed results that cannot be directly compared to any 'reptation-like' regime. In section 5.3 we devise a means to show how reptation dynamics can be achieved with linear polymers in a tube.

We also studied the mean radius of gyration, $\langle R_g^2 \rangle$ of flexible linear polymers in a dense periodic lattice of obstacles (shown in Table 5.2 and Figure 5.4C). In Figure 5.4C we extrapolate the large M scaling exponent by using consecutive (local) slope values and achieve results that are consistent with the theoretical prediction established in eq. 5.6. We used both a linear extrapolation (solid line) and a 2nd order polynomial fit (shown by dotted line) to find $\upsilon_{(M\to\infty)}$ and see that both fits achieve fairly close results.

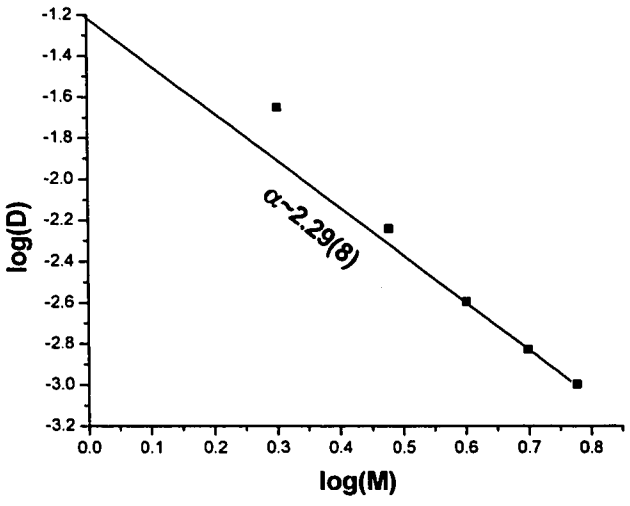

Figure 5.4A: Log-Log plot of the diffusion coefficient, D, vs molecular size M of a flexible chain in a dense lattice of periodic obstacles. The slope of the graph gives the scaling α of D(M). We see the value α~2.29 when taking the slope of the last 3 points .

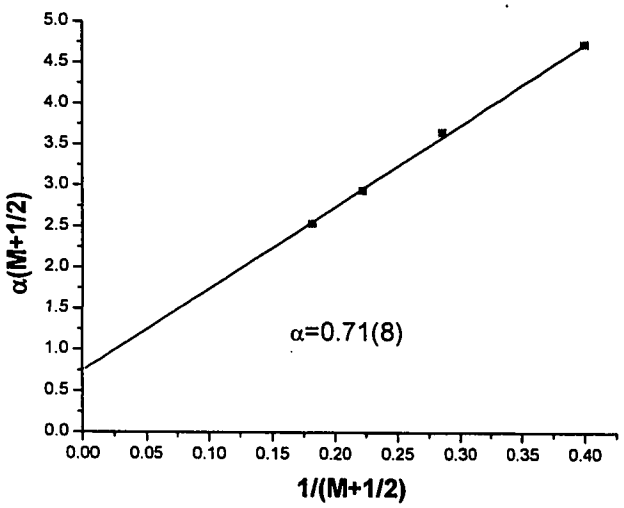

Figure 5.4B: The finite-size scaling parameter of the end-to-end distance $\alpha(M+1/2)$ according to size of a flexible chain in a dense lattice of periodic obstacles. Once again, we do not achieve desired results due to

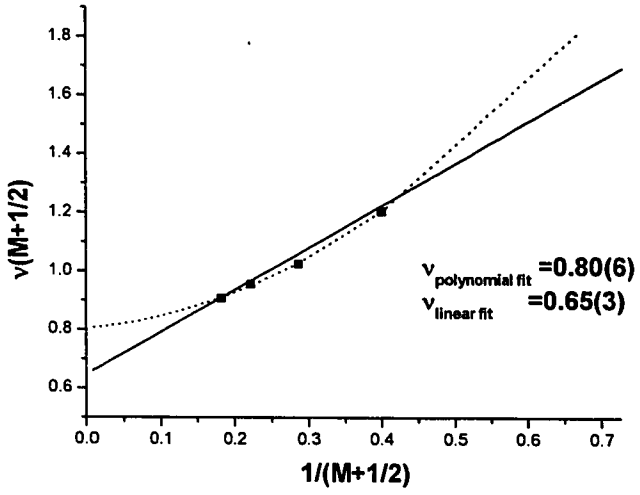

Figure 5.4C: The finite-size scaling exponent $\upsilon(M+1/2)$ vs. $(M+1/2)^{-1}$ of a flexible chain in a dense lattice of periodic obstacles. The y-intercept should yield the large M scaling parameter. We see from the linear fit we achieve relatively close values $\upsilon_{(M\to\infty)}$.

5.3. Anisotropic periodic Gels

In this obstacle lattice, we retain the same idea of periodicity with an important difference: The periodicities are not the same in each Cartesian coordinates ($L_x \neq L_y$). Specifically, we will be keeping the periodicity L_y constant and increase the periodicity in the x direction. This is shown in Figure 5.5.

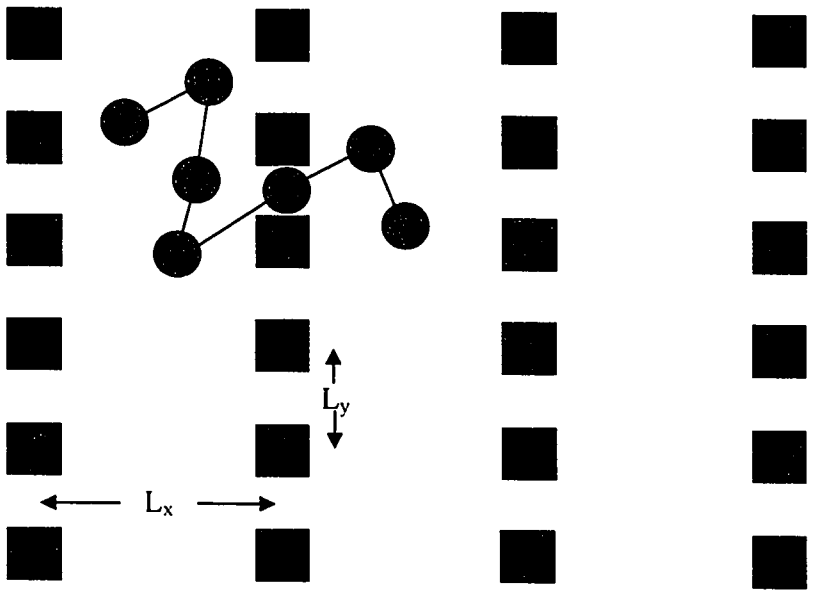

Figure 5.5: Schematic representation of a periodic lattice of obstacles. The squares represent obstacles and the grey circles depict individual monomers. The periodicity in x and y, denoted by L_x and L_y respectively is also shown.

This can be viewed as a stack of filters where the molecule must traverse a certain distance L_x between filters. Results for the mobility of flexible linear chains are shown in Figure 5.6. Interestingly enough, we see an initial increase in the scaled mobility as we start increasing L_x followed by a dramatic drop in the scaled mobility. The phenomenon is known as entropic trapping (ET) [29,30]. ET of macromolecules during gel electrophoresis has been reported previously for small DNA molecules in polyacrylamide gels[31]. Figure 5.6 can be viewed as follows: When the spacing in L_x initially begins to increase the molecule finds itself with more free volume to manoeuvre and we see a corresponding increase in mobility. Note, however, that the molecule is still in a reptation regime at this point. When the spacing $L_x \approx 2R_g$ the molecule can resume a more entropically favourable conformation and consequently finds itself trapped between the 2 opposing walls. To traverse the walls, the molecule must lose entropy to assume a conformation more appropriate to reptation in order to cross the barrier.

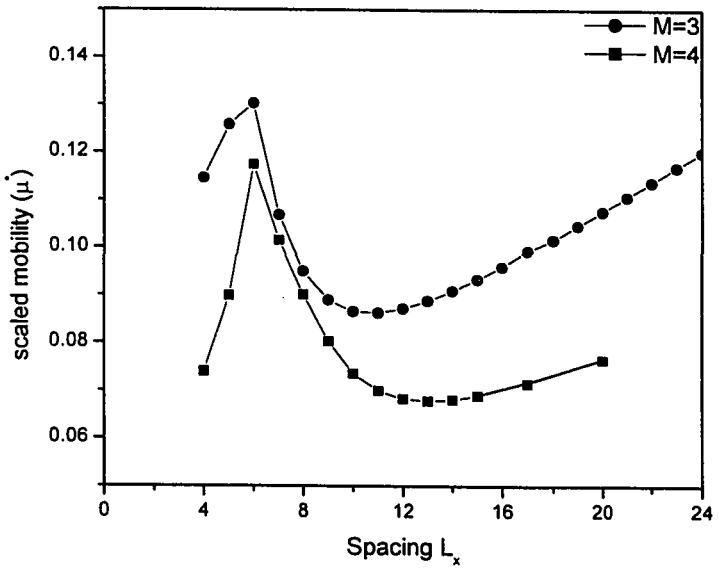

Figure 5.6: The scaled mobility, μ^*, is shown for flexible linear chains (M=3,4) migrating in a periodic anisotropic lattice of obstacles ($L_x \geq L_y = 4$). We see that as the spacing in L_x increases the mobility quickly falls to a minimum due to the entropic trapping effect. The mobility then slowly increases with L_x for both molecules studied here

Studying the mean orientation of our flexible chain in the same anisotropic gel can be a more illustrative demonstration of ET. The following relationship was used to determine the orientation of our molecule:

$$S = 2\langle \cos^2 \theta \rangle - 1 \tag{5.7}$$

where θ is measured by taking the vector from the first to the last monomer of the linear chain (θ =0 being defined along the x-axis). Figure 5.7 demonstrates how the orientation factor is defined.

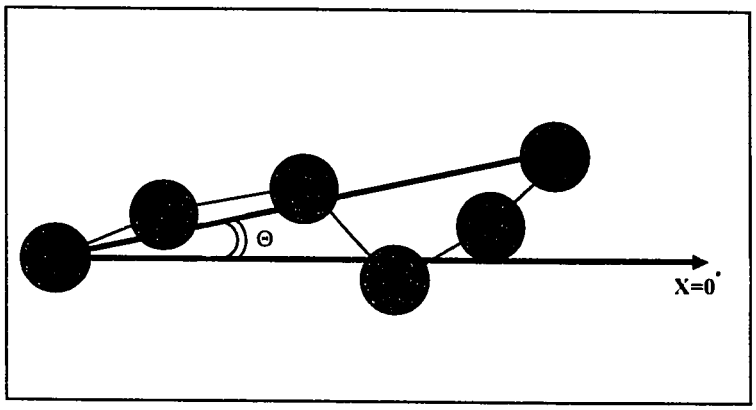

Figure 5.7: A schematic depiction of how the orientation factor S is found for linear polymers.

An isotropic system gives us S=0 while a molecule predominately oriented along the x (y) axis would yield values closer to S=1 (S=-1). Figure 5.8 shows our results for the orientation factor of our flexible chain in a periodic anisotropic gel. As we can see, at L_x=L_y=4 we have S=0, as expected. Increasing the spacing L_x causes the chain to be predominately oriented along the y-axis, reaching a minimum orientation value at L_x=7 (S≈-0.14). And, obviously, we have:

$$\lim_{L_x \to \infty} S = 0 \tag{5.8}$$

Entropic trapping can be viewed as a very effective tool for sieving molecules according to size since longer chains will require a larger spacing in L_x before trapping can effectively occur. In fact, our results indicate that it would be possible to have longer chains elute faster in such a gel than shorter ones. Unfortunately, we could not observe this in our simulations given the limited size range of our molecules. Another popular technique for sieving molecules is capillary electrophoresis (including the use of microchannels). In the next section we will attempt to study this effect by studying the mobility of molecules in narrow tubes.

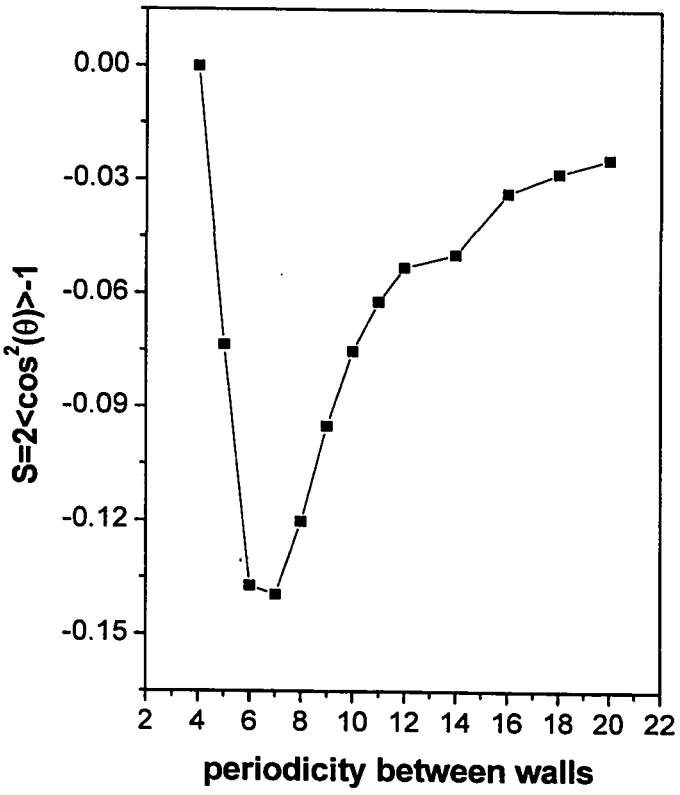

Figure 5.8: The orientation factor $S = 2\langle \cos^2 \theta \rangle - 1$ vs. lattice spacing L_x for the anisotropic gel system with L_y=4.

5.4. Tubes

We studied a system based on the principle of capillary electrophoresis. We designed a narrow channel where our polymer is confined in a narrow tube (L_y=3) of infinite length. Figure 5.9 shows the lattice used. We expect to see our polymer behave as a one-dimensional Rouse chain ($D \sim M^{-\alpha}$, where α=1). Results are shown in Table 5.3 and Figure 5.11. A log-log plot of the scaled diffusion constant (D^*) vs. molecular mass (M) reveals a scaling parameter $\alpha(M) \sim 1.41$ (Results not shown). This result is higher than expected but a linear extrapolation of the finite size scaling parameter (eq 4.4) shows that the value approaches what is expected of a Rouse chain (shown in Figure 5.11). Again, higher molecular weights will need to be studied before making any definite conclusion as to the exact value of α. The scaling parameter of the mean square end-to-end distance $\langle h^2 \rangle$ provides a non-monotonous progression towards the large M limit and we are

unable to draw any conclusions as the value of $\upsilon_{(M\to\infty)}$ from the available results. Logically, in this case, we would presume that the large M exponent of $\langle h^2 \rangle$ would be: $\upsilon \to 1|_{M\to\infty}$ given the one-dimensional aspect of our system (shown below).

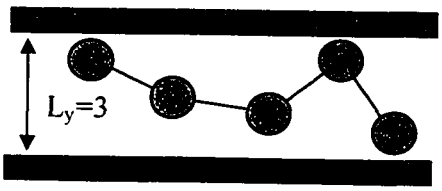

Figure 5.9: Schematic representation of a polymer confined in a two-dimensional tube

In a second attempt to view ET, we modified the same "channel" by adding obstacles to create large compartments separated by narrow doors with a small opening. Figure 5.10 shows an example of our gel. The parameters L_x correspond to the length of the compartment and L_y as its width. The opening is only large enough to permit the passage of one monomer at a time. Once again, we used flexible linear chains to study this system. In Figure 5.12 we plotted $\log(D^*)$ vs. $\log(M)$ for various channel lengths L_x. From Figure 5.12, we see that we have two distinct regimes for the mobility of our chains. The first is the small M regime where $\mu \sim 1/M^b$, with $b>3/2$. The scaling parameter typically associated with ET for large chains are in the range of $3/2<b<3$ [29-31]. Our results for small chains correspond to these values but more data needs to be collected to make any firm conclusions about the existence of ET. The second regime is the large M regime where $\mu \sim 1/M^c$ with $c<2$. In the second regime, we expect the chain to behave as a one dimensional Rouse chain ($D \sim 1/M$) and our data seems to be asymptotically converging towards that result but, once again, more data needs to be collected to confirm that hypothesis. Therefore, the two regimes correspond to entropic trapping (small M) and reptation (large M) respectively. We should also mention that to see any pronounced ET using larger chains we would need to increase the size ($L_y>3$) of the gap to allow for our flexible chain to assume its proper ellipsoidal conformation. (Since the polymer coil is commonly described as a random walk, its shape will not typically resemble a sphere but rather an ellipsoid because the random walker considers neither is past nor future. Consequently, the path described by the polymer coil will tend to explore an area rather thoroughly before moving on to the next area. This causes

anisotropy in the shape of the polymer that makes it look like an ellipsoid as opposed to a sphere.)

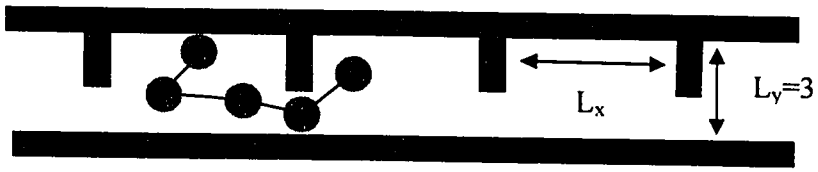

Figure 5.10: Schematic representation of a polymer in a tube with obstacles that serve as entropic traps.

Table 5.3: Flexible Chain in a narrow tube

LEGEND: M=# of monomers, D=Diffusion Coefficient, $\langle h^2 \rangle$ =end-to-end distance, α(M)=scaling exponent of D, υ(M)=scaling exponent of $\langle h^2 \rangle$					
M	D	Number of conformations	$\langle h^2 \rangle$	α(M+½)	ν(M+½)
2	0.077381	42	7.3810	1.5427	1.12465
3	0.041398	396	18.3737	1.44092	1.18462
4	0.027350	3 224	36.3251	1.29223	1.25483
5	0.020499	24 588	63.5943	1.20643	1.22226
6	0.016451	186 120	99.3068		
∞				**0.95 ± 0.08**	**N/A**

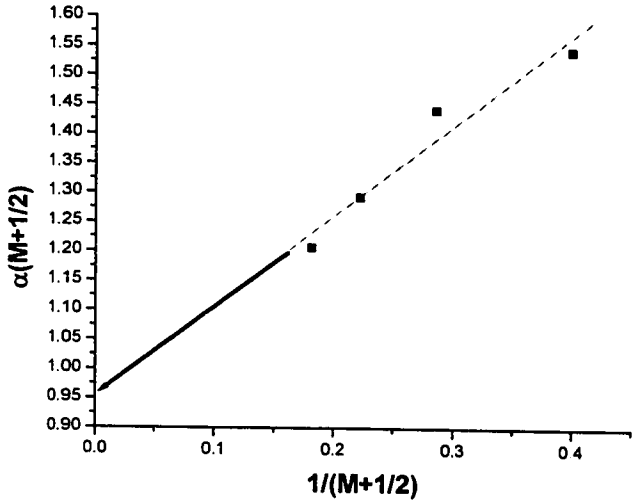

Figure 5.11: Diffusion scaling exponent α of a flexible polymer in a narrow tube (L_y=3). We see that the linear extrapolation yields near Rouse-like dynamics from the arrow extending the linear fit.

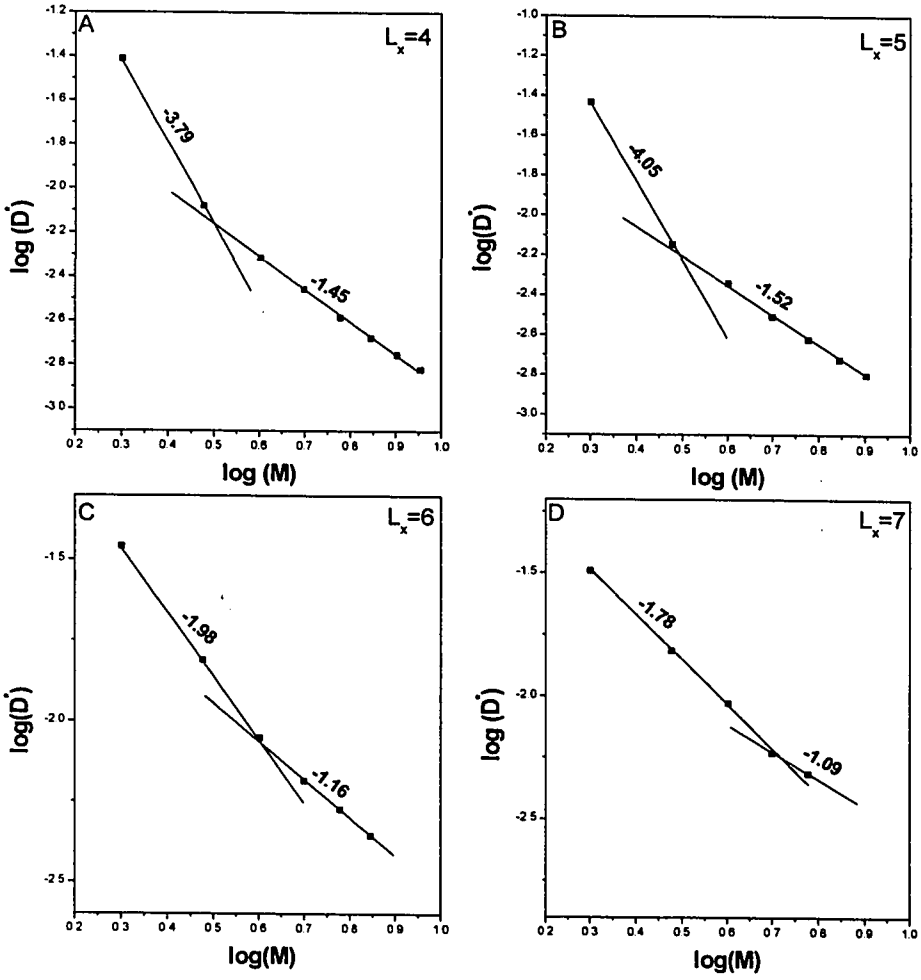

Figure 5.12: Log (μ^*) vs Log (M) for the tunnel system (Fig. 5.10). Lattice spacings are: L_x=4 (A), L_x=5 (B), L_x=6 (C) and L_x=7 (D). Power law fits $\mu^* \sim M^h$ are shown, and the exponents h are given.

Chapter 6

Discussion

In this section we globally discuss our results in general terms in hopes of gaining a big-picture perspective of what was achieved in this thesis. We will start with a synopsis of what has been achieved and review the goals set forth at the beginning of this project. We will then discuss the importance of the OMRC model despite our findings that it may lead to erroneous assumptions.

In chapters 2 to 6 we successfully improved an existing model and were able to properly simulate the behaviour of various molecules in solution. With the exception of the star chains, all our results correspond to expected results. More importantly, we were able to find proper results without having to resort to stochastic algorithms. This is significant since we achieved better results in a fraction of the time it would take for, say, Lattice Monte Carlo simulations.

The first part of this thesis focussed on the exactness of our data and this focus paid off. We uncovered the extent to which entropic trapping can be useful in separating molecules. One of the goals of this thesis was to have smaller molecules diffuse more slowly than larger ones using the right sieving gel. Unfortunately, we were never able to achieve this but we are confident that it is still a possibility using larger molecular sizes and appropriate entropic trapping gels. Several papers have subsequently found a use for entropy using micro fabricated devices. Meller and Branton[32] studied diffusion of linear polymers through a channel and reported that the most probable time of passage, τ_p, follows two regimes: One for small molecular sizes and one for larger one. The transition between regimes seemed to be heavily influenced by the length of the entropic channel (which in this case was a single passage). We also identified two regimes based on the size of the molecule with regard to diffusion of linear polymers in tubes separated by

periodic walls (Figure 4.1B). This reinforces our hypothesis that we can exploit entropic traps to sieve molecules. Cabodi, Turner and Craighead[23] studied a system to separate long DNA chains by exploiting entropy in a micro fabricated system of periodic obstacles. The idea was to apply an electric field for a given amount of time. Smaller chains were able to insert themselves completely in the device while the longer chains were only partially inserted. Shutting off the electric field created a difference of potential in the chains that were only partially inserted. These chains found it more favourable to pull out of the lattice and return to their initial state. The smaller chains that were completely inserted had a mean square displacement of 0, allowing it to diffuse without bias, thus separating longer chains from the smaller ones.

What about the Ogston model? We spent a great deal of energy highlighting the deficiencies inherent in the OMRC model. This does not mean that the model is no longer useful. The inherent simplicity of the model is still attractive and can be used to determine mean properties of the diffusion of molecules. This thesis allows the reader to understand that there are other variables that need to be taken in consideration when performing the separation of molecules. What can be viewed as fine tuning our knowledge becomes increasingly important as we develop technology that allows us to micro-fabricate sieving devices and take advantage of the finer details of molecular interaction. The Ogston model does not consider gel description and molecular architecture. Our results indicate that they can play a vital role in the diffusion of macromolecules. As an example, we found that the effective fibre radius of the gel is dependant on the molecule diffusing in the gel. The fibre radius for linear chains was 4 times that of the circular chains. This effect becomes greater as we increase molecular sizes. This knowledge can be exploited to achieve better separation between linear and circular DNA molecules, for example.

To be thorough we will also see what this model does not accomplish. The foremost limitation would be our inability to simulate larger molecular sizes. This was a necessary trade off for the exactness of our results. The BFM uses a coordination number of 36, meaning that two joint monomers can combine in 36 different ways. Our data agree that, using the BFM, the number of conformations follows the relationship:

$$\Omega(M) = \Omega_o \bullet Z^{M-1} \tag{6.1}$$

Table 6.1 shows our data fits using various molecules in different gel systems. It is possible to use a lattice description that has a much lower coordination number and allow us to study molecular sizes as large as M=10 in solution, or M~15 when introducing obstacles. Unfortunately, this still falls in the realm of very small molecular sizes. Heudkelum, Barkema and Bisseling[34] were able to study reptation dynamics of chains up to M=15 exploiting symmetries in polymer conformations and using parallel processing for computation. The coordination number used was Z=6 in 3D and they limited molecular dynamics to the reptation regime.

Table 6.1: # of Conformations: $\Omega(M) = \Omega_o \bullet Z^{M-1}$

Molecule/Lattice	Ω_0	**Z**
Flexible chain/solution	1.34	27.84
Circular chain/solution	0.85	14.41
Stiff chain/solution	3.40	10.57
Flexible chain/ periodic array of obstacles (L_x=L_y=4)	9.73	9.48

A common theme throughout this first part of the thesis is that we make extrapolations that are based of just a few points. The results of our extrapolations indicate that the study of larger molecules using this exact model will provide very good results. Unfortunately, a common goal in the study of polymer physics is to develop universal relationships. Given the small range of molecular sizes that we studied, it is unreasonable to make any type of universal assertions. Along those same lines, certain extrapolations that were presented can be viewed as dubious since they are made using only 2 or 3 data points. Examples of this are found throughout this work. The fact that, in several instances, our extrapolations come very close to theoretically accepted results offers credulity to our methodology even if results were obtained using minimal data.

PART II

Chapter 7

Anomalous Diffusion

7.1 Introduction

In Part II of this thesis, we study the displacement of a particle in various media impeding the particle's movement, or more precisely, its mobility (if a net external field is applied) and diffusion. Most works concentrate on the long-term effects or steady state solutions and emphasis is rarely made to study the short-term effects. How does a particle achieve a steady state? How fast does it achieve this state? Which factors affect the particles 'journey' to a steady state? Is this transient regime something that can be observed? Can it be exploited in new separation devices? All of these questions lead us back to the OMRC model and its inability to describe short-term effects due to inhomogeneity of the medium and the anisotropy of the system caused by the presence of an external electric field. For example, it was reported[39,40] that gels with fractal geometry[41] are much more effective at trapping particles in dead-ends than homogeneous random gels. An experimental study conducted by Sturm et al.[16] was presented to ascertain the dynamic behavior of latex beads in an agarose gel whose concentration ranged from 0.6% to 1.4%. Specifically, it was a study of the short-time scaling behavior of the particle's mean square displacement. Therefore, it seems appropriate to investigate these same issues using a theoretical model and to compare our results to those of Sturm et al.[16]. In Part II, we will use an exact enumeration method to follow and characterize the displacement of a particle at various time intervals using a variety of obstacle

distributions. In Section 7.2, we will discuss the relevant theory while Section 7.3 introduces the numerical model we will be using.

7.2 Theory

Normally, the steady state diffusion of an analyte follows a linear regime with time, t (eq 1.4):

$$\langle r^2(t)\rangle = 2dD_o t \tag{7.1}$$

where d is the dimensionality, D_o is the diffusion constant and $\langle r^2(t)\rangle$ is the mean square displacement. In the short time regime, on the other hand, we often find that $\langle r^2(t)\rangle$ is not a linear function of time because the analyte has not had sufficient opportunity to fully explore its surroundings. The phenomenon is even more pronounced when the particle moves in a fractal environment. This is rarely a typical experimental situation, however, since the fractality of all real systems are limited both at the small and large length scales. The short-time anomalous diffusion regime can often be described by the scaling law:[35-37]

$$\langle r^2(t)\rangle = 2dD^* \cdot t^{2/d_w} \tag{7.2}$$

where d_w is the fractal dimension of the walk and is usually greater than 2 due to the possibility of the particle being impeded within the lattice. The term fractal dimension is a misnomer. It makes reference to the initial belief that anomalous diffusion can only be observed in the diffusion of particles in a fractal gels. We will show in this second part that anomalous diffusion can be observed regardless of whether the distribution of obstacles is fractal or not. Also, D^* is the effective anomalous diffusion coefficient, valid for the transient regime only. Sturm et al.[16] found that d_w was independent of the gel concentration in the absence of an electric field (within error bars). Moreover, Sturm et al.[16] found that the mean square displacement of the particles scales less than linearly with time when no electric field was applied (d_w>2). This result indicated that the agarose gel is indeed a fractal[36,37](at least over the length scales probed by their experimental system) whose structure is independent of gel concentration. These results

are shown in Figure 7.1. Comparing eq (7.1) and eq (7.2) we get the transition time solving:

$$\begin{aligned} 2dD_o t &= 2dD^* t^{2/d_w} \\ t^{2/d_w - 1} &= \frac{D_o}{D^*} \end{aligned} \tag{7.3}$$

or,

$$t_{ss} = \left(\frac{D_o}{D^*}\right)^{d_w/2-d_w} \tag{7.4}$$

where t_{ss} is thus the time of transition between short-time and the steady state diffusion of particles. Equivalently, substituting eq (7.4) into eq (7.1) we obtain:

$$r_{ss} = \sqrt{2dD_o t_{ss}} \tag{7.5}$$

where r_{ss} is the distance at which the transition to steady-state motion of particles will take place within the system. A system may thus look fractal over length (time) scales shorter than r_{ss} (or t_{ss}), and normal otherwise.

Theory holds that an applied field will add a term to eq (7.1). Hence we have[16]:

$$\left\langle r^2(t) \right\rangle \approx 6Dt + v^2 t^2 \tag{7.6}$$

where v is the mean drift velocity. So far, we have only expressed the movement of particles in terms of $\left\langle r^2(t) \right\rangle$. Slater, Guo and Gauthier[42,44] have reported that the addition of an electric field creates an anisotropy in the system causing a difference in the transverse and longitudinal diffusion constants. To study this anisotropy, we will thus define the electric field along the x-axis and study the first and second moments of the displacement in each Cartesian direction. We then have:

$$\begin{aligned} &\left\langle x(t) \right\rangle = v_x t \\ &\left\langle x^2(t) \right\rangle - \left\langle x(t) \right\rangle^2 \propto t^{2/d_w}, \text{ for } t < t_{ss}. \\ &D_x = \frac{1}{2}\lim_{t\to\infty} \frac{d\left(\left\langle x^2(t) \right\rangle - \left\langle x(t) \right\rangle^2\right)}{dt} \end{aligned} \tag{7.7}$$

where $\langle x(t) \rangle$ is the drift of the particle along the x-axis and the variance $\langle x^2(t) \rangle - \langle x(t) \rangle^2$ behaves as a pure diffusive process for times $t >> t_{ss}$[43]. The above equations are equivalent in the y,z-directions with $v_y = v_z = 0$. In contrast to the field-free experiments, the value of d_w was smaller in the presence of an electric field (10V/cm) using the same gel. Moreover, d_w was an increasing function of the gel concentration. Figures 7.1 and 7.2 show these results. On the one hand, while the bead is moving within a gel pore, its dynamics are governed by a drift process (2nd term of eq. 7.6). On the other hand, once the bead collides with a gel fiber, the bead movement is impeded by the field pushing the bead against the gel strand. As the concentration increases, the time between collisions shortens and the bead dynamics are predominantly governed by collisions (hence by random processes). Consequently, at low concentrations, we expect the particle's movement to be dominated by the second term of eq. (7.6) (i.e. drift process). At higher concentrations, the combination of increased collisions and the electric field pushing the particle against the gel strands causes the particle's overall dynamics to be dominated by a diffusion-like process. This explains why values of $d_w < 2$ were obtained for low concentrations and an increase in d_w was observed as the concentration increased.

Using the theoretical elements presented in this section, we will be able to use our theoretical model to characterize the anomalous diffusion of particles and compare our results with those found in ref [16]. The next section will introduce the model used to study the motion of particles on short time scales.

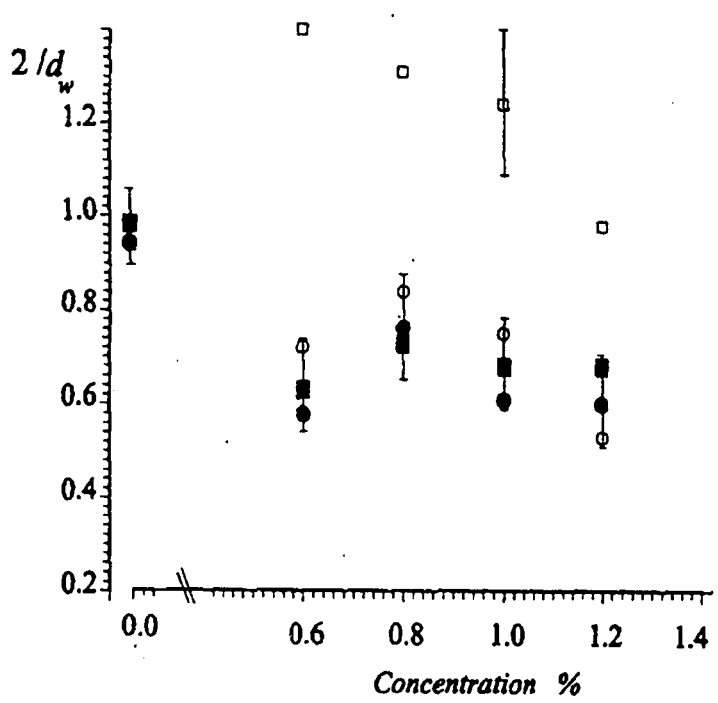

Figure 7.1: Results of Ref [16], showing $2/d_w$ vs. gel concentration. The following legend is used:

- □ x direction, E=10V/cm
- ○ y direction E=10V/cm
- ■ x direction E=0
- ● y direction E=0

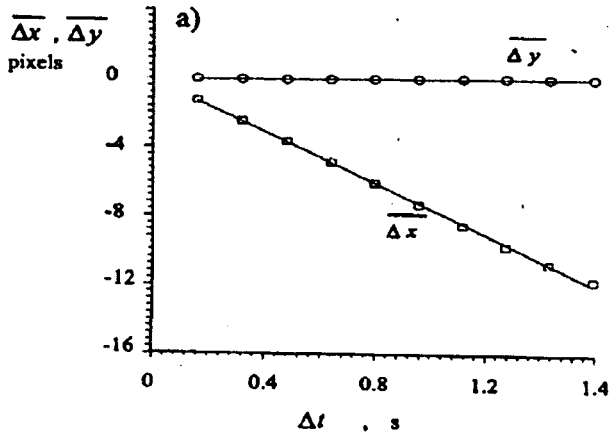

Figure 7.2A: Results of ref [16] showing the first moment of the mean displacement in the x and y directions vs. time with an applied external field of 10V/cm applied in the x-direction. The lines represent the best linear fit of the data.

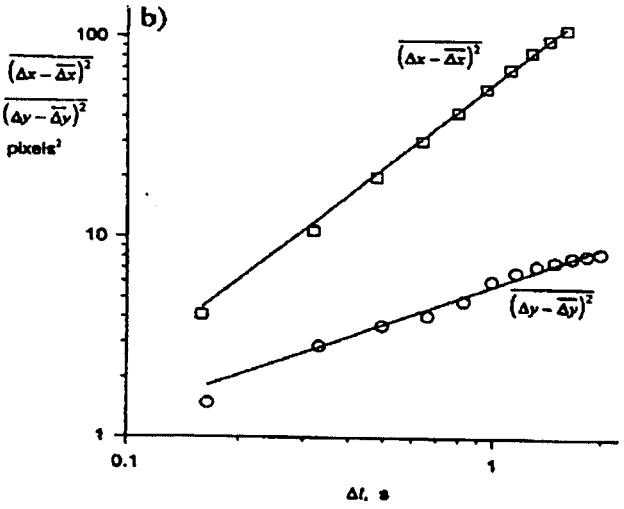

Figure 7.2B: Results of ref [16] showing the second moment of the mean displacement in the x and y directions vs. time with an external field of 10V/cm applied in the x-direction. The lines represent the best linear fit of the data.

7.3 The model

As mentioned before, this model will involve an exact enumeration of all particle trajectories. Using a cubic lattice in 3D, we enumerate all these trajectories of the particle based on an initial starting point. We can compute probabilities associated with each trajectory and derive $\langle x(t)\rangle$ and $\langle x^2(t)\rangle$ (or $\langle y(t)\rangle, \langle y^2(t)\rangle$ and $\langle z(t)\rangle, \langle z^2(t)\rangle$) for a given time t. Taking an averaging over all initial conditions (weighted equally) we can determine those values exactly. To illustrate this exact enumeration approach, Figure 7.3 shows a simple unbiased diffusion problem in 2 dimensions on a lattice without obstacles:

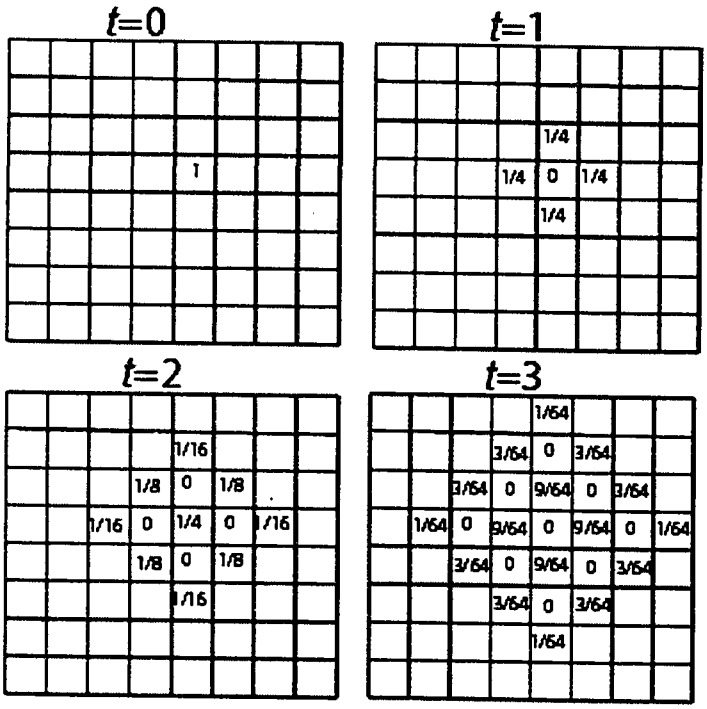

Figure 7.3: We show the unbiased distribution of probabilities of a particle in 2D at times t= 0, 1, 2, and 3.

In three dimensions, the probabilities for jumping are given by:

$$p_{\pm x} = p_{\pm y} = p_{\pm z} = \frac{1}{6} \tag{7.8}$$

The general expression for the probability of presence $n_{xyz}(t)$ on site (x,y,z) at time t is given by the equation:

$$n_{xyz}(t) = n_{x-1,y,z}(t-1)p_{+x} + n_{x+1,y,z}(t-1)p_{-x} + n_{x,y-1,z}(t-1)p_{+y} + \tag{7.9}$$
$$n_{x,y+1,z}(t-1)p_{-y} + n_{x,y,z-1}(t-1)p_{+z} + n_{x,y,z-1}(t-1)p_{-z}$$

Using this method we also have the luxury of introducing an electric field (or another driving force) by modifying the probabilities of transition accordingly. We will use the same approach discussed in section 2.2. Hence,

$$p_{\pm x} = \frac{1}{3} \cdot \frac{e^{\pm \varepsilon}}{e^{+\varepsilon} + e^{-\varepsilon}} \tag{7.10}$$

where ε is the scaled field defined by eq (2.8). The probabilities in the ±y,z directions remain unchanged and are given as follows:

$$p_{\pm y} = p_{\pm z} = \frac{1}{6} \tag{7.11}$$

Unlike the model described in chapter 2, this model does not strictly define the electric field as 'vanishing'. Therefore, we can choose stronger values of the electric field in our study. That being said, however, our intent is to learn of the short time dynamics of particles and is not a study of the drift velocity. Hence, we will be keeping the value of the electric field relatively small.

The presence of obstacles will, of course, affect the distribution of probabilities and we need to define a methodology for treating obstacle interactions with regard to the model: If a move leads to a lattice site containing an obstacle, the move is rejected and the probability of moving towards the obstacle is then applied to the particle's initial location on the lattice. This is standard in Monte Carlo simulations.

The short time dynamics of a particle is incumbent upon many parameters. Foremost of which is the nature of the obstacles and their distribution. The presence alone of obstacles may cause anomalous short-time dynamics but if the concentration of obstacles is small we expect that this effect will be negligible. When the concentration approaches the percolation limit we expect that the anomalous diffusion will be more prevalent. Finally, when the array of obstacles becomes fractal we can argue that the particle never reaches a state of steady motion because the correlation length of the fractal aggregates diverges, and the long term anomalous diffusion exponent d_w would scale to a factor larger than 2. The extent to which the diffusion is anomalous will likely depend on the fractal dimension of the obstacle distribution and the length scale over which this fractal nature applies. We will also investigate how the application of an external field affects the short-term dynamics of particles. Chapter 8 will focus on validating our model by studying various lattice systems with and without an applied external field.

Chapter 8

Anomalous Diffusion: Results

8.1 Validation of the model (ε=0)

The first step is to verify the enumeration method in the unbiased (no external field) limit to make certain that it yields proper values of the diffusion constant for long times. We will start with a particle in solution (no obstructions) and follow through with simple periodic obstruction schemes. We will compare our values with those found in the literature to validate our method.

We will start with a particle in free solution. Mercier and Slater[13] devised an exact method of extracting the steady-state diffusion constant of an analyte in 3 dimensions. We will be using results found in that paper as a basis for our comparison. We expect the diffusion process to follow the scheme in eq (7.1). The diffusion coefficient of a particle in free solution is expected to be D=1/6 if we use our notation and dimensionless units. The results of our simulations using the model presented in Section 7.3 provide identical values of the diffusion constant (shown in Figure 8.1). Of note is the fact that there is no transient to the steady-state diffusion constant. This means that the transition to a steady state regime is only non-trivial when obstacles are present. This is an expected result.

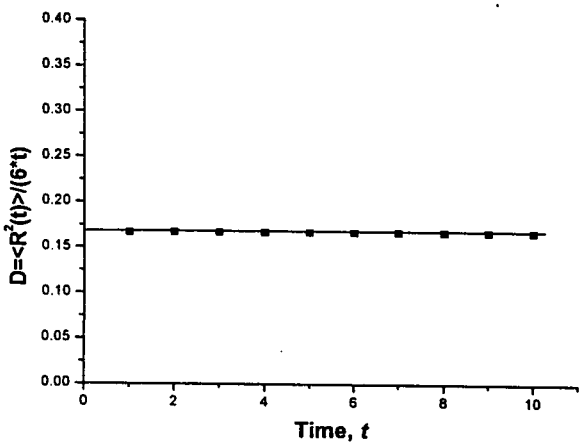

Figure 8.1: Diffusion of a particle in solution (no obstacles) and without bias (ε=0). The solid line represents the steady state solution D=1/6.

Our results for $\langle x^2(t)\rangle$ and $\langle y^2(t)\rangle$ are shown in a different way in Figure 8.2. We see that in the absence of obstacles and external biases the components are equivalent, i.e., the system is isotropic for all times $t \geq 0$. Furthermore, the slope is 1 which indicates that the diffusion coefficient is constant (see eq (7.1)) and that there is no transient behavior. This was also expected. Moreover, from eq. 7.1, we have:

$$\log[x^2(t)] = \log(t) + \log(2dD) \qquad (8.1)$$

which implies that the intercept on the vertical axis should be: $\log(2dD) = -0.4771$ (by substituting the values d=1 and D=1/6). In Figure (8.2), we see the plot of eq (8.1) and find that both slope and y-intercept confirm the fact that there is no transient behavior.

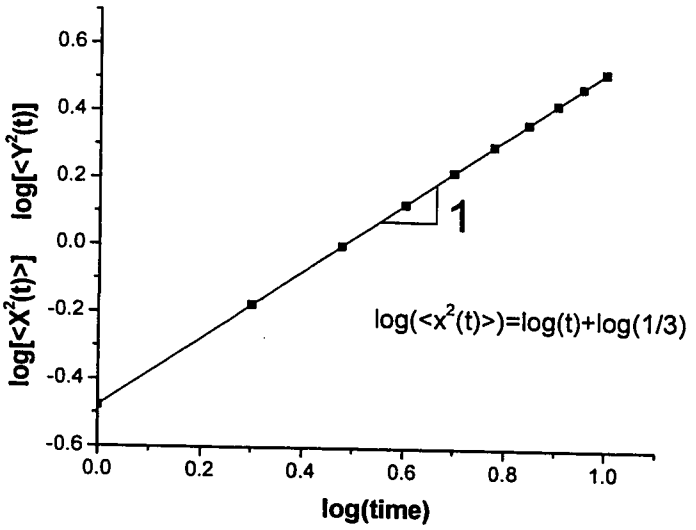

Figure 8.2: Log-log plot of the unbiased (ε=0) mean square displacement vs. time of a particle in solution (no obstacles). We see that both components overlap (the points are absolutely identical) and that the slope is 1, as expected.

We thus conclude that in the absence obstacles, our model provides the expected (trivial) results. The addition of obstacles in our lattice will cause the particle to undergo a transient regime where the mean square displacement will not scale linearly with time. Before presenting our results it would be useful to discuss how the values of D^*, D_o and d_w are going to be computed. After running several test simulations on a variety of periodic lattices it became quite clear that, in most cases, the transition from an anomalous diffusive regime to the steady-state regime is done smoothly and we generally have:

$$d_w \to 2 \text{ as } t \to \infty \tag{8.2}$$

Although we knew to expect such a transition we did not anticipate its smoothness. The value of d_w was found by taking consecutive slope values of eq (7.2). In other words, from eq. (7.2), we have:

$$\left\langle r^2(t)\right\rangle = 2dD^* t^{2/d_w} \tag{8.3A}$$

$$\log\left(\left\langle r^2(t)\right\rangle\right) = \log\left(2dD^*\right) + \frac{2}{d_w}\log(t) \tag{8.3B}$$

$$\left(\frac{2}{d_w}\right)_{t,t+1} = \frac{\log\left(\left\langle r^2(t+1)\right\rangle - \log\left(\left\langle r^2(t)\right\rangle\right)\right)}{\log(t+1) - \log(t)} \tag{8.3C}$$

$$\left(\frac{2}{d_w}\right)_{t,t+1} = \frac{\log\left[\left\langle r^2(t+1)\right\rangle \Big/ \left\langle r^2(t)\right\rangle\right]}{\log\left[1+1/t\right]} \tag{8.3D}$$

From eq. (8.3D), we can easily find the "instantaneous" value of d_w for all times t. Equivalently, we can express eq. (8.3D) in terms of its component in x,y and z. This becomes necessary when an external field is applied because the effective fractal dimension, d_w, may then be different for each Cartesian coordinates. In fact, we would have to study the components $d_{w,x}$, $d_{w,y}$ and $d_{w,z}$ of the fractal dimension for the study of anisotropic gels. Using the second moment of displacement (eq 7.7) to determine the value of the fractal dimension of the particle, we will effectively factor out the particle drift to study the particle's diffusive properties. To avoid confusion, we will use the notation: ($d_{w,x}$, $d_{w,y}$, $d_{w,z}$) to distinguish which component of the fractal dimension we are studying.

Figure (8.3) shows how $d_{w,x}$ evolves for a lattice of periodic obstacles while Figure (8.4) shows the same graph for a lattice of infinitely long periodic fibers.

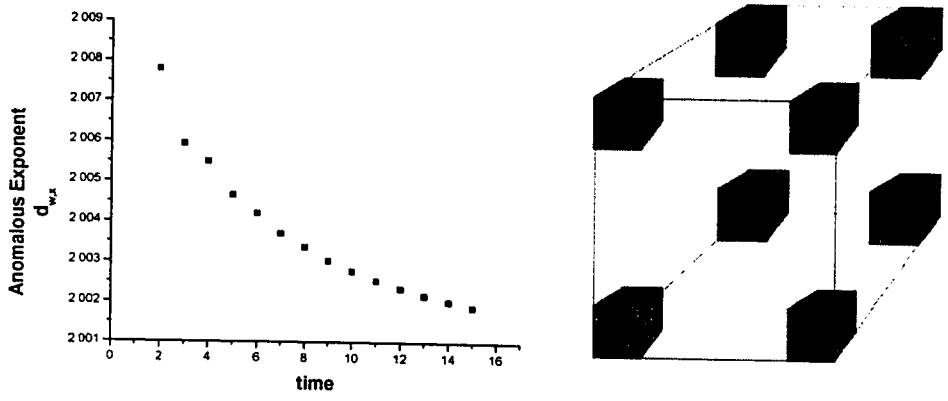

Figure 8.3: Anomalous exponent $d_{w,x}$ vs. time in a lattice of periodic obstacles with an obstacle periodicity, P=4 (shown on the right). The steady-state value is $d_{w,x}\,|_{t\to\infty} = 2.0$

In a lattice of periodic obstacles, we observe how $d_{w,x}$ monotonously transitions to its steady state value ($d_{w,x}$=2), in accordance with eq (8.2). We also note that at t=4 we see a slight kink in the value of $d_{w,x}$ which corresponds with the obstacle's periodicity (P=4).

Since the gel architecture is uniform in all Cartesian coordinates and no external field is applied we have:

$$d_{w,x} = d_{w,y} = d_{w,z} = d_w \tag{8.4}$$

In Figure (8.4) we see quite a different picture for the evolution of $d_{w,x}$ vs. time: the value of $d_{w,x}$ reaches a maximum value before resuming a monotonous decrease towards the steady-state value. The value of $d_{w,x}$ shown here and in Fig 8.3 is always subdiffusive (d_w>2). This is consistent with the findings of Starchev et al.[16] for the short-time displacement of a particle in the absence of an applied field (see our Fig. 7.1). The central question of this chapter is whether we will observe any superdiffusion effects when a field is applied. This will be investigated in the next section. We also observed a direct correlation between the periodicity of the lattice and the time at which the maximum value of $d_{w,x}$ is reached. In Figure 8.5A, we see the anomalous exponent, $d_{w,x}$, vs. time, t for a particle in a lattice of infinitely long periodic fibres (ε=0) for several periodicities, P. We see that in most instances, the value of $d_{w,x}$ reaches a maximum value before making the transition described in eq. (8.2) (the only exception is for P=3 where the value of $d_{w,x}$ starts at a local maximum value). We will call the time at which this maximum value is reached t_{max}. In Figure (8.5B) we see a plot of t_{max} vs. P. Except for P=3 (this case has 2 maxima), the relationship between t_{max} and P is linear and exactly depicted by the following relationship:

$$t_{max} = 2 + P, \quad P > 3 \tag{8.5}$$

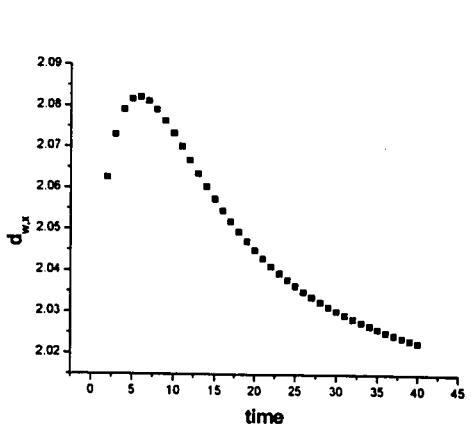

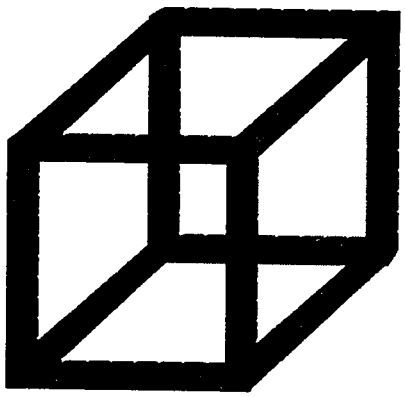

Figure 8.4: Anomalous diffusion exponent $d_{w,x}$ vs. time for a lattice of infinitely long periodic fibers. The periodicity in this example is P=4 (the lattice is shown on the right with P=9 for clarity). The value of $d_{w,x}$ reaches a maximum before making a monotonous transition to its steady-state value, d_w=2.

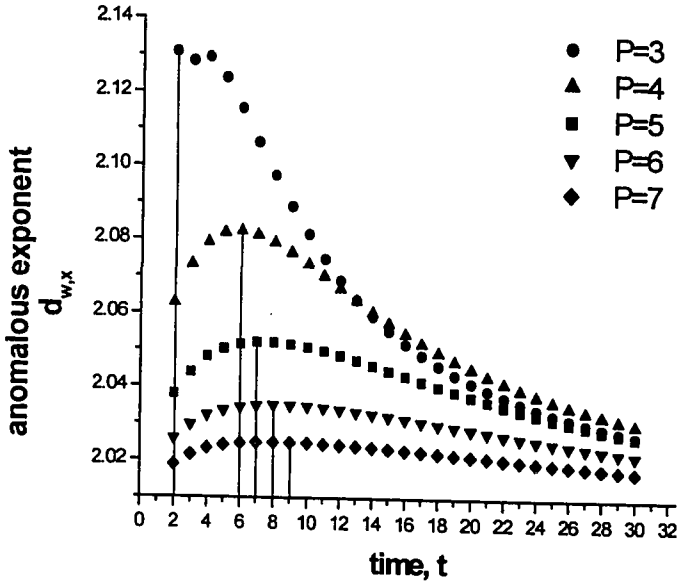

Figure 8.5A: Anomalous diffusion exponent, $d_{w,x}$ vs. time in a lattice of infinite periodic fibers (ε=0) for several periodicities, P. The vertical lines depict the point at which the maximum value of $d_{w,x}$ is obtained.

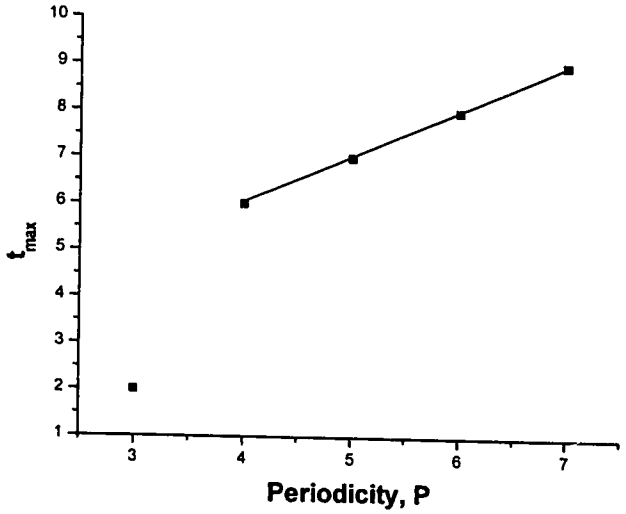

Figure 8.5B: t_{max} vs. Periodicity in a lattice of periodic infinite fibers (ε=0). Here, t_{max} is defined as the time at which the anomalous exponent d_w reaches a maximum. We see that after P=3, we have a linear progression of t_{max}. The linear fit represents the expression:

$$t_{max} = 2 + P$$

Given the various ways in which d_w can evolve in time, we are faced with having to choose a definition of d_w which will be used for all systems. To ensure consistency, we will always choose d_w based on the slope of the first 2 times ($d_w|_{t=1,2}$). In other words, we use eq. (8.3D) using times t=1,2. Consequently, the value of D^* will be found by finding the y-intercept of eq. (8.3B), using only times t=1,2. We illustrate how this is accomplished in Figure (8.6).

Note that we also define the "current" diffusion coefficient $D(t)=\langle r^2\rangle/6t$. By definition, we expect:

$$D(t)\to D_o \text{ as } t\to\infty \tag{8.5}$$

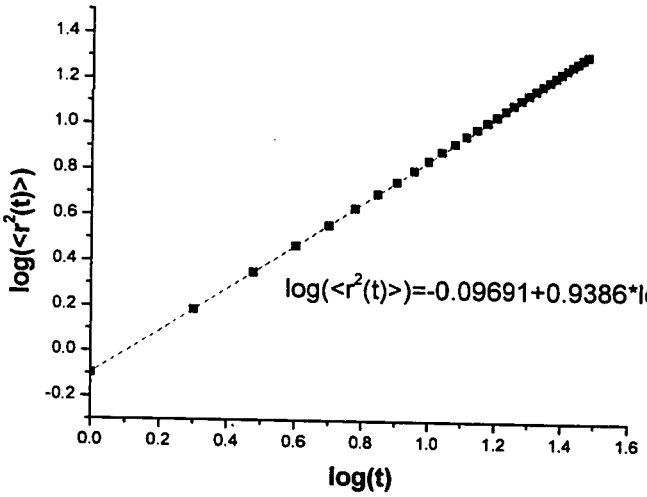

Figure 8.6: We illustrate the manner in which the value of D^* is found. The results shown are for a particle in a lattice of infinite periodic fibres (P=3, ε=0). The equation shown is taken from eq. (8.3B) and the slope is given by eq. (8.3D). The linear extrapolation used to find D^* is done using times t=1, 2. In this case, $D^*=10^{-0.09691}=0.13333$ and $2/d_w=0.9386$.

To find the value of the steady-state diffusion constant D_o we have two options: The first was already mentioned and that is to take values of the exact steady-state diffusion constant (D_o=0.1309799) found in ref [37]. The second option is to graph the current diffusion coefficient $D(t)$ against $1/t$. Since D(t) is defined as the time evolution of the diffusion coefficient to its steady-state value, we can extrapolate the two values of D(t) corresponding to the highest times to find a reasonable approximation of the steady-state diffusion constant, D_o, by taking the y-intercept. In Figure 8.7A, we test this methodology using a lattice of infinitely long fibers. The thin solid line represents the linear extrapolation while the thick horizontal solid line is the actual steady state value reported in ref [37]. Surprisingly, the value found using the linear extrapolation is exactly the steady-state value reported in ref [37] (to the 7th decimal). In fact, taking a linear extrapolation of D(t) using t= {30...40} reproduced the value of the D_o to the same precision!! This result shows that after a certain time, D(t) approaches its steady-state value linearly. We suspect that this transition time is strongly linked to the periodicity of the system. In Figure 8.7B, we test this linear relationship by plotting (D(t)-D_o) vs. ($1/t$). If the progression of D(t) towards D_o is indeed linear, the slope of the resulting log-log

plot should be 1. The linear fit shown in Figure 8.7B is accomplished using the last 3 points. We see that the value of the slope is indeed very near unity indicating a linear convergence: $D(t) = D_o + A/t$ for $t >> 1$.

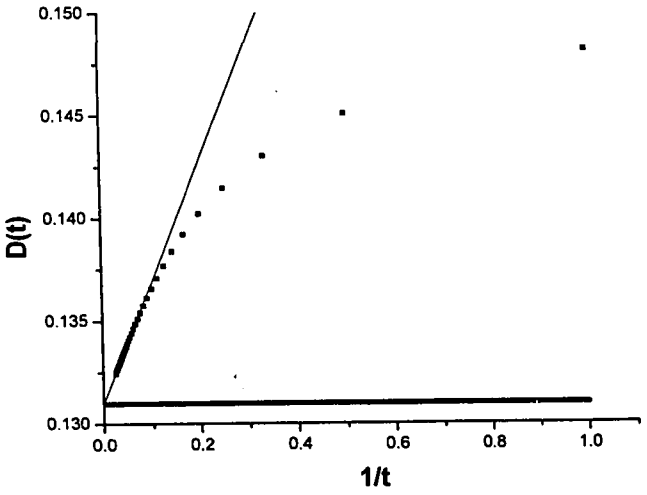

Figure 8.7A: The unbiased short time diffusion constant, *D(t)* vs. $1/t$ in a lattice of infinite periodic fibers (P=4). The black squares represent D while the thin solid line is the linear extrapolation of the last 3 points (D at t=38-40). The extrapolation reveals: $D(t)|_{t\to\infty} = 0.13098000(2)$ The thick horizontal solid line represents the exact steady state value (D_o=0.13097999) reported in ref [37].

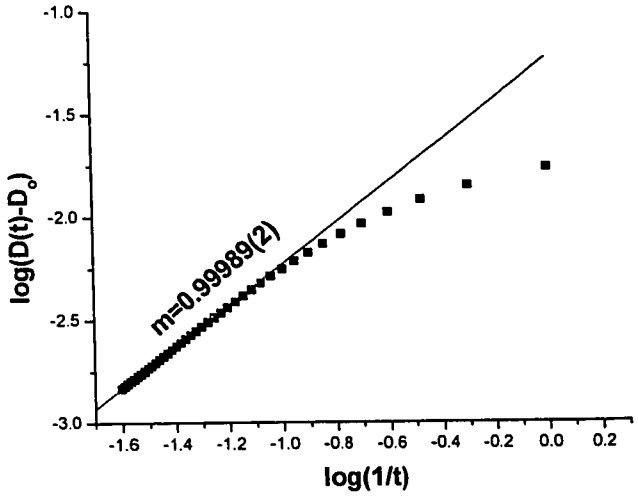

Figure 8.7B: Log-log plot of ($D-D_o$) vs. 1/t. The slope m~1 indicates that the progression of D to D_o does indeed become linear after a certain time. This greatly facilitates the calculation of the steady-state value D_o in cases where no exact result exists.

In this section we presented basic results that were designed to validate the model and we provided details on how we extract the values of d_w, D^* and D_o. We showed that in the absence of obstacles there is no transient behavior of the diffusion constant. We also

demonstrated that all three components of the mean square displacement provide expected results when no obstacles are present. In the presence of obstacles, we described how the values of d_w and D^* are defined. We also showed that we can obtain the steady-state value of the diffusion coefficient by linearly extrapolating the values of the current diffusion coefficient $D(t)|_{t\to\infty}$. In fact, we can also plot the local anomalous exponent ($d_w(t)$-2) vs. $1/t$. The extrapolation to $t\to\infty$ should prove eq. (8.1) and provide a final validation of the model. Results are shown in Figure 8.8.

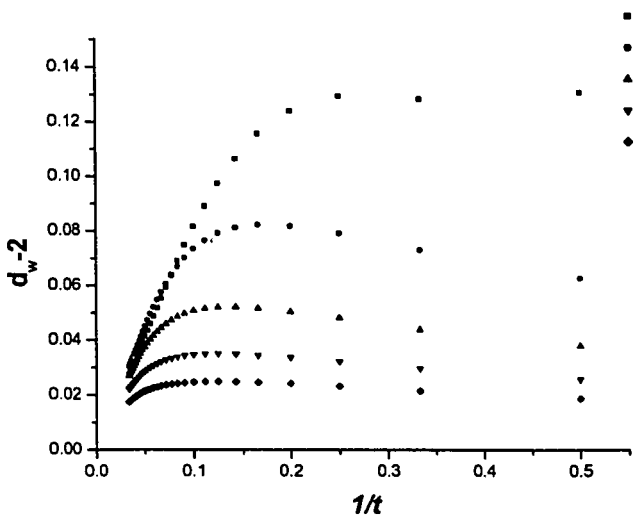

Figure 8.8: (d_w-2) vs. $1/t$ in a lattice of infinite periodic fibers (ε=0) for several periodicities. At low periodicities, a linear extrapolation of the last 2 times (t=29,30) reveals $d_w\to 2$ as $t\to\infty$ (to the 4th decimal place), confirming eq. (8.1). At higher periodicities, we need to see longer times to see the appropriate extrapolation of d_w.

In the next section, we elaborate on these results by investigating the manner in which the field driven displacement of the particle achieves the steady-state regime.

8.2 Results in the presence of a field

In this section, we will attempt to reproduce results similar to those reported in ref [16] and Figure 7.1. To accomplish this, we will be using two different systems. The first, already discussed and depicted in Figure 8.4, is the lattice of periodic fibers. We will use this lattice to determine the extent to which the disorder in the system might be a contributor to the anomalous, short-time displacement observed experimentally in an agarose gel. We will study this lattice by varying two parameters: the first is the periodicity (or the obstacle concentration) and the second is the value of the scaled applied external field, ε. In this manner, we will be able to determine if the applied

external field has a significant impact on the effective anomalous scaling exponent. The second lattice studied simulates a succession of periodic traps. The obstacles are placed in a way that will effectively impede the movement of the particle in the direction of the external field. This lattice will be depicted in Figure 8.12

8.2.1 Periodic Fibres

Results for a lattice of infinite periodic fibers in the absence of an electric field have already been presented while testing the validity of the model (Figures 8.4-8.8). With ε=0, we actually had the trivial results (not shown):

$$\langle x\rangle = \langle y\rangle = \langle z\rangle = 0$$
$$\left\langle \left(x - \langle x\rangle\right)^2 \right\rangle = \langle x^2\rangle = \langle y^2\rangle = \langle z^2\rangle \qquad (8.6)$$

These relations are intuitive and expected. With the application of a field, eq (8.6) no longer applies. In Figure 8.9 we show our results with ε=0.38.

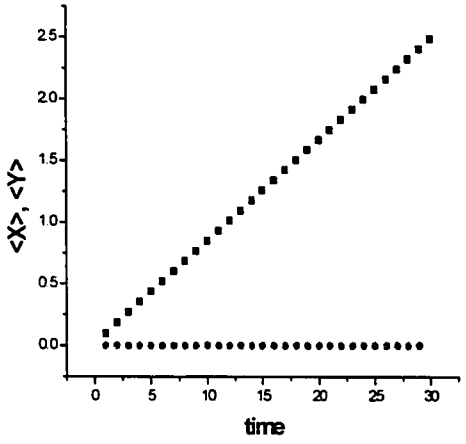

Figure 8.9A: The mean displacement of a particle against time in a lattice of periodic and infinitely long fibers (P=3) with an applied field parallel to the x-axis (ε=0.38). The squares represent the movement along the x-axis while the circles show the movement along the y-axis.

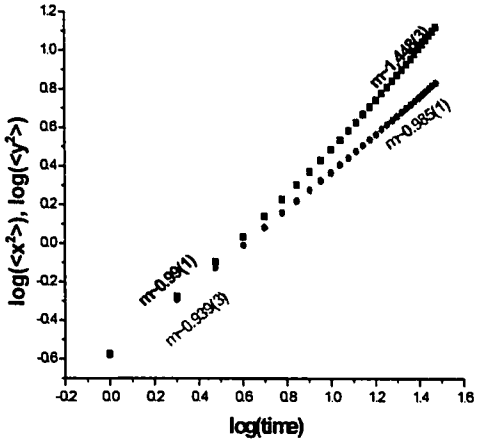

Figure 8.9B: Log-log plot of the mean square displacement of a particle vs. time in a lattice of periodic and infinitely long fibers (P=3) with an applied field parallel to the x-axis (ε=0.38). The squares represent the movement along the x-axis while the circles show the movement along the y-axis.

Figure 8.9A, shows the mean displacement along both the x and y-axis. Once averaged over all initial conditions, the data provide a constant value of the velocity in the x-direction while showing no bias in the y-direction (ie: $\langle y\rangle = 0$). Equivalently, we also

have $\langle z \rangle = 0$ (results not shown). The results of Figure 8.9A are equivalent to those obtained by Sturm et al. [16] (see our Figure 7.2). In Figure 8.9B, we show a log-log plot of the mean square displacement against time in both the x and y directions. Recall that the value of the slope, m, is given by $m = 2/d_w$ in the zero field limit. In the y-direction, we see a sub-linear scaling parameter for short times that slowly makes the transition to the expected linear regime (ie: $2/d_{w,y} = 1$). The results for the movement in the y-direction are consistent with those found in the previous section (ε=0) since the applied external field is perpendicular to the y-axis and should not directly affect displacement in that direction. In the x-direction, however, our results are consistent with eq (7.6) and Figure 8.9A. The initial scaling is close to unity and steadily increases with time, showing a value of $m \cong 1.45$ at times t=29,30. For larger times, we expect that the scaling of the mean square displacement, $\langle x^2 \rangle$ will reach the asymptotic value of m=2, as predicted by eq (7.6) (the drift regime). While Starchev et al. [16] reported an elaborate interplay between drift and trapping, we don't observe this using a lattice of periodic fibers. This is not a very surprising result since an ordered, periodic lattice is not expected to generate any trapping mechanism (e.g., dead-ends). We also plotted the second moment of the displacement in both the x and y-directions. Results are shown in Figure 8.10.

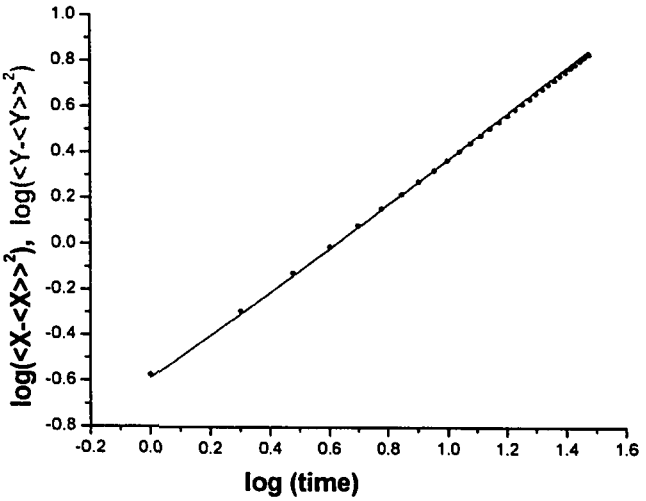

Figure 8.10: The second moment of the displacement in both the x and y directions for a particle in a lattice of periodic fibres (P=3) in the presence of an external field (ε=0.38). The line represents the second moment in the x-directions while the points show the second moment in the y-direction.

Although it may be difficult to see in Figure 8.10, we observe that the second moment in the x-direction is initially lower than the second moment in the y-direction but has a slightly higher slope. Consequently, the second moment in x eventually overtakes the second moment in the y-direction (this occurs at time $t \cong 8$ in this case). In ref [16], there is no such overlap (see our Figure 7.2). We can reason this major difference because the time scales in both problems differ greatly. The range of times studied in ref [16] is of the order of 1 second (see Figure 7.2) while the times studied in our lattice model are closer to the order of 10^{-5} seconds (see eq (2.6)). Another way to look at this is to compare the distance traveled in both cases. In terms of the number of pores traveled, the particle in our computer simulation travels, on average, no more than 1 pore length at maximum time t~30 (see Fig. 8.9A) while, experimentally, the distance traveled can be approximated by:

$$d = vt \cong (2\times10^{-5}\ {}^{m}\!/\!_{s})\cdot(1\,s) = 2\times10^{-5}\ m \qquad (8.7)$$

Assuming a pore size of $p \cong 200$nm (this is a typical value for an agarose gel) we have a total distance traveled of about 100 pores. This is over 100 times the distance traversed in our own numerical study. Keeping the difference in the number of pores visited in mind, we can see how our results are consistent with those found in ref [16]. Unfortunately, it is not reasonable to perform any comparative analysis for the second moment.

We also want to study how the anomalous exponent, $d_{w,x}|_{t\to 0}$, evolves with the concentration. Figure 8.11 shows these results.

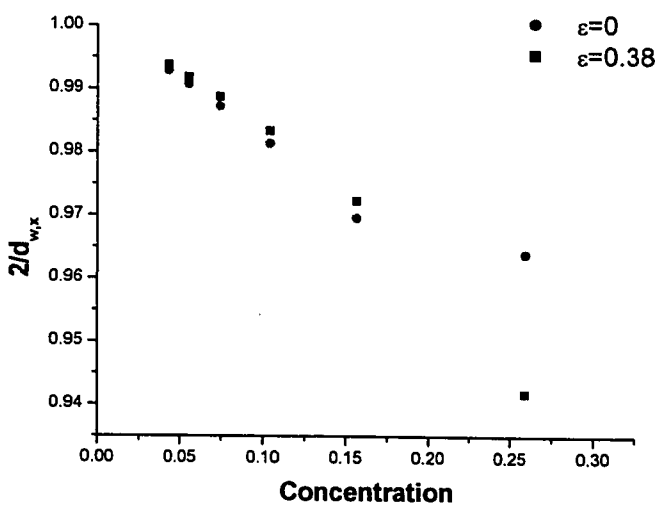

Figure 8.11: $2/d_{w,x}$ is plotted against the concentration, C. Results are shown for a particle in a lattice of infinite fibers. The circles represent results with no bias (ε=0) and the squares represent results with bias (ε=0.38). $2/d_{w,x}$ was obtained using eq. (8.3D) and times t=1,2.

The value of the concentration can be expressed in terms of the periodicity by the relation:

$$C = \frac{3P-2}{P^3} \tag{8.8}$$

In the absence of an electric field, we observe the expected transition from anomalous (subdiffusive) behavior ($2/d_{w,x} < 1$) to normal diffusion ($2/d_{w,x} \to 1$) as the concentration C→0. Although this is consistent with the findings of Sturm et al.[16], we do not achieve the same values of $d_{w,x}$. In fact, the field has little effect on $d_{w,x}|_{t\to 0}$, except at the highest possible concentration C=7/27 corresponding to P=3. This behavior indicates that the electric field does inhibit the particle's diffusion by 'trapping' the particle against the fiber. Note that since the value of $d_{w,x}$ is obtained from times t=1,2, we do not observe the drift portion of the displacement, which will cause the particle to undergo greater displacement in the x-direction than either of its transverse directions. To see this, we plot the time-dependent value of $d_{w,x}(t)$ for various field strengths. This is shown in Figure 8.12.

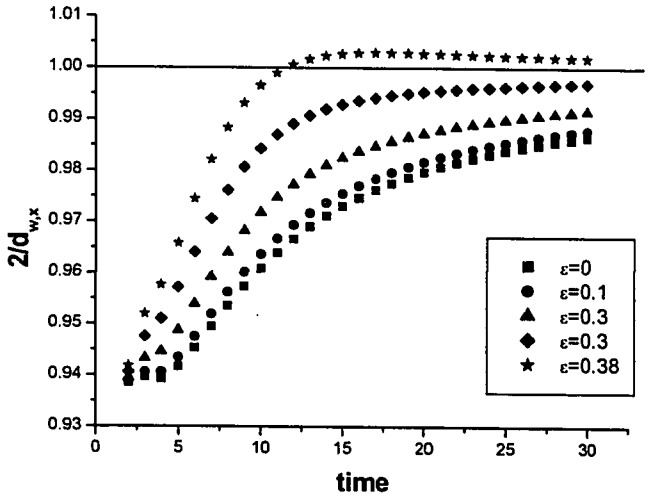

Figure 8.12: The anomalous exponent $2/d_{w,x}$ is plotted against time in a lattice of periodic fibers (P=3) for various values of the external field, ε. The horizontal line represents the value $d_{w,x}=2$ for clarity.

For low values of the applied external field, we see subdiffusive behavior for times. Conversely, at higher field strengths, we observe that the exponent eventually goes into a superdiffusive regime and achieves the nominal, long-term value of $d_{w,x}=2$ for very long times. With an applied external field, Starchev et al.[16] observed a transition from the superdiffusive regime to the subdiffusive regime as the concentration increased (see our Figure 7.1). In Figure 8.13, we plot the anomalous exponent $d_{w,x}$ as a function of time for a particle in the presence of a strong external field (ε=0.38) for several concentrations.

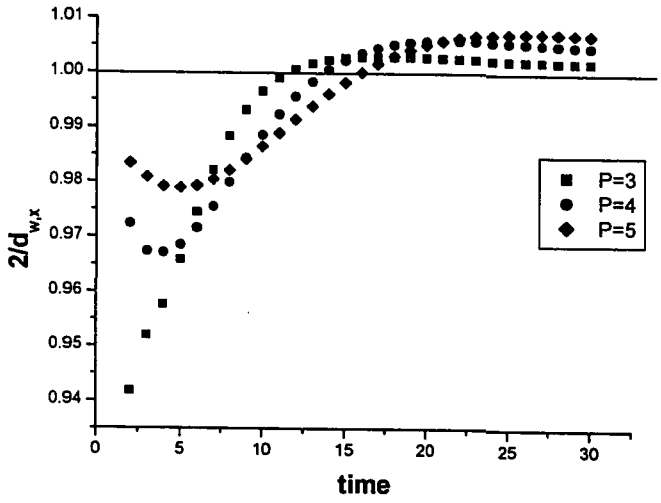

Figure 8.13A: The anomalous diffusion exponent $2/d_{w,x}$ vs. time of a particle in a lattice of periodic fibers in the presence of an external field (ε=0.38) for several periodicities. The horizontal line represents the value of $d_{w,x}$=2.

At a value of ε=0.38, all concentrations exhibit crossover behavior to the superdiffusive regime. Moreover, this crossover time consistently occurs earlier for higher concentrations. While Starchev et al.[16] reported a transition from superdiffusive to subdiffusive behavior as the concentration increases (see Figure 7.1), it is difficult to draw any parallel conclusions since we do not know how to compare our fields to these used in their experimental work.

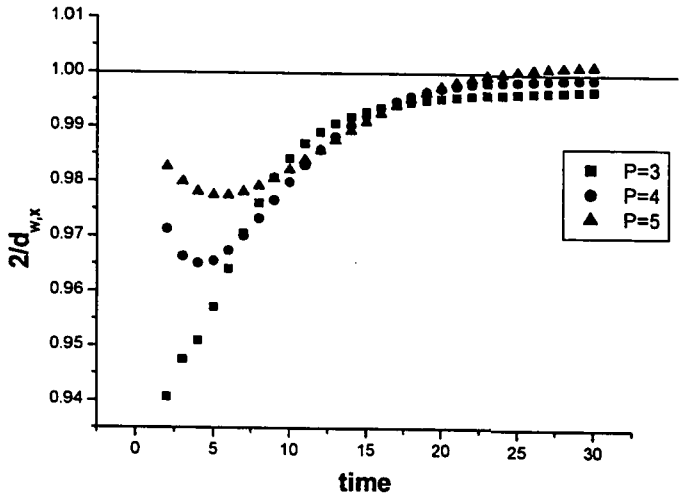

Figure 8.13B: The anomalous diffusion exponent $2/d_{w,x}$ vs. time of a particle in a lattice of periodic fibers in the presence of an external field (ε=0.30) for several concentrations. The horizontal line represents the value of $d_{w,x}$=2.

In Figure 8.13B, we show data for a slightly lower field intensity ε=0.30. For higher concentrations, the long-term behavior of the anomalous diffusion exponent is subdiffusive for all times. As the concentration decreases however, we now clearly see a transition from the subdiffusive regime to the superdiffusive regime. Therefore, choosing an appropriate value of the electric field, we succeeded in reproducing (qualitatively) the results of ref [16]. This is an important finding because it allows us to theoretically reproduce experimental results thus validating both the results of ref [16] in addition to our own model.

In section 8.2.1, we explored the dynamics of a particle in a lattice of periodic obstacles in the presence of an external field. We presented the trivial results showing that the mean motion in directions perpendicular to the external field is zero. We also showed that the mean square displacement of the particle in the direction of the external field is consistent with eq. (7.6), showing a transition from the diffusion towards the drift regime. Nevertheless, the study of drift was not strictly the purview of the work so we can simply resign ourselves to the statement that our results, so far, are consistent with basic knowledge of diffusion dynamics, and, more to the point, consistent with the experimental results of Starchev et al.[16].

Staying faithful with the work of ref [16], we studied the second moment of displacement (eq. 7.7) to effectively filter out the drift portion of the displacement in the direction of the external field and study the diffusive properties of our particle. In doing so, we studied the anomalous diffusion exponent, $d_{w,x}$, by changing 2 parameters: the obstacle concentration and the value of the external field.

By varying the external field, we discovered that the anomalous exponent made the transition from subdiffusion to superdiffusion as the external field increases (Figure 8.12). Since Starchev et al.[16] did not change their value of the external field we have no basis for comparison. Nevertheless, we do observe for the first time that the electric field does have an effect on the scaling exponent of the diffusion constant instead of simply contributing to the particle's drift. Therefore, when studying the short time displacement of particles, we have to take this factor into consideration to obtain exact results. By changing the lattice concentration, we successfully reproduced the results of Starchev et

al.[16]: Using an appropriate value of the external field (Figure 8.13B) we observed a transition from subdiffusion to superdiffusion as the concentration was decreased.

The overall results reported so far in this section can be viewed as qualitatively consistent with those found in ref [16]. The quantitative differences between our results and those of Starchev et al.[16] can be explained as follows: Firstly, the lattice used does not adequately simulate the agarose gel used experimentally. The lattice of periodic fibers used in this work is significantly different than an agarose gel and so we do not make any claim to their similarity. Despite this important difference in gel architecture, we reproduced similar qualitative results. The only remaining difference between our theoretical results and those of ref [16] is the amplitude of the anomalous diffusion exponent, d_w, (Starchev et al.[16] reported values of d_w ranging from approximately d_w=1.42 – 3.64) presumably caused by the fractacality of the agarose gel. Secondly, the disparity in the time and length scales may not allow us to compare results quantitatively. We can then speculate that the strong anomalous diffusion observed experimentally might be due either to the disorder of the distribution of obstacles or the trapping that occurs within the gel due to its fractal nature, or both. To distinguish the importance in these two factors, we propose a second gel, designed to isolate the trapping effect in particle displacement while maintaining the idea of periodicity. Our goal is to confirm whether trapping alone can reproduce results observed experimentally using an agarose gel. The proposed lattice is shown in Figure 8.14 and the following section presents our results using this new lattice.

8.2.2. A system with periodic traps

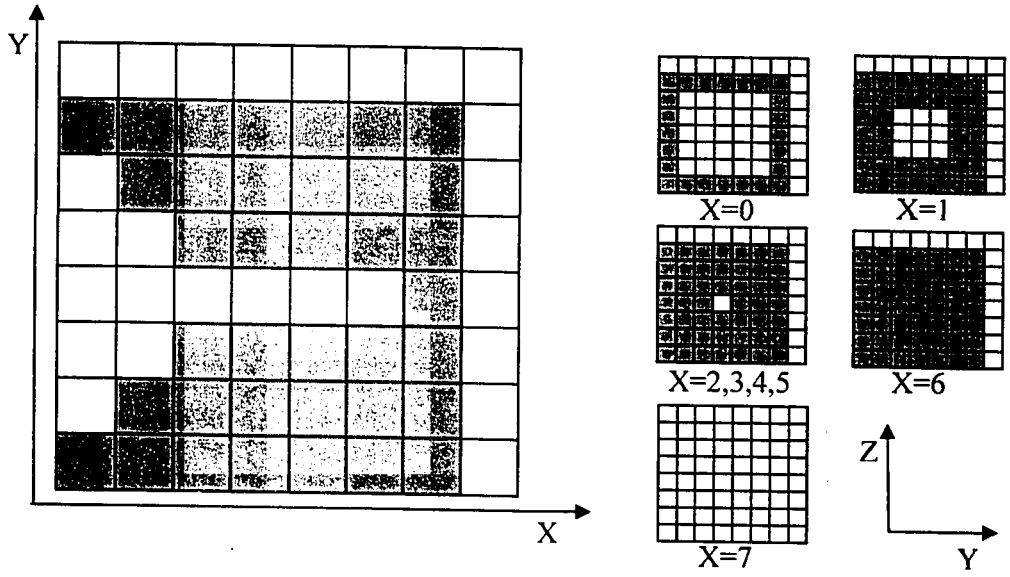

Figure 8.14: A cross-section view of the dead-end matrix. On the left side we see the x-y plane. From this view we can see how the obstacles are arranged like a funnel, effectively trapping the molecules in the x-direction. On the right we see the Y-Z plane. The size of the whole cell is 8x8x8=512 lattice sites.

In Figure 8.14 we see 2 views of the proposed system. As can be seen, the purpose is to impede the particle's movement in the x-direction by introducing a periodic, funnel shaped and hollow obstacle. In Figure 8.15A, we see the fractal dimension, $d_{w,x}$, of the diffusive motion of the particle as a function of time for several values of the external field. The data shown for the particle without external field is qualitatively similar to what was obtained in the lattice of periodic fibers. The important distinction, however, is that convergence to the steady-state values appears to be much slower. Comparing with Figure 8.5A, we can see that the amplitude of $d_{w,x}$ is indeed greater than what was observed for the lattice of periodic obstacles and that the anomalous diffusion does persist for much longer times. In fact, a long intermediate regime exists where $2/d_{w,x} > 1.1$ if the field exceeds about ε=0.2. This is a new effect. In Figure 8.15B, we see the transverse fractal dimension, $d_{w,y}$. The data shown indicates that for all field strengths, we have subdiffusive behavior. Ironically, in an attempt to trap a particle's movement in the x-direction, we also succeeded in achieving trapping dynamics in the y and z-directions. For $\varepsilon \leq 0.2$, we can see how $d_{w,y}$ begins the slow transition to $d_{w,y}$=2 at

the steady-state. Longer times would have to be studied to observe this effect for larger values of ε.

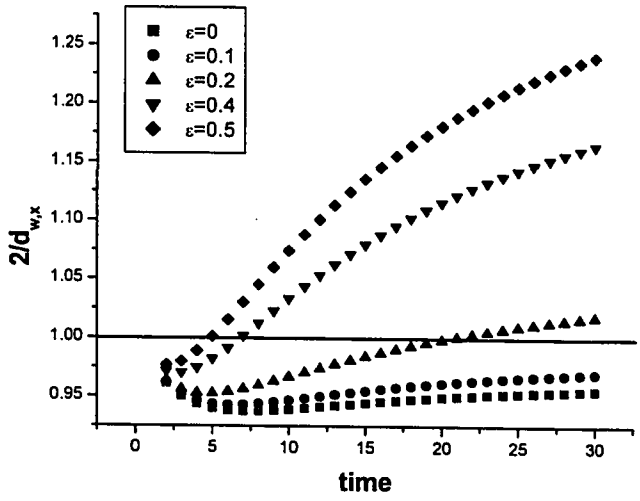

Figure 8.15A: $2/d_{w,x}$ vs. time, t in a lattice of periodic traps for various values of the external field. The horizontal line indicates the value $2/d_{w,x}=1$.

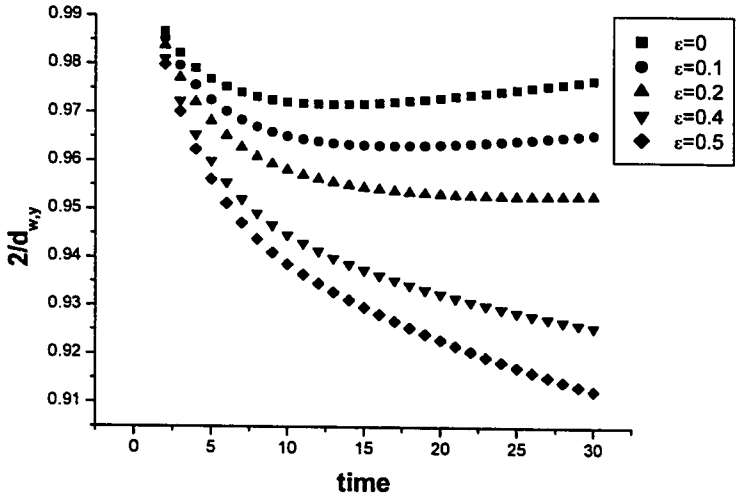

Figure 8.15B: $2/d_{w,y}$ vs. time, t in a lattice of periodic traps for various field strengths.

In Figures 8.16 and 8.17, we show the mean displacement and the mean square displacement of a particle with a value of ε=0.2.

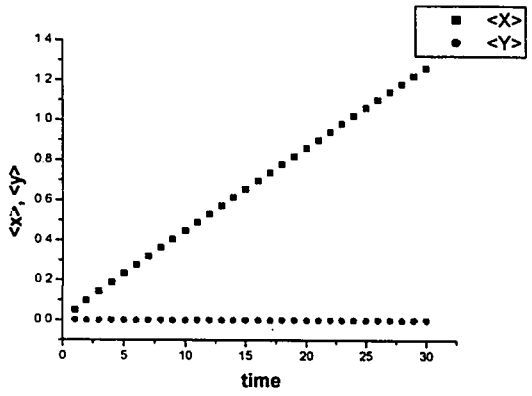

Figure 8.16: The mean displacement of a particle against time in a lattice of periodic funnel-shaped traps with an external field parallel to the x-axis (ε=0.2). The squares represent the movement along the x-axis while the circles show the movement along the y-axis

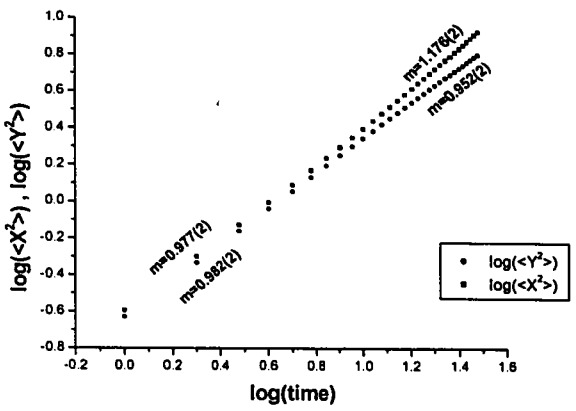

Figure 8.17: Log-log plot of the mean square displacement of a particle against time in a lattice of periodic funnel-shaped traps with an applied field parallel to the x-axis (ε=0.2). The squares represent the movement along the x-axis while the circles show the movement along the y-axis. The values, m of the slopes for the first and last 3 points of each curve are shown.

Figure 8.16 depicts the same physical behavior as the particle in a lattice of periodic fibers: the velocity in the direction of the field is constant while the orthogonal velocities are zero. Results shown in Figure 8.17 for the mean square displacement are interesting. As in Figure 8.9B, the value of the slopes, m, provide the scaling exponents at t=1-3 and t=27-30 for the displacement in the x and y directions respectively. We see that, initially, the scaling exponent for both directions is subdiffusive $\left(m = 2/d_w < 1\right)$. However, the scaling of the mean square displacement is greater in the y-direction than the x-direction. As the time increases, the diffusion exponent resumes its expected behavior: in the x-direction we have a transition to the drift regime caused by the presence of the electric field. In the y-direction, not only does the scaling remain subdiffusive but it is lower than its initial value. We observed a much more rapid progression of the value of the scaling exponent to its characteristic steady-state value $(2/d_w = 1|_{t\to\infty})$ in the lattice of periodic

fibers (see Figure 8.9B). The funnel-shaped lattice depicts a much slower transition to the expected long-term behavior, as can clearly be seen in both Figures 8.15 and 8.17. Since the transition to the steady-state regime is so slow, we plotted $(d_w\text{-}2)$ vs. $1/t$ in Figure 8.18 to try to estimate the likely long-term behavior of the displacement of the particle.

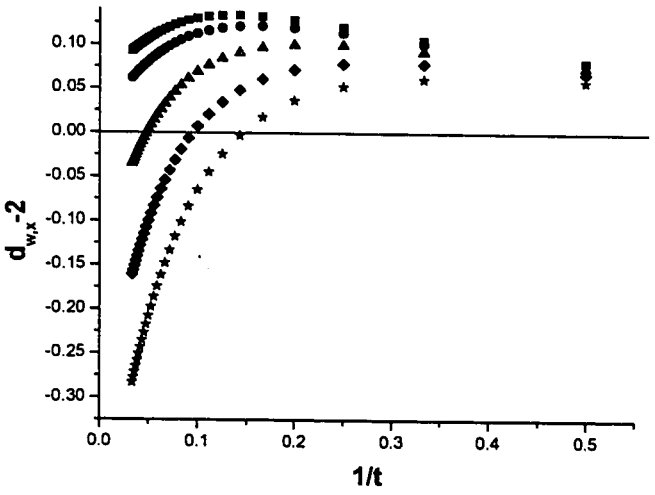

Figure 8.18: $(d_{w,x}\text{-}2)$, vs. $1/t$ of a particle in a lattice of funnel -shaped traps for several values of the external field. The horizontal line represents the value $d_w=2$. The legend is as follows:

Symbol	ε
■	0
●	0.1
▲	0.2
◆	0.3
*	0.4

The conclusion to be drawn from Figure 8.18 is that much longer times will need to be studied to determine the way the anomalous exponent converges towards its asymptotic value 2.

When we studied the lattice of periodic fibers, we plotted the second moment of the displacement against time and showed how there is a crossover behavior at time $t\sim8$ where the second moment in the x-direction overtakes the second moment in the y-direction. Results for the second moment of a particle in our lattice of periodic traps are shown in Figure 8.19.

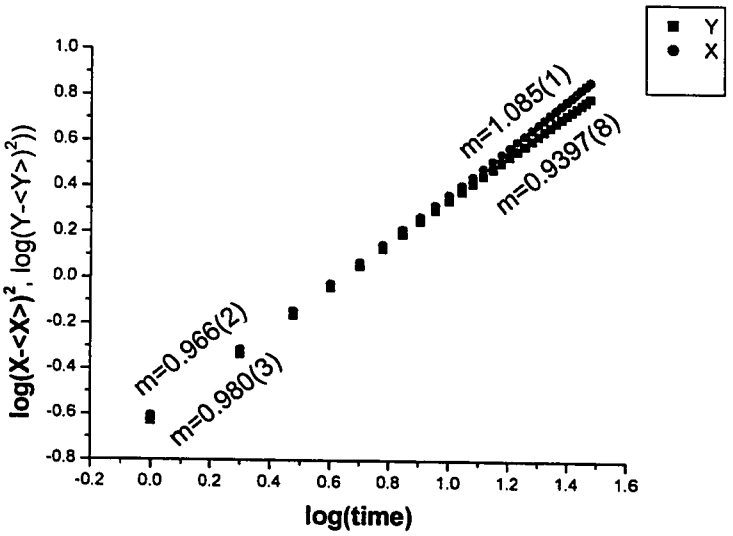

Figure 8.19: log-log plot of the second moment of the displacement against time of a particle in a lattice of periodic, funnel-shaped obstacles in the presence of an external field (ε=0.3). Circles and squares represent the displacement in the x and y direction, respectively.

In the funnel-shaped lattice, the second moment in the x-direction is always greater than the second moment in the y-direction (ie: $\left\langle (x-\langle x\rangle)^2 \right\rangle > \left\langle (y-\langle y\rangle)^2 \right\rangle, \forall t$). In terms of their scaling exponent (which is indicated by the slope, *m*, of Figure 8.19), it is initially lower in the x-direction and gradually increases in value until it is slightly higher than the diffusion scaling in the y-direction. Consequently, short-time trapping the molecule in the direction of the field is observed. As time increases, we see a transition to the super-diffusive regime in the x-direction while we have sub-diffusion in the y-direction.

8.3 Discussion

In this section, we will go over all results obtained in the second part of the thesis to gain a better appreciation of this new model's strong and weak points. After the presentation of the model (Section 7.3), we showed that, in the absence of obstacles, there is no transient regime and that the diffusion constant is not a function of time (Figure 8.1). Adding the presence of obstacles will cause the displacement of the particle to undergo a sub-diffusive regime for short times when no external field is present. We call this regime: 'anomalous diffusion'. The extent and duration of the anomalous diffusion regime is a function of the obstacle concentration and their distribution. One of our goals was to determine how the transition from anomalous to steady-state diffusion is achieved.

In all cases studied, we found that this transition was a smooth function and not strictly delimited by two distinct regimes of displacement. In fact, we determined that the progression of the scaling of the diffusion coefficient towards its steady-state value became a linear function of $1/t$ (Figure 8.8) in a lattice of periodic infinite fibers. Moreover, we were able to find the mathematical relationship depicting the time, t_{max}, at which the maximum value of d_w was found (eq. 8.5) for a lattice of periodic infinite fibers.

The time at which the maximum value of $d_{w,x}$ was achieved and a linear progression towards the value $d_{w,x}=2$ was subsequently observed was dependent on the periodicity, or pore size, in our lattice of periodic infinite fibers. In contrast, no such linear relationship was found for the lattice of periodic obstacles. Consequently, the relationship between the gel architecture and the manner in which a particle makes the transition to steady-state diffusion dynamics is not always easy to determine.

In the absence of an external field, the obstacle distributions that we studied did not play a large role in the magnitude of $d_{w,x}$. The maximum value of the fractal dimension found using infinite periodic obstacles ($d_{w,x}=2.131$, P=3, Figure 8.12) was about the same as that which was found in a lattice of periodic traps ($d_{w,x}=2.132$, Figure 8.15A). Despite similar results with regards to the magnitude of the fractal dimension, the time spent in an anomalous regime appears to be quite sensitive to the gel architecture. For example, by comparing Figures 8.12 and 8.15A, we see how the particle spends a much longer time in a subdiffusive regime in the lattice of periodic traps ($d_{w,x}\sim 2.10|_{t=30}$) than the lattice of periodic infinite fibers ($d_{w,x}\sim 2.04|_{t=30}$). Indeed, the convergence of the fractal dimension to the steady-state value is much slower in the lattice of periodic traps.

In all gels studied (periodic obstacles, infinite fibers and periodic traps), the value of the fractal dimension was always close to 2 ($2/d_w \cong 0.93-1$) when no external field was applied. Starchev et al.[16] reported values of $2/d_w$ ranging from approximately 0.50-0.85 (see our Figure 7.1). Since our lattices do not simulate an agarose gel we can reasonably state that the fractacality and/or disorder of the gel can also play an important role in the amplitude of the anomalous diffusion effect.

When we consider the movement of the particle under the effect of an external field, we showed that the initial (t=1-2) scaling exponent, $2/d_{w,x}$ of the diffusion constant is a decreasing function of the obstacle concentration (Figure 8.11). We also observed that in a lattice of periodic obstacles, the particle can exhibit superdiffusive behavior when the external field is sufficiently high (Figure 8.13A, 8.13B). Starchev et al.[16] reported similar findings. However, for small values of the external field we did not observe any superdiffusive behavior $\left(d_{w,x} > 2 \,\forall\, t,\ \varepsilon \le 0.2\right)$. At higher values of the external field, we initially (i.e. short times) have a subdiffusive regime ($d_{w,x}$>2) followed by a superdiffusive regime ($d_{w,x}$<2). The exact value of the external field at which such a transition is observed will depend on the obstacle concentration but is typically found to be in the range $\varepsilon = 0.2 - 0.4$ for the concentrations studied in this work. We predict that the transition from sub to super-diffusion can be expressed as a function of time. This new effect was never previously observed either experimentally, or numerically. Since ref [16] only examined a single value of the external field, they were not able to recognize how the magnitude of the external field can be significant when studying the anomalous diffusion of particles. Moreover, the value of $d_{w,x}$ for a particle in a lattice of periodic fibers was still much smaller than those reported by ref [16] when an external field was applied. Although superdiffusion was observed, the observed range was typically: $1.0 < 2/d_{w,x} < 1.2$. Starchev et al.[16] observed values the were slightly larger (up to $2/d_{w,x} \cong 1.3$ (see our Figure 7.1)).

When we applied an external field to our funnel lattice, the transition to the steady-state diffusion regime was very slow. If the external field was sufficiently low (ε<0.2), we observe subdiffusion in all directions. For larger values of the external field (ε>0.2), we observe a transition from the subdiffusive to the superdiffusive regime in the direction of the external field (x) and very strong subdiffusive behavior in the other 2 directions (y,z). The transverse fractal dimension was typically in the range: $0.9 < 2/d_{w,y} < 1.0$. Ref [16] reports values of the transverse fractal dimension to be in the same range as those found in the absence of an applied external field (i.e.: 0.55-0.85). However, we see in Figure 8.15B that for larger values of the external field (ε>0.3), the maximum value of $d_{w,yz}$ has not yet been reached and the transition towards the steady state value was not

observed. Therefore, our reported values of the fractal dimensions are somewhat understated because the study of longer times would obviously indicate larger values of the fractal dimension. When the external field is sufficiently high our lattice of periodic funnels acts as an effective trap. Larger times will need to be studied to obtain more consistent quantitative results.

In summary, we conclude that trapping does indeed play an important role in the magnitude of d_w. Since our reported values of the fractal dimension of the particle were not as high as those found by Starchev et al.[16] (or in the literature for that matter[37,47,48]) we can only conclude that while trapping plays an important role in the particle's short-time subdiffusive behavior, the disorder and the fractacality of the gel also need to be considered. A likely next step would be to study the short-time diffusion of particles in disordered and fractal gels. Regular fractals, with periodic boundary conditions, would be particularly useful.

The model proposed in the second part to this thesis does have inherent disadvantages. Firstly, while any enumeration method has the advantage of providing exact results, we do have to contend with the fact that we were only able to simulate very short times. Exceeding t~50 becomes extremely time-consuming in three dimensions. The study of t>50 is better left using stochastic algorithms. Secondly, it is not always possible to extrapolate steady-state values for the displacement of particles. Although we were able to find some exact values of the long term diffusion coefficient, we do not yet have an expression linking the time at which progression towards the steady state value becomes a linear function of $1/t$, allowing us to reliably extrapolate our results

$$\text{Without field}: \langle h \rangle = 4\left(\frac{1}{4}\right)+5\left(\frac{1}{4}\right)+5\left(\frac{1}{4}\right)+6\left(\frac{1}{4}\right) = 5$$

$$\text{With field}: \langle \mathrm{h} \rangle = 4\left(\frac{1}{4}\right)+5\left(\frac{1}{4}+\frac{\varepsilon}{8}\right)+5\left(\frac{1}{4}-\frac{\varepsilon}{8}\right)+6\left(\frac{1}{4}\right) = 5$$

to $t \to \infty$ $F_k = \sum C_i \; \upsilon \to 1|_{M\to\infty} \; 1/\sqrt{M}$

$1/t \to 0$. Moreover, our model will never be able to bridge the gap between anomalous and steady-state behavior because we are limited to t<50. The studied particle would have to traverse a distance that is several times greater than its average pore size before achieving steady-state motion. In our model, being limited to t<50, the average distance

traversed by our particle is always of the order of a single pore size, even when the external field is relatively high. Therefore, the use of exact enumeration models will have to rely on extrapolation to determine the long term behavior of a particle.

PART III

Chapter 9

Conclusion

In this part of the thesis, we conclude by providing a discussion on the broad strokes of what we accomplished. In each part of the thesis, we introduced a model that studied various aspects of polymers physics. For each of these parts, we will present a short synopsis of the model followed by a brief review of our major findings.

In the first part of the thesis we improved upon an existing model which found exact values of the mobility of particles. We restructured the model to include the study of small macromolecules. This improvement allowed us to study various new problems because the molecular architecture is taken into consideration. Since the model was independent of the molecular lattice description we opted to use the bond fluctuation model to maximize the precision of our results at the expense of being limited to very small molecular sizes.

The strong points of this new model is that you can obtain highly precise results for the mobility (or diffusion coefficient) of a molecule without having to resort to lengthy stochastic simulation algorithms. Moreover, our method provides complete flexibility with regard to lattice descriptions, allowing for different rule sets for both molecule-molecule and molecule-obstacle interactions. In other words, we can alter the lattice description to suite our needs for the study of molecules in either 2 or 3 dimensions.

To accentuate the usefulness of this model, we will briefly reiterate some of our key results. Firstly, we were able to clearly show the existence of entropic trapping. Previous studies only speculated that entropic trapping may be exploited in sieving

matrices. In our study, we clearly showed how a molecule can be trapped between 2 walls and that the extent of the trapping will be a function of the molecular size. Unfortunately, we were not able to study a large enough sample of molecular sizes to determine how effectively we can sieve molecules using this technique. Secondly, we used standard Ogston tools[25] to determine that the effective gel radius is, in fact, a function of molecular architecture. This means that the gel fibers will be able to affect the mobility of the molecule, even when the two are far apart and that we must now consider the gel along with the molecule to determine how the gel will affect the mobility of the analyte. These were only two of many dynamic effects that we were able to investigate using this model.

The model introduced in the first part of the thesis investigated systems in two-dimensions, using only the bond fluctuation model to describe how the particles interact with one another. A likely next step would be to study various lattice descriptions in two-dimensions and compare our results to ascertain the importance of how we describe our molecular interactions. Since our model can easily accommodate three-dimensional systems, we can also study analytes in 3D. This would be the next step, especially if we wish to use this model to aid in the development of experimental sieving systems.

In the second part of the thesis, we focused on the short-time anomalous diffusion of particles. We proposed an exact enumeration model designed to study the short-time displacement of point-like molecules. We enumerated all possible particle trajectories and associated probabilities to each trajectory to determine the exact displacement of the particle. Quantities that were studied included the time-dependent diffusion constant $D(t)$ and the fractal dimension, d_w, whose value translates directly to the scaling of the particle's displacement. We studied these system parameters by varying the obstacle distribution, concentration (C) and applied (dimensionless) external field (ε) to determine how these factors affect the manner in which a particle achieved its characteristic steady-state displacement.

To validate the model, we studied a particle in both solution (ie: C=0, no obstacles) and by using simple obstruction schemes (ie: periodic obstacles and periodic infinite fibres). Our results corresponded very well to both theoretical predictions and comparison with published results. During our validation process, we identified that, in

some cases, the long-term steady-state solution to the diffusion constant, D_o, can be extrapololated linearly to $1/t \to 0$. Additionally, we were also able to duplicate (qualitatively) all the results reported by Starchev et al.[16]. Specifically, we observed transition from subdiffusive to superdiffusive behavior of the particle in the presence of an applied external field as the concentration decreases (Figure 8.13B).

We also studied a potential trapping lattice (shown in Figure 8.14) to determine the extent to which the anomalous diffusion effect is caused by trapping within a gel (as opposed to gel disorder). We determined that this trapping lattice displayed anomalous diffusion for much greater times than in a lattice without trapping. In other words, the transition to the steady state regime was decidedly much slower. We also showed that for higher values of the external field, the particle in the funnel shaped lattice displayed significant superdiffusion in the direction of the field while in the y,z directions, we observed significant subdiffusion. The general theme identified with this lattice was that much longer times would need to be studied to fully characterize the extent of the anomalous diffusion for both magnitude and time scales.

In this second part, we showed that the physics involved in the short-time displacement of particles are indeed significant and deserve to be studied in more detail to gain a better understanding of the short-time displacement of particles. We only began this study by showing a few interesting lattice models that were designed to show the validity and scope of this new model. A more detailed investigation using disordered gels seems in order. A model that can study longer times would also prove quite useful to help bridge the gap in our understanding between the short time and steady-state regimes of displacement.

References

1. Stellwagen, N., Gelfi, C., Righetti, P.G., Electrophoresis, 2002, 23, 167-175
2. Krylov, S.N., Dovichi, N.J., Analytical Chemistry, Vol. 72, No. 12, June 15, 2000
3. Marquet, C., Buguin, A., Talini, L., Silberzan, P., Physical Review Letters , Vol 88, No. 16, 22 April 2002
4. Huang, L.R., Tegenfieldt, J.O., Kraeft, J.J., Sturm, J.C., Austin, R.H., Cox, E.C., Nature Biotechnology, 2002, 20, 1048-1050
5. Morris, C.J.O.R., in: Peeters, H. (Eds.), Protides of the Biological Fluids, Elsevier, New York 1967, pp. 543-551.
6. Rodbard, D., and Chrambach, A., Proc. Nat Acad. Sci. USA 1970, 65, 970-977.
7. Tietz, D., in: Chrambach, A., Dunn, M. J., Radola, B. J. (Eds.) Advances in Electrophoresis Volume 2, VCH Publishers, Weinheim 1988, pp. 109-169
8. Mercier, J,-F., Slater, G. W., J. Chem. Phys. 1999, 110, 6050-6056.
9. Mercier, J,-F., Slater, G. W., J. Chem. Phys. 1999, 110, 6057-6065
10. Slater, G. W., Guo, H. L., Electrophoresis. 1996, 17, 977-988.
11. Slater, G. W., Guo, H. L., Electrophoresis. 1996, 17, 1407-1415.
12. Treurniet, J. R., Slater, G. W., J. Chromatography A 1997, 772, 39-48.
13. Mercier, J.-F., Slater G. W., Electrophoresis 1998, 19, 1560-1565.
14. Doi M., Edwards S. F., The theory of Polymer Dynamics, Clarendon Press, Oxford 1986
15. R.K. Pathria, Statistical Mechanics 2nd ed. (Butterworth Heinemann, Oxford, (1996)
16. Starchev, K., Sturm, J., Weill, G., Brogren, C.-H., *Journal of Physical Chemistry B*, 1997, 101, 5659-5663
17. Ogston, A.G., *Trans. Faraday Soc.* 1958, 54, 1754-1757.
18. Ferguson, K. A., *Metabolism* 1964, 13, 985-1002.
19. Slater, G. W., Guo, H. L., *Electrophoresis* 1995, 16, 11-15
20. Mercier, J. F., Slater, G. W., *Electrophoresis* 1998, 18, 1560-1565

21. Labrie, J., Mercier, J.-F., Slater, G. W, *Electrophoresis* 2000, 21, 823-833.
22. Reif, F., *Fundamentals of statistical and thermal physics*, McGraw-Hill, 1965.
23. G. W. Slater, J. Rousseau and J. Noolandi, *Biopolymers* 26, 863 (1987).
24. D. W. Heermann, *Computer simulation methods*, 2nd ed. (Springer-Verlag. 1990)
25. Slater, G.W., "Theory of band broadening for DNA gel electrophoresis and sequencing" *Electrophoresis* 14, 1-7 (1993)
26. Carmesin I., Kremer K., *Macromolecules* 1988, 21, 2819-2823
27. Press, W. H., Flannery, B. P., Teukolsky, S. A., Vetterling, W. T., *Numerical Recipes: The Art of Scientific Computing (fortran version),* Cambridge University Press, Cambridge (1989)
28. Bishop, M., Michels, J. P. J., *J. Chem. Phys.* 1985, 83, pp. 4791-4792.
29. Nixon, G. I., Slater, G. W., *Phys. Rev. E* 1999, 60, pp. 3170-3173.
30. Slater, G. W., Nixon, G. I., *Physics in Canada* 1997, 53, pp. 177-183
31. Rousseau, J., Drouin, G., Slater, G. W., *Phys. Rev. Lett.* 1997, 79, pp. 1945-1948
32. A. Meller, D Branton, *Electrophoresis 2002*, 23 pp. 2583-2591
33. Cabodi, M., Turner, S. W. P., Craighead, H., G., *Analytical Chemistry,* Vol. 74, No. 20, October 15, 2002
34. Heukelum, A. V., Barkema, G. T., Bisseling, R. H., *Journal of Computational Physics 180*, pp. 213-326 (2002)
35. Stauffer, D., *Introduction to Percolation Theory*: Taylor & Francis: London, 1985: p. 95
36. Havlin, S. Molecular Diffusion and Reactions, *In The fractal Approach to Heterogenous Chemistry*; Avnir, D., Ed.; John Wiley & Sons: New York, 1989
37. Havlin, S.; Ben-Avraham, D. *Adv. Phy.* 1987, 36, pp. 695-798
38. De Gennes, P. G., *J. Chem. Phys.*, 22, 1971, pp. 572-579
39. Saxton, M. J. *Biophys. J.* 1992, 61, 119-128
40. Saxton, M. J. *Biophys. J.* 1993, 64, 1053-1062
41. Mandelbrot, *The Fractal Geometry of Nature*; W.H. Freeman and Co.: New York, 1982.
42. Slater, G. W.; Guo, H. L. *Electrophoresis* 1995, 16, 11-15.
43. Starchev, K.; Avramov, M.; Radoev, B. *Langmuir* 1995, 11, 1731-1734.

44. Gauthier, M. G., Slater, G. W., *J. Chem. Phys.*, 117, 2002, pp. 6745-6756
45. Slater, G.W.; Wu, Y.S., *Phys. Rev. Lett.*, 1995, 75, 164-167
46. Majid, I., Ben-Avraham, D., Havlin, S., Stanley, H. E., *Phys, Review B*, 1984, 30, 1626-1628
47. Rampino, N. J, Chrambach, A. J., Chromatogr. 1992, 596, 141-149
48. Havlin, S., Molecular Diffusion and Reactions. *In The Fractal Approach to Heterogeneous Chemistry;* Avnir, D., Ed.; John Wiley & Sons: New York, 1989
49. B. Maier and J. O. Radler, *Phys Rev. Lett.*, 1999, 82, 1911
50. P. Cicuta and I. Hopkinson, *J. Chem Phys.*, 114, 2001, pp. 8659
51. Grant I. Nixon, Gary W. Slater, *J. Chem. Phys.*, 117, 2002
52. Mercier, J-F., Slater, G.,W., *Macromolecules* 2001, 34, 3437-3445